

X-RAY CRYSTALLOGRAPHIC STUDY OF A TRINUCLEAR RUTHENIUM ORGANO-METALLIC
COMPLEX

by

Loganathan ⁷⁰⁰ Subramony

Submitted in partial fulfilment of the requirements for the Degree of
Master of Science in the Department of Physics in the Faculty of
Science at the University of Durban-Westville

Supervisor : Professor D.W. Engel

Co-Supervisor: Dr K.G. Moodley

[S.I.] : [S.M.]

Date submitted: January 1984

ACKNOWLEDGEMENTS

I would like to record my appreciation to the following:

Professor D.W. Engel, Department of Physics, University of Durban-Westville, under whose direction this research was undertaken, for his constant encouragement, interest, constructive criticism and invaluable suggestions.

Dr K.G. Moodley, Department of Chemistry, University of Durban-Westville, for the preparation of single crystals and for most valuable discussions.

Mr S. Baboolal, Assistant Director, Computer Centre, University of Durban-Westville, for help in sorting out the numerous computing difficulties.

Mr J. Albain, CSIR, Pretoria, for collecting intensity data on single crystals.

Dr D.H. Pienaar, Department of Chemistry, University of Durban-Westville, for help with the production of molecular diagrams.

Professor K. Bharuth-Ram, Head of the Department of Physics, University of Durban-Westville, for support and encouragement.

The University of Durban-Westville for the use of the library, laboratory and computer facilities.

Finally, I am most grateful to my wife, Penelope Vijayalakshmi, for the typing of this thesis, for her patience and moral support.

ABSTRACT

The crystal structure of $\text{Ru}_3(\text{CO})_{10}(\text{C}_6\text{H}_5)_2\text{PN}(\text{C}_2\text{H}_5)\text{P}(\text{C}_6\text{H}_5)_2$ (RUCOPNP) has been determined by single crystal X-ray analysis. The crystals are triclinic with space group $\bar{P}1$. The unit cell of dimensions $a = 14,732$; $b = 12,386$; $c = 10,982 \text{ \AA}$; $\alpha = 104,52$; $\beta = 100,64$; $\gamma = 94,89^\circ$ contains two formula units. The unit cell and space group were determined by photographic deJong-Bouman and precession techniques using $\text{CuK}\alpha$ radiation. A procedure was developed for more accurate alignment of the crystal for rotating crystal techniques. Intensity data were collected on a Philips PW1100 four-circle diffractometer with $\text{MoK}\alpha$ radiation. The positions of the Ru atoms were determined from Patterson syntheses and the remaining atoms located using successive Fourier synthesis. The structure was refined by blocked full-matrix least-squares methods to a residual of $R = 0,0537$ for 3538 independent reflections with $I > 5\sigma(I)$ with 300 parameters in the final refinement. The phenyl rings and the CH_2 and CH_3 moieties were refined as rigid groups with H-atoms included at fixed positions. A difference Fourier synthesis was done and showed no significant peaks.

RUCOPNP is derived from $\text{Ru}_3(\text{CO})_{12}$ by substitution of two equatorial carbonyl ligands by the P atoms of a single edge-bridging $(\text{C}_6\text{H}_5)_2\text{PN}(\text{C}_2\text{H}_5)\text{-P}(\text{C}_6\text{H}_5)_2$ ligand (PNP). In both complexes the Ru atoms are arranged in a triangle and have distorted octahedral geometry. The introduction of the PNP ligand to the symmetrical parent $\text{Ru}_3(\text{CO})_{12}$ has the following effects: (a) It causes a contraction of the ligand-bridged Ru-Ru bond distance to $2,798 \text{ \AA}$ whereas the other Ru-Ru distances are $2,860$ and $2,848 \text{ \AA}$ which are close to the distances in the parent compound; (b) It causes the adjacent equatorial carbonyl ligands to rotate towards the PNP ligand by $11,4^\circ$. (c) It causes considerable deviations of some of the axial carbonyl ligands from the normal to the plane containing the Ru atoms.

CONTENTS

		PAGE
<u>CHAPTER ONE</u>	INTRODUCTION	1
<u>CHAPTER TWO</u>	PHOTOGRAPHIC TECHNIQUES FOR SINGLE CRYSTAL ANALYSIS BY X-RAY DIFFRACTION	3
2.1.1	X-RAY DIFFRACTION	3
2.1.2	THE RECIPROCAL LATTICE AND THE EWALD CONSTRUCTION	4
2.2.1	THE ROTATION TECHNIQUE AND THE FORMATION OF LAYER LINES	7
2.2.2	DETERMINATION OF THE LATTICE PARAMETER c	10
2.2.3	DETERMINATION OF c FROM A FLAT FILM	11
2.2.4	CRYSTAL ALIGNMENT ON THE LATTICE EXPLORER	14
2.3	THE deJONG-BOUMAN TECHNIQUE	22
2.4.1	THE BUERGER PRECESSION TECHNIQUE	27
2.4.2	BUERGER PRECESSION ALIGNMENT PHOTOGRAPHS	31
<u>CHAPTER THREE</u>	DETAILS OF APPARATUS USED	34
<u>CHAPTER FOUR</u>	DETERMINATION OF UNIT CELL CONSTANTS OF RUCOPNP	36
4.1	PHOTOGRAPHY OF THE RECIPROCAL LATTICE	36
4.2.1	BEST RECIPROCAL UNIT CELL	52
4.2.2	RECIPROCAL UNIT CELL PARAMETERS	52
4.2.3	REAL (DIRECT SPACE) UNIT CELL PARAMETERS	57
4.3	DETERMINATION OF THE NUMBER OF MOLECULES IN THE UNIT CELL	58

	PAGE
4.4	OPTIMUM THICKNESS OF CRYSTAL FOR INTENSITY MEASUREMENT 60
4.5	SUMMARY OF CRYSTAL DATA 61
<u>CHAPTER FIVE</u>	INTENSITY MEASUREMENT 62
5.1	IDENTIFICATION OF CRYSTAL HABIT 62
5.2	CHOICE OF CRYSTAL FOR INTENSITY MEASUREMENT 63
5.3	INTENSITY DATA FROM THE CSIR 64
<u>CHAPTER SIX</u>	STRUCTURE DETERMINATION - THEORY 67
6.1	RELATIONSHIP BETWEEN ELECTRON DENSITY FUNCTION AND STRUCTURE FACTORS 67
6.2	THE PHASE PROBLEM 69
6.3	THE FOURIER METHOD 69
6.4.1	THE PATTERSON SYNTHESIS 70
6.4.2	CHARACTERISTICS OF A PATTERSON VECTOR MAP 71
<u>CHAPTER SEVEN</u>	STRUCTURE DETERMINATION OF RUCOPNP 73
7.1.1	APPLICATION OF HEAVY ATOM METHOD 73
7.1.2	CALCULATION OF PATTERSON SYNTHESIS 73
7.1.3	DISTINCTION BETWEEN P_1 AND $P\bar{1}$ 74
7.1.4	IDENTIFICATION OF HEAVY ATOM PEAKS INSIDE THE MOLECULE 76
7.1.5	IDENTIFICATION OF HEAVY ATOM PEAKS BETWEEN MOLECULES 78

		PAGE
7.2.2	FOURIER SYNTHESIS - IDENTIFICATION OF ATOMS IN STRUCTURE	84
7.3	REFINEMENT OF THE STRUCTURE	93
<u>CHAPTER EIGHT</u>	DISCUSSION OF STRUCTURE	100
8.1	EFFECT OF THE LIGAND ON THE Ru_3 CORE	100
8.2	THE CO GROUPS	106
8.3	THE EQUATORIAL BOND ANGLES	107
REFERENCES		110
APPENDIX 1	ERROR CALCULATION FOR RECIPROCAL LATTICE PARAMETERS	113
APPENDIX 2	TRANSFORMATION MATRIX FROM SKEW TO ORTHOGONAL COORDINATES	121
APPENDIX 3	THE SHELX PROGRAM	124
APPENDIX 4	LIST OF OBSERVED AND CALCULATED STRUCTURE FACTORS	128

CHAPTER ONE

INTRODUCTION

The study of bridged metal-organic complexes is of interest as these compounds could serve as models for the better understanding of catalysis in processes such as the Fischer-Tropsch process being used at Sasol. Synthesis and study of complexes containing iron or ruthenium thus has potential commercial and industrial value. Various bidentate ligands have been used in such work and a new ligand $(C_6H_5)_2PN(C_2H_5)P(C_6H_5)_2$, synthesized according to a modified literature method⁽¹⁾ by Dr K.G. Moodley, is being studied in the Chemistry Department at the University of Durban-Westville.

Single crystal X-ray structure analysis is a powerful tool in such studies as the technique can provide accurate bond lengths and bond angles involved in bridged or chelated complexes and can reveal small deviations and distortions when comparing similar structures which may be of importance in understanding the catalytic processes.

Single crystals of the trinuclear ruthenium compound $Ru_3(CO)_{10}(C_6H_5)_2-PN(C_2H_5)P(C_6H_5)_2$ were prepared as follows: 0,38 g ruthenium dodecacarbonyl ($Ru_3(CO)_{12}$) (obtained from Strem Chemicals, USA) and 0,74 g of the $(C_6H_5)_2PN(C_2H_5)P(C_6H_5)_2$ ligand were placed in a 250 ml flat-bottomed flask together with a stirring bar. 100 ml of distilled cyclohexane were added to the flask. The flask was evacuated and then filled with pure dry nitrogen gas. A constant atmosphere of nitrogen was maintained over the flask which was irradiated with UV light from a sun-lamp (Philips). The solution was stirred throughout the irradiation which lasted for 7 hours. The reaction product (a red-brown solution) was filtered through

a sintered glass crucible. The solvent from the filtrate was removed on a rotary evaporator. The residual solid was dissolved in a 1:1 mixture of dichloroethane and hexane and chromatographed on a silica gel column. The solid from the main red-brown band was recrystallized from the same solvent mixture. Single crystals were obtained by cooling the mixture in a refrigerator.

Analysis of the product prior to recrystallization gave the results:

43,60% C, 2,51% H and 1,4% N; for the formula $\text{Ru}_3(\text{CO})_{10}(\text{C}_6\text{H}_5)_2\text{PN}(\text{C}_2\text{H}_5)\text{P}(\text{C}_6\text{H}_5)_2$, the expected analysis is 43,60% C, 2,63% H and 1,53% N. The spectral data (ir) indicate that the structure may be similar to that for $\text{Ru}_3(\text{CO})_{10}(\text{C}_6\text{H}_5)_2\text{PCH}_2\text{P}(\text{C}_6\text{H}_5)_2$ ⁽²⁾. The ligand in the latter compound has yielded bridged dinuclear complexes for both Fe and Ru whereas all efforts to synthesize the analogous bridged dinuclear complex with $(\text{C}_6\text{H}_5)_2\text{PN}(\text{C}_2\text{H}_5)\text{P}(\text{C}_6\text{H}_5)_2$ have to date proved fruitless. Before making further attempts to prepare bridged dinuclear species with this ligand it would be useful to compare its bonding mode with that for $(\text{C}_6\text{H}_5)_2\text{PCH}_2\text{P}(\text{C}_6\text{H}_5)_2$ which has been shown to have a propensity for bridging.

A full characterization of the trinuclear ruthenium complex prepared with the new ligand would help in the understanding of the role of the X group in ligands of the type R_2PXPR_2 in conferring bridging properties on such ligands. It was therefore decided to determine its crystal structure. The proposed molecular structure of the complex (abbreviated RUCOPNP) is shown in Fig. 1.1.

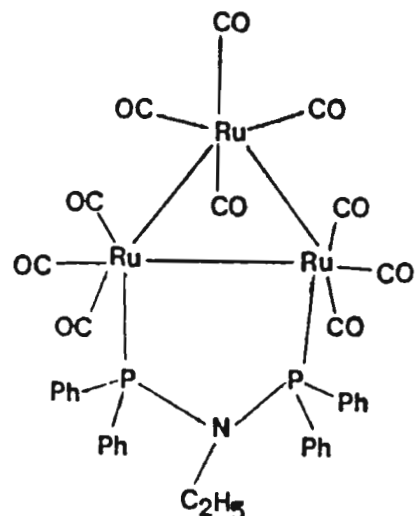


Fig. 1.1 The proposed molecular structure of RUCOPNP.

CHAPTER TWOPHOTOGRAPHIC TECHNIQUES FOR SINGLE CRYSTAL ANALYSISBY X-RAY DIFFRACTION

In this chapter the basic concepts of X-ray diffraction by crystals are explained (Section 2.1.1 and 2.1.2). The apparatus used in this study was the STOE Reciprocal Lattice Explorer⁽⁵⁾. With this apparatus photographs can be taken according to three different techniques, namely the rotation, deJong-Bouman and precession techniques. These techniques are discussed in detail in this chapter. In the case of the rotation technique the formation of layer lines of diffraction spots on a cylindrical film, and the calculation of the length of the direct axis (c) parallel to the rotation axis are discussed (Sections 2.2.1 and 2.2.2). As the Lattice Explorer has a flat film cassette the formula required to calculate the axial length is modified (Section 2.2.3). An improved method of aligning a crystal on the Lattice Explorer by X-ray methods is developed (Section 2.2.3).

2.1.1 X-RAY DIFFRACTION

X-ray diffraction may be considered as reflection from sets of planes through the points of the direct (or crystal) lattice. The direct lattice is a purely imaginary construct which functions as a co-ordinate system to which an actual crystal structure is referred. For each direct lattice, a corresponding reciprocal lattice may be postulated. It has the same symmetry as the direct lattice and is derived from it mathematically.

Reflection occurs at angles θ for which there is constructive interfer-

ence between successive planes in the lattice according to Bragg's law:

$$n\lambda = 2d \sin\theta \quad (2.1)$$

where d is the interplanar spacing and n the order of the reflection (Ref. 3, p. 22).

The planes are indexed with reference to unit lattice vectors defining the Miller indices hkl of a particular set of planes as the reciprocals of the intercepts on the three crystal axes of the plane closest to the origin (Ref. 3, p. 20).

The geometry of X-ray diffraction is most easily understood with reference to the so-called reciprocal lattice which is discussed in the next section.

2.1.2 THE RECIPROCAL LATTICE AND THE EWALD CONSTRUCTION

The reciprocal lattice is defined as follows: Choosing as the origin some lattice point in the direct lattice, normals to all the possible direct planes are constructed such that each normal terminates at a point a distance $1/d_{hkl}$ from this origin where d_{hkl} is the perpendicular distance between the hkl planes. All such points determined from this construction constitute a lattice which is called the reciprocal lattice (Ref. 3, p. 24) (abbreviated to r.l.). The unit vectors of the direct lattice are designated by a , b and c and those of the reciprocal lattice by a^* , b^* and c^* .

The relation between the direct lattice and the reciprocal lattice for a monoclinic system is shown in Fig. 2.1.

The direct lattice, identified by solid circles, is oriented in this diagram with the b -axis normal to the page; hence all $h0l$ planes are

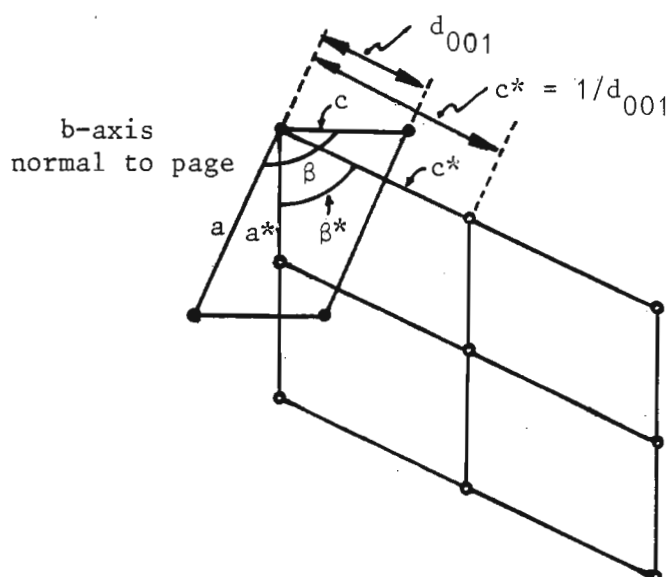


Fig. 2.1 Relationship between direct and reciprocal lattice. Parameters with asterisks refer to the reciprocal lattice.

also normal to the page. Each set of planes of the direct lattice is represented by a point (open circle) in the reciprocal lattice.

The relationship between the unit vectors in the direct lattice \underline{a} , \underline{b} , \underline{c} and those in the reciprocal lattice \underline{a}^* , \underline{b}^* , \underline{c}^* are as follows:

$$\underline{a}^* = \frac{\underline{b} \times \underline{c}}{V}, \quad \underline{b}^* = \frac{\underline{c} \times \underline{a}}{V}, \quad \underline{c}^* = \frac{\underline{a} \times \underline{b}}{V} \quad (2.2)$$

where $V = \underline{a} \cdot \underline{b} \times \underline{c}$ is the volume of the unit cell.

From this definition it can be seen that

\underline{a}^* is perpendicular to \underline{b} and \underline{c}
 \underline{b}^* " " " \underline{c} " \underline{a}
 \underline{c}^* " " " \underline{a} " \underline{b} .

Conversely,

\underline{a} is perpendicular to \underline{b}^* and \underline{c}^*
 \underline{b} " " " \underline{c}^* " \underline{a}^*
 \underline{c} " " " \underline{a}^* " \underline{b}^* .

This means that, in general, any direct axis has a family of r.l. planes

perpendicular to it, each plane containing points of constant value for the index associated with that axis.

The reciprocal lattice construction makes possible the interpretation of Bragg's law which is very useful in practice. In Fig. 2.2a a section of a reciprocal lattice plane of the crystal is shown. X-rays of wavelength λ are assumed to be parallel to this plane. XO defines the direction of the primary beam with O the origin of the r.l. Now a circle passing through O of radius $1/\lambda$ is constructed with centre C located on the direct beam.

For a r.l. point lying on this circle, the angle \widehat{OPB} is a right angle (angle is a semicircle). Therefore

$$\sin(\widehat{OBP}) = \sin \theta = \frac{OP}{OB} = \frac{1/d_{hkl}}{2 \cdot 1/\lambda}$$

since the length of the r.l. vector OP is $1/d_{hkl}$.

Therefore

$$\lambda = 2d \sin \theta. \quad (2.1)$$

which is Bragg's law with $n = 1$ and θ is the Bragg angle.

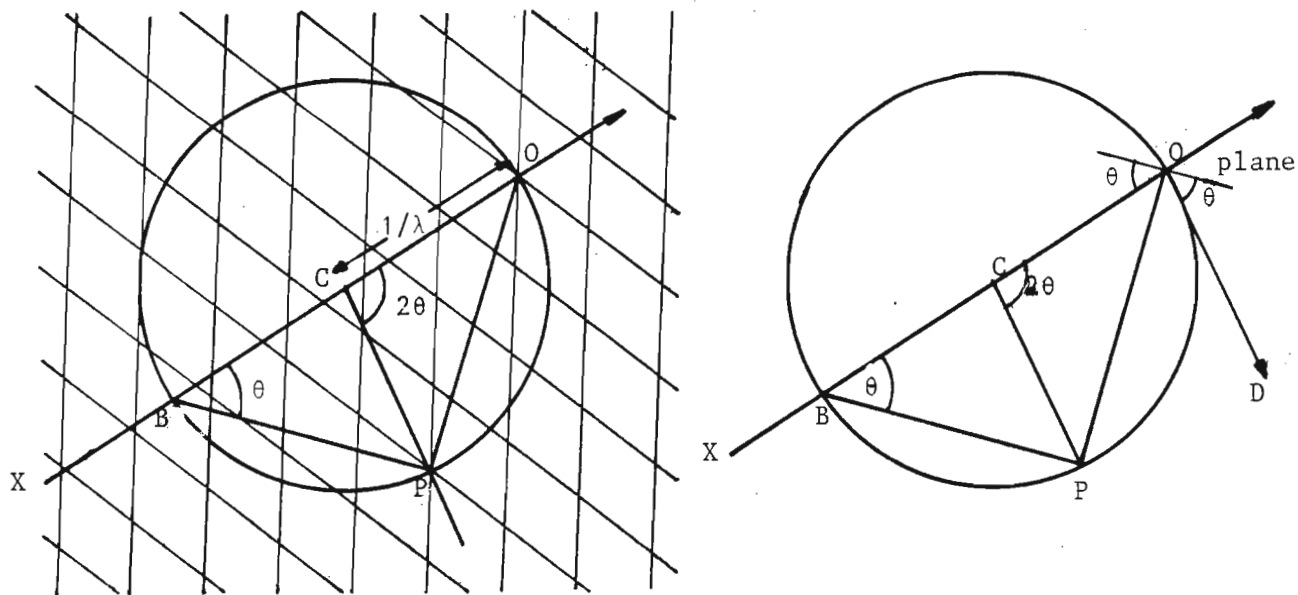


Fig. 2.2a The Ewald construction. Fig. 2.2b The direct plane.
(Ref. 3, p. 32, Fig. 2.21a, b).

BP is parallel to the real plane because it is perpendicular to the r.l. vector OP, and BP makes an angle θ with the direct beam. The diffracted beam makes angle 2θ with the direct beam (angle at B is twice angle at centre, both subtended by OP). Therefore CP is in the direction of the diffracted beam. Fig. 2.2b shows the real plane and the diffracted beam at O.

When the circle is rotated about the diameter OB the sphere that is generated is called the Ewald sphere. Any r.l. point lying on this sphere will give rise to a reflection. When the crystal (with its reciprocal lattice) is rotated, many r.l. points pass through the Ewald sphere and the corresponding reflections are observed.

Several techniques of photography of the reciprocal lattice are based on a rotating motion of the crystal. 1) Photographs taken with a stationary film are called rotation photographs or oscillation photographs if the crystal oscillates through a small angle. 2) The deJong-Bouman technique provides an undistorted image of a r.l. plane perpendicular to the rotation axis and roughly parallel to the X-ray beam. The film rotates synchronously with the crystal. 3) In the Weissenberg technique the motion of the film is a translation parallel to the rotation axis and a distorted image of the same r.l. plane as in 2) is obtained. This technique has not been used in this investigation. 4) The commonly used precession technique of Buerger is based on a precession motion of the crystal and the film. This technique produces undistorted images of r.l. planes perpendicular to the X-ray beam.

2.2.1 THE FORMATION OF LAYER LINES

The discussion in this section is based on descriptions found in standard texts^(3, 4) on X-ray crystallography.

To take oscillation or rotation photographs, a beam of characteristic X-rays is directed at 90° to the chosen axis, say \underline{c} , which has been aligned parallel to the rotation axis of the camera.

Fig. 2.3 shows the relation between the X-ray beam direction and the rotating crystal axis through O at the centre of the Ewald sphere (Ref. 4, p. 284).

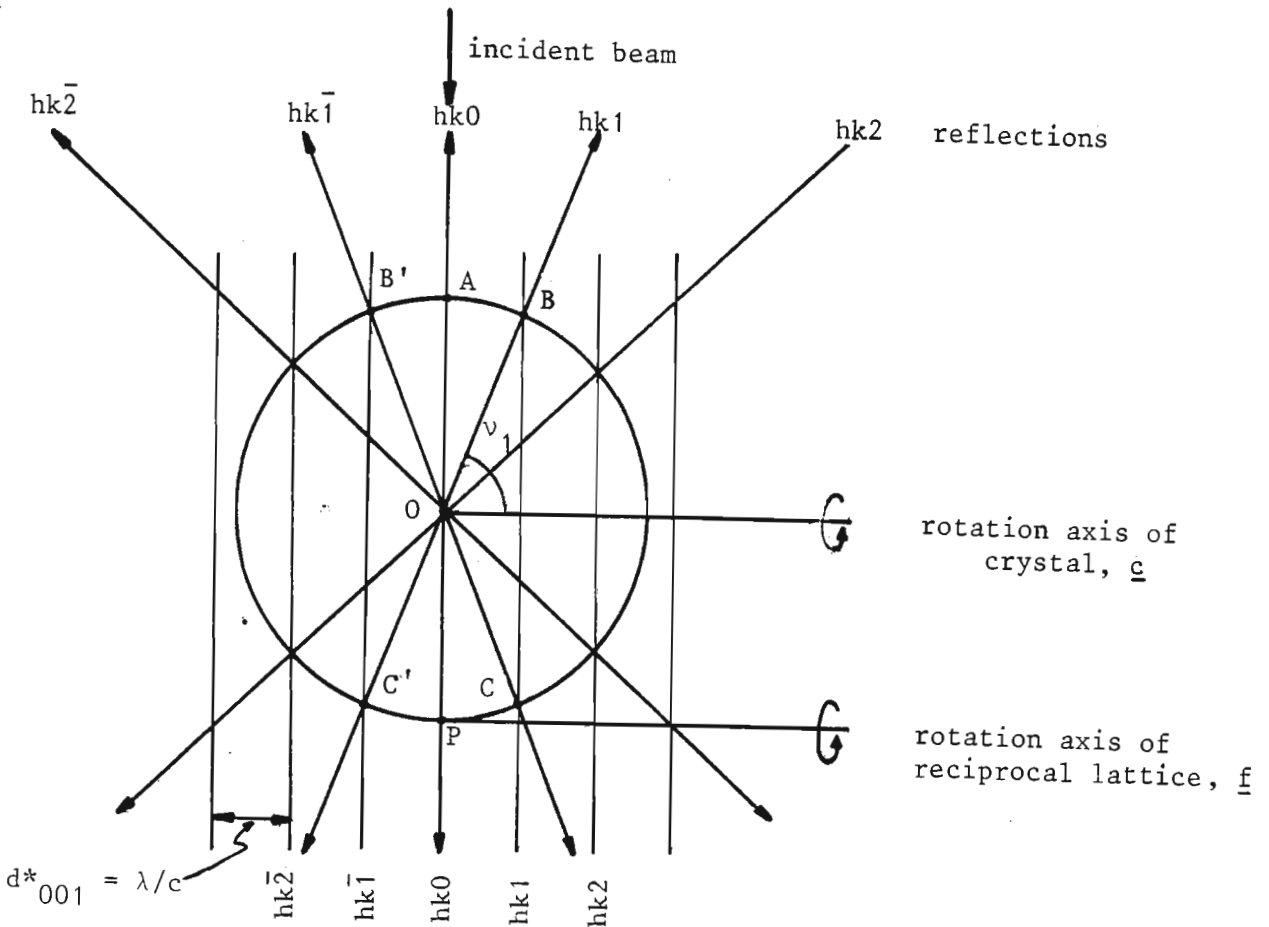


Fig. 2.3 A section through the Ewald sphere showing r.l. planes and associated Laue cones for a crystal rotating about the \underline{c} -axis (Ref. 4, p. 284, Fig. 10-2).

The undeviated beam emerges from the sphere at P , and consequently this point marks the origin of the reciprocal lattice. The reciprocal planes which are normal to the \underline{c} -axis and consist respectively of $hk0$, $hk1$, and $hk2$, points, simultaneously rotate about a parallel axis through P . (The planes are spaced at intervals $d^*_{001} = \lambda/c$).

During the rotation, the $hk0$ reciprocal points pass through the surface of the sphere whose trace is AP and as they touch the Ewald sphere, Bragg's condition for reflection is satisfied (Ref. 3, p. 32). The corresponding $hk0$ reflections emanate from O and lie in the plane of this circle, that is, on the surface of a "flat-cone". The $hk1$ and $hk\bar{1}$ reciprocal planes cut the Ewald sphere in circles whose traces are respectively BC and B'C'. The corresponding $hk1$ and $hk\bar{1}$ reflections are lines in symmetrical Laue cones, coaxial with the rotation axis, and characterised by the half-apex angle ν_1 . Similarly, the $hk2$ and $hk\bar{2}$, and other reciprocal planes which happen to cut the sphere, result in pairs of symmetrical Laue cones, also coaxial with the rotation axis, but with smaller half-apex angles.

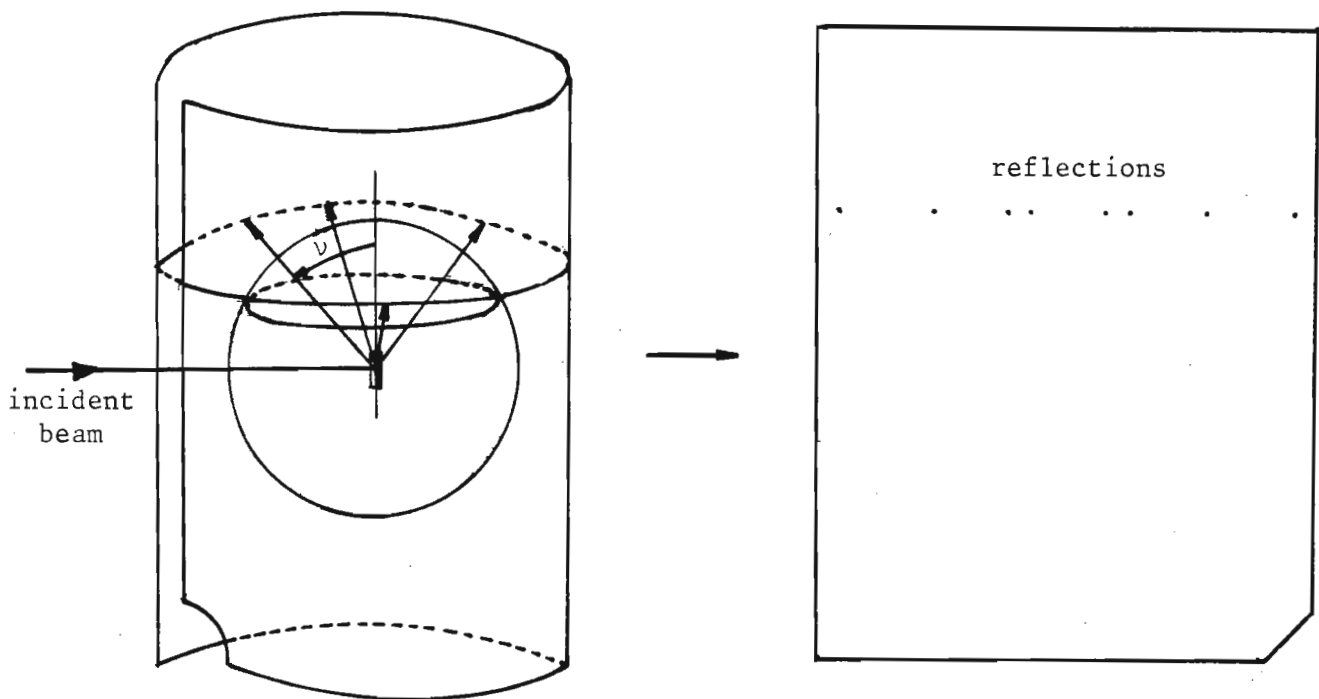


Fig. 2.4 The Laue cones and formation of reflections on a cylindrical film (Ref. 3, p. 85, Fig. 5.6).

The reflected rays from the r.l. lie on cones. If a cylindrical film is now placed around the crystal (which is assumed to be at the centre of the Ewald sphere) then these cones will intersect the film in a circle of points all of which will be at the same height. When the film is

unrolled, the diffraction spots will lie on a straight line as is shown in Fig. 2.4.

2.2.2 DETERMINATION OF THE LATTICE PARAMETER c

Fig. 2.5 shows a section through the cylindrical film, parallel to and including the rotation axis. The half-apex angle ν of a diffraction cone depends on the spacing of the reciprocal planes.

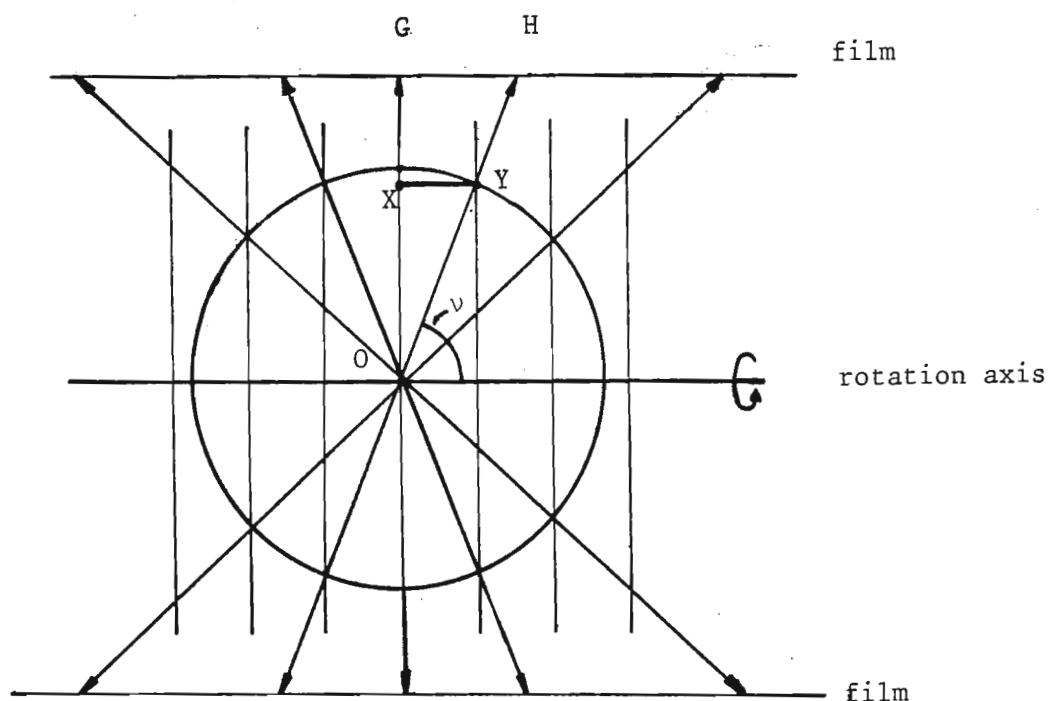


Fig. 2.5 Relationships between a film measurement and the cone angle ν on a rotation photograph (Ref. 4, p. 286, Fig. 10-5).

The spacings between the planes are equal, and the spacing between the zero layer and the n^{th} layer is $n \cdot \frac{1}{c}$.

For the n^{th} order diffraction cone

$$\cos \nu_n = \frac{n \cdot \frac{1}{c}}{OY} = \frac{n \cdot \frac{1}{c}}{1/\lambda} = n \cdot \frac{\lambda}{c}$$

$$\text{Hence } c = \frac{n\lambda}{\cos \nu_n} \quad (2.3)'$$

The angle ν is determined from measurements on the film. $\Delta OGH \equiv \Delta OXY$, OG is the radius R of the camera and GH is the distance y between the zero and first layers as measured on the film. Generalizing, for the n^{th} layer

$$\tan \nu_n = \frac{R}{y_n}, \quad \text{and}$$

$$c = n \frac{\lambda}{\cos(\tan^{-1} \frac{R}{y_n})} \quad (2.3)''$$

2.2.3 DETERMINATION OF c FROM A FLAT FILM

The STOE Reciprocal Lattice Explorer⁽⁵⁾ makes use of flat films rather than cylindrical films. The resulting lines of diffracting spots (layer lines) from rotation photographs will not be parallel straight lines but will be curved away from the centre on either side of the straight zero layer line as in Fig. 2.6.

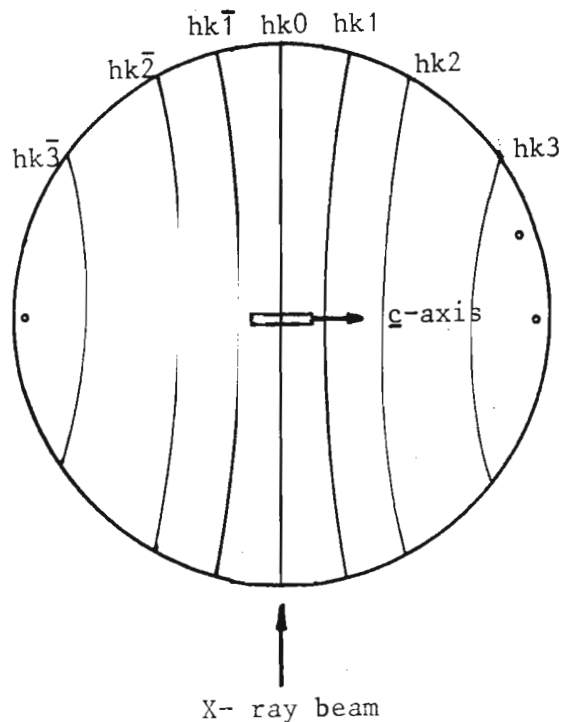


Fig. 2.6 Appearance of layer lines on a flat film from rotation photography.

The explanation for this is as follows. For any set of n^{th} layer reflections the half-apex angle ψ is the same for each reflection. If a cylindrical film of radius R is now placed around the crystal, with the crystal on its axis, then the distance travelled by each n^{th} layer reflected ray to reach the film is the same. For a flat film placed a distance R from the crystal, the distance travelled (by each reflected ray of the n^{th} layer) is not constant. Compare A, B, C, D on cylindrical film with A', B', C', D' respectively on flat film in Fig. 2.7.

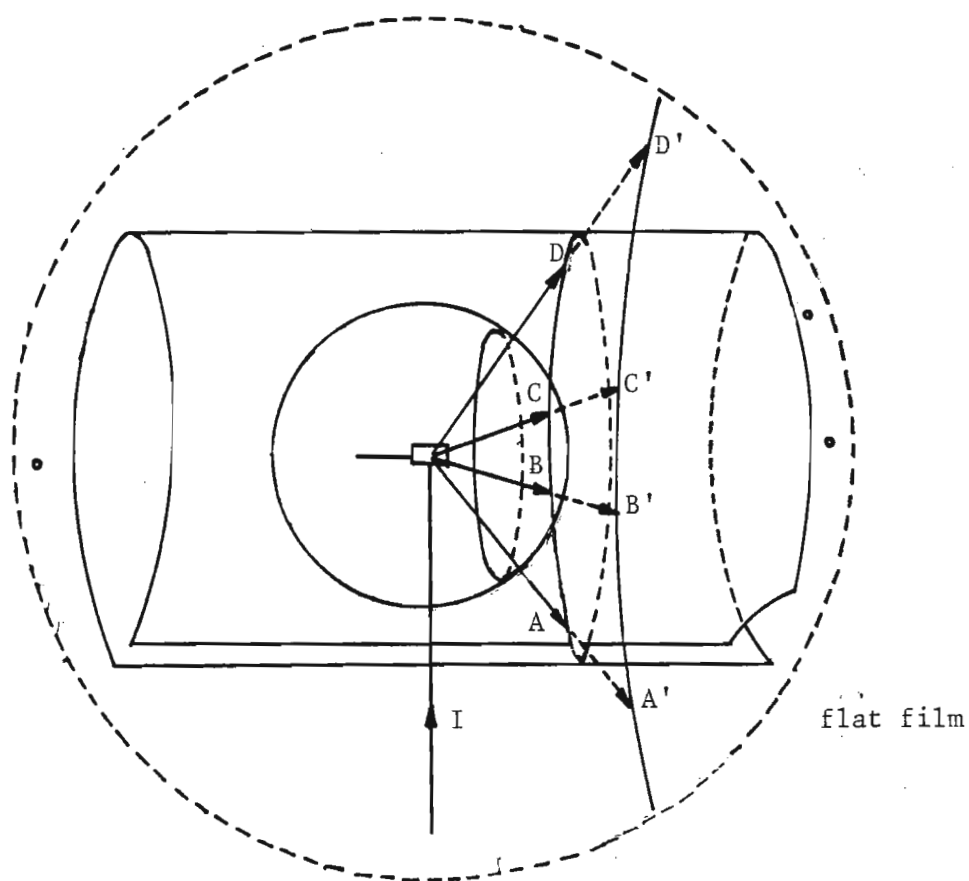


Fig. 2.7 Comparison of reflections seen on flat and cylindrical films from rotation photographs.

Fig. 2.8 shows the position of the crystal and film looking down the incident X-ray beam ($CO = R = 60,00 \text{ mm}$). O, P, T and Q are points on the film. OP lies on the zero layer line. T is the point of intersection of

Since the rotation photograph is symmetric about the zero layer line, y_n can be determined by measuring $2X$, $2Y$ and using equation (2.5). With this value of y_n , c can be calculated from equation (2.3)" as for a cylindrical film.

2.2.4 CRYSTAL ALIGNMENT ON THE LATTICE EXPLORER

An improved method of aligning a crystal axis with the rotation axis of the STOE Reciprocal Lattice Explorer by X-ray methods is developed in this section.

Two alignment methods are discussed by Stout and Jensen (Ref. 3, p. 92). According to Method 1 the angle between the two zero layer lines at the centre of a double exposure oscillation photograph gives the corrections to be made on the vertical goniometer arc. This method is also recommended in the instruction manual for the Lattice Explorer, but is not very accurate (Fig. 2.9). The reason for this is that for small misalignment angles the lines are not resolved except near the edge of the film where the curvature of the lines makes direct measurement of an angle impossible.

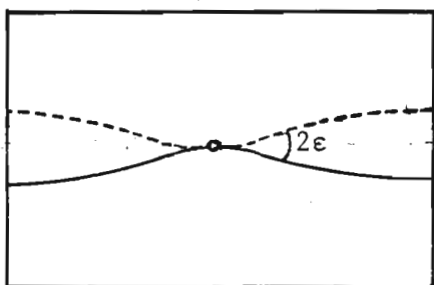


Fig. 2.9a Zero-layer trace on film resulting from error in plane A only i.e. bow error.

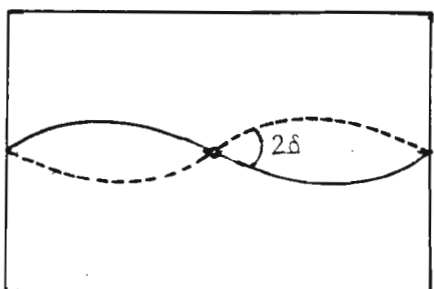


Fig. 2.9b Zero-layer trace on film resulting from error in plane B only i.e. tilt error.

The second method is that due to Weisz and Cole⁽⁶⁾. They use a formula of Hendershot⁽⁷⁾ for calculation of goniometer corrections from separations Δr and $\Delta \ell$ on a double exposure film. (In a double exposure photograph two exposures are taken on the same film with one of the goniometer arcs vertical. After the first exposure is taken, the goniometer is rotated through 180° and the second exposure is taken for a shorter time than the first in order to distinguish the one from the other). The separations are measured at $2\theta = 90^\circ$ (Fig. 2.10). If the crystal is nearly aligned the two lines overlap, and in order to make accurate measurements the film is displaced a known amount between exposures.

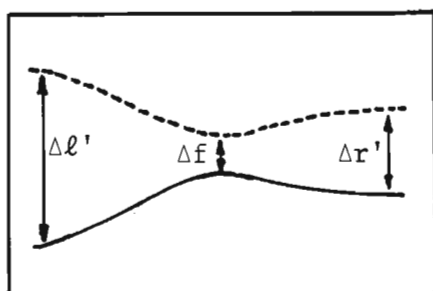
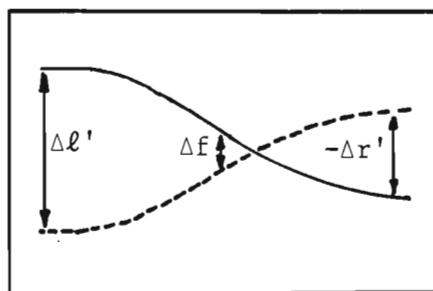


Fig. 2.10a, b Appearance of zero-layer lines on double oscillation photographs of a misaligned crystal (Ref. 3, p. 93, Fig. 5.14).

The sign convention is illustrated for two cases:

- a) $\Delta \ell'$ and $\Delta r'$ have the same sign
- b) $\Delta \ell'$ and $\Delta r'$ have opposite sign.



$$\text{Errors } \Delta r = \Delta r' - \Delta f$$

$$\Delta \ell = \Delta \ell' - \Delta f$$

Corrections ($^\circ$):

$$\text{tilt error} = \left| \frac{\Delta r - \Delta \ell}{2} \right|$$

$$\text{bow error} = \left| \frac{\Delta r + \Delta \ell}{2} \right|$$

However, the facility which enables the film to be displaced is available on a Weissenberg camera but not on the Lattice Explorer. Moreover for a flat film, measurement at $2\theta = 90^\circ$ is not possible (max. possible 2θ is 45°) and the film-crystal distance is a variable factor R' . The method of Weisz and Cole has to be looked at more carefully if a crystal has to be orientated for rotation photographs or deJong-Bouman photographs, i.e. with a real lattice vector parallel to the rotation axis on the Lattice Explorer. For precession photographs (real axis \parallel to X-ray beam) the normal orientation procedures are quite satisfactory.

In the method described below, the line separation $2Y$ is considered as a function of missetting angles ϵ (or δ) and 2θ values.

$$Y = f[\epsilon(\text{or } \delta), 2\theta(\text{or } x)] \quad (2.6)$$

where x is the distance along the zero layer line, and ϵ or δ , the correction angles on the goniometer.

In order to derive the misalignment formulae, a missetting is first considered of the arc which tilts the crystal towards the X-ray beam (bow error), i.e. a setting error in plane A (Fig. 2.11) with the horizontal arc misset an angle ϵ . The situation is illustrated in Figs. 2.12a, b and c.

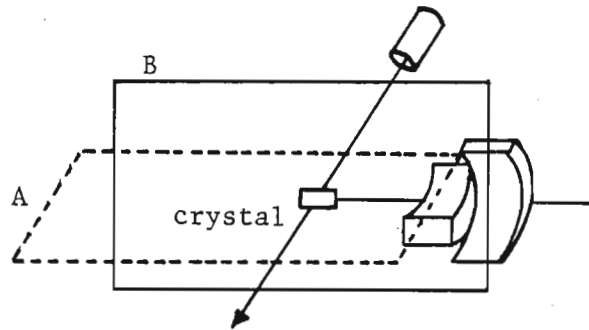


Fig. 2.11 Planes A and B in relation to X-ray beam (Ref. 3, p. 91, Fig. 5.12).

In Fig. 2.12a CO is the primary beam and OX the zero layer reciprocal lattice plane tilted at angle ϵ . CP is the reflected ray which leaves the Ewald sphere y reciprocal units below the horizontal plane, and makes an angle α with the horizontal.

From Fig. 2.12b $\sin \alpha = \frac{y}{r}$ r - radius of Ewald sphere.

From Fig, 2.12c $p = r(1 - \cos 2\theta)$ 2θ - Bragg angle

From Fig. 2.12a $\frac{y}{p} = \tan \epsilon$.

Therefore $\frac{y}{r} = \frac{y}{p} \cdot \frac{p}{r} = (1 - \cos 2\theta) \tan \epsilon$

From Fig. 2.13 $\frac{Y}{R'} = \frac{y}{r}$,

where $2Y$ is the distance between zero layer lines on the film and R' is

Fig. 2.12
(a) Plan

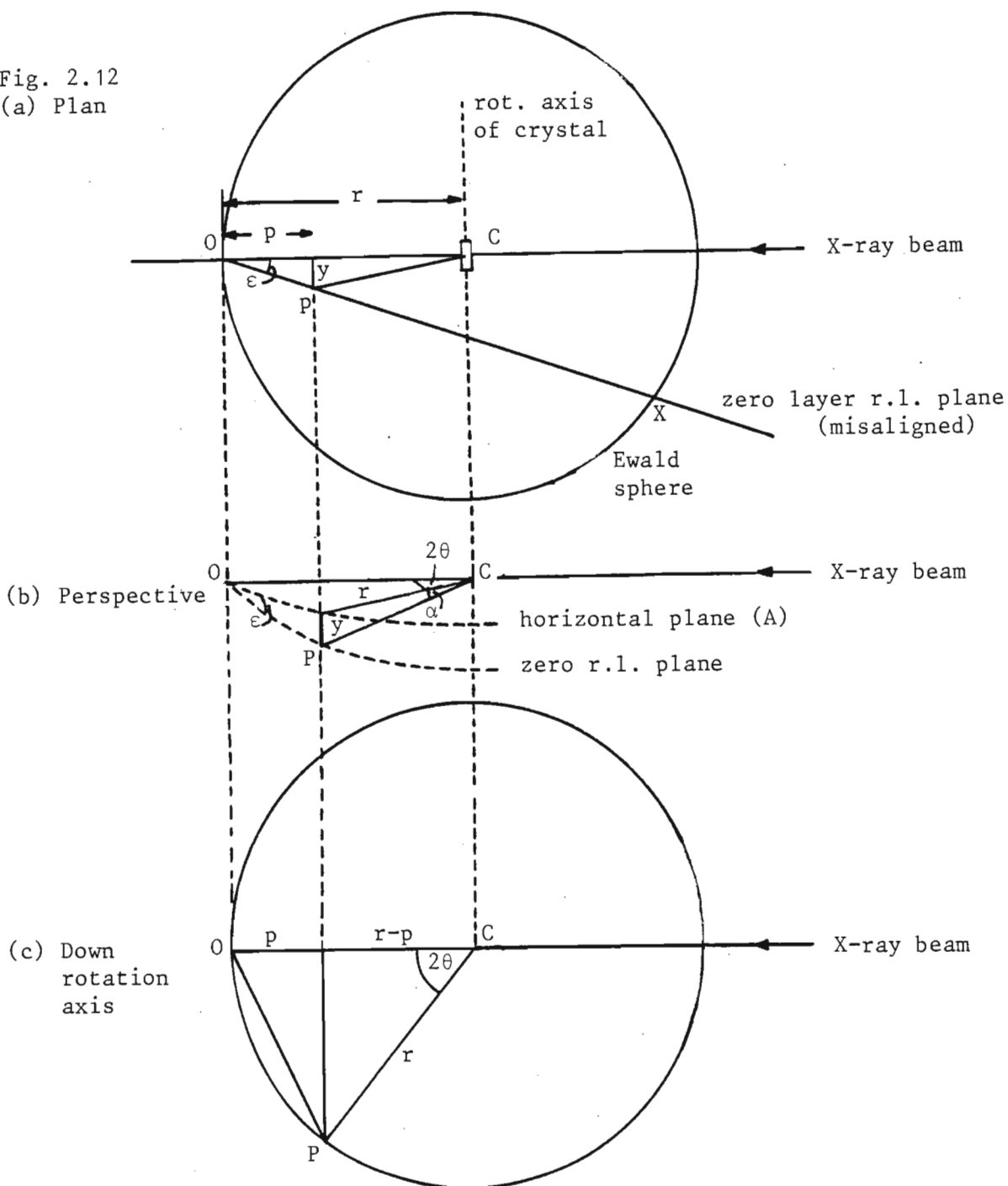


Fig. 2.12(a) A section through the Ewald sphere centre C viewed perpendicular to plane A (plan view). This plane contains the X-ray beam and the horizontal arc of the goniometer. The zero layer r.l. plane which is misaligned by angle ϵ (bow-error) passes through O and is perpendicular to the plane of the paper.

(b) Perspective view.

(c) View along rotation axis of crystal.

the crystal-film distance.

Thus

$$\frac{Y}{R'} = \frac{y}{r} = (1 - \cos 2\theta) \tan \epsilon$$

$$\text{i.e.} \quad Y = R'(1 - \cos 2\theta) \tan \epsilon \quad (2.7)$$

If R is the film-crystal distance for $2\theta = 0$, then $R' = R/\cos 2\theta$.

The relationship between R and R' is shown in Fig. 2.14.

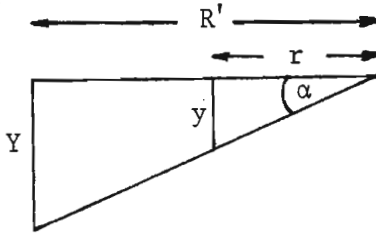


Fig. 2.13 Relationship between Y and y .

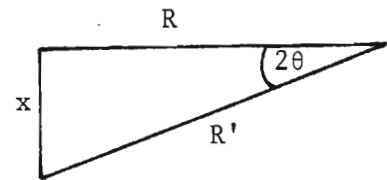


Fig. 2.14 Relationship between R and R' .

Next consider a missetting of vertical arc which tilts the crystal through an angle δ w.r.t. the X-ray beam (tilt), i.e. a setting error in plane B. The situation is illustrated in Figs. 2.15a, b and c.

$$\text{Here} \quad \frac{p}{r} = \sin 2\theta \quad \text{and} \quad \frac{y}{p} = \tan \delta.$$

$$\text{Therefore} \quad \frac{Y}{R'} = \frac{y}{r} = \frac{y}{p} \cdot \frac{p}{r} = \sin 2\theta \tan \delta$$

$$\text{i.e.} \quad Y = R' \sin 2\theta \tan \delta. \quad (2.8)$$

The results can be summarized as follows:

$$Y_1 = R' (1 - \cos 2\theta) \tan \epsilon \quad (2.7)$$

$$Y_2 = R' \sin 2\theta \tan \delta \quad (2.8)$$

where ϵ = bow missetting (in horizontal arc)

δ = tilt missetting (in vertical arc)

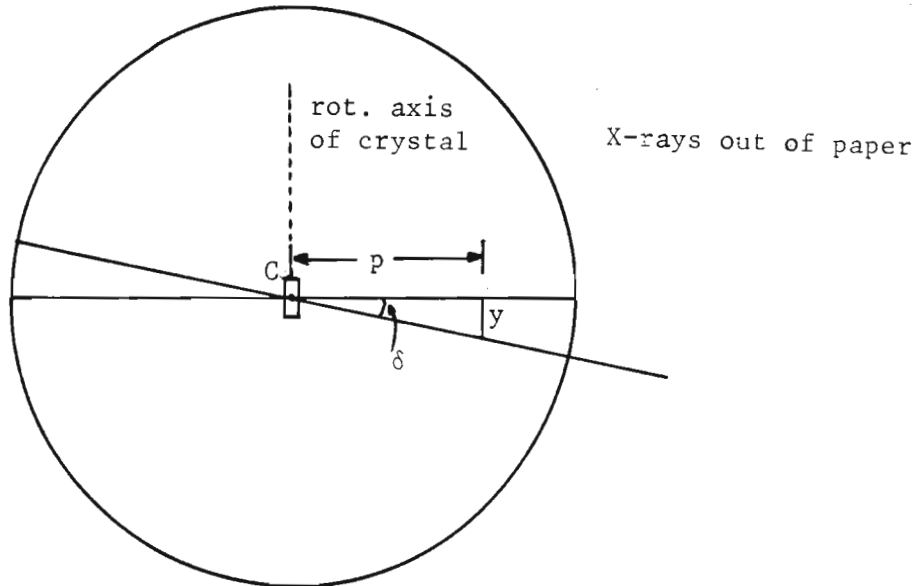
R' = crystal-film distance

Y_1 = half-distance between lines of spots

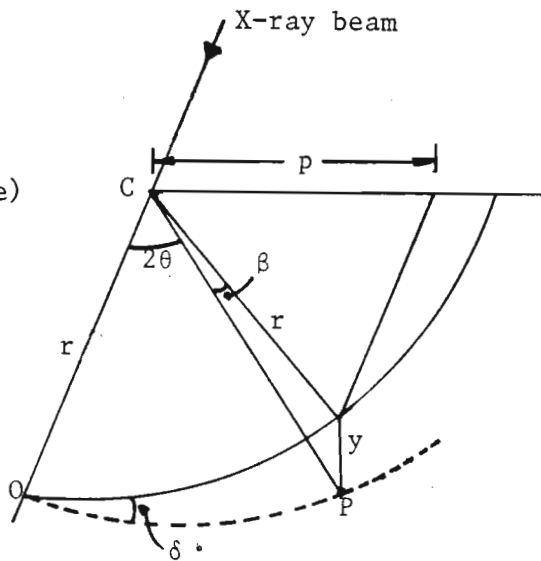
for bow missetting only

Fig. 2.15

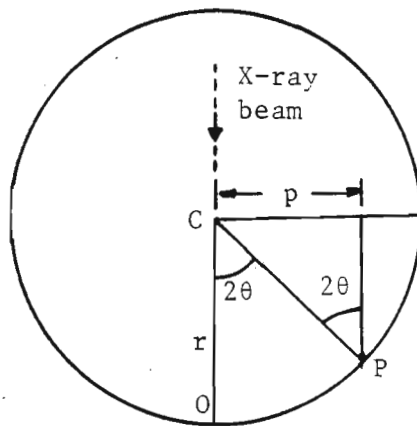
(a) Plan



(b) (Perspective)



(c) Down rotation axis



- Fig. 2.15(a) A section through the centre of the Ewald sphere perpendicular to the plane B (see Fig. 2.11). The X-rays emerge out of the paper. The zero-level r.l. plane is misaligned by angle δ , a setting error in plane B (tilt error).
- (b) Perspective view.
- (c) View down rotation axis.

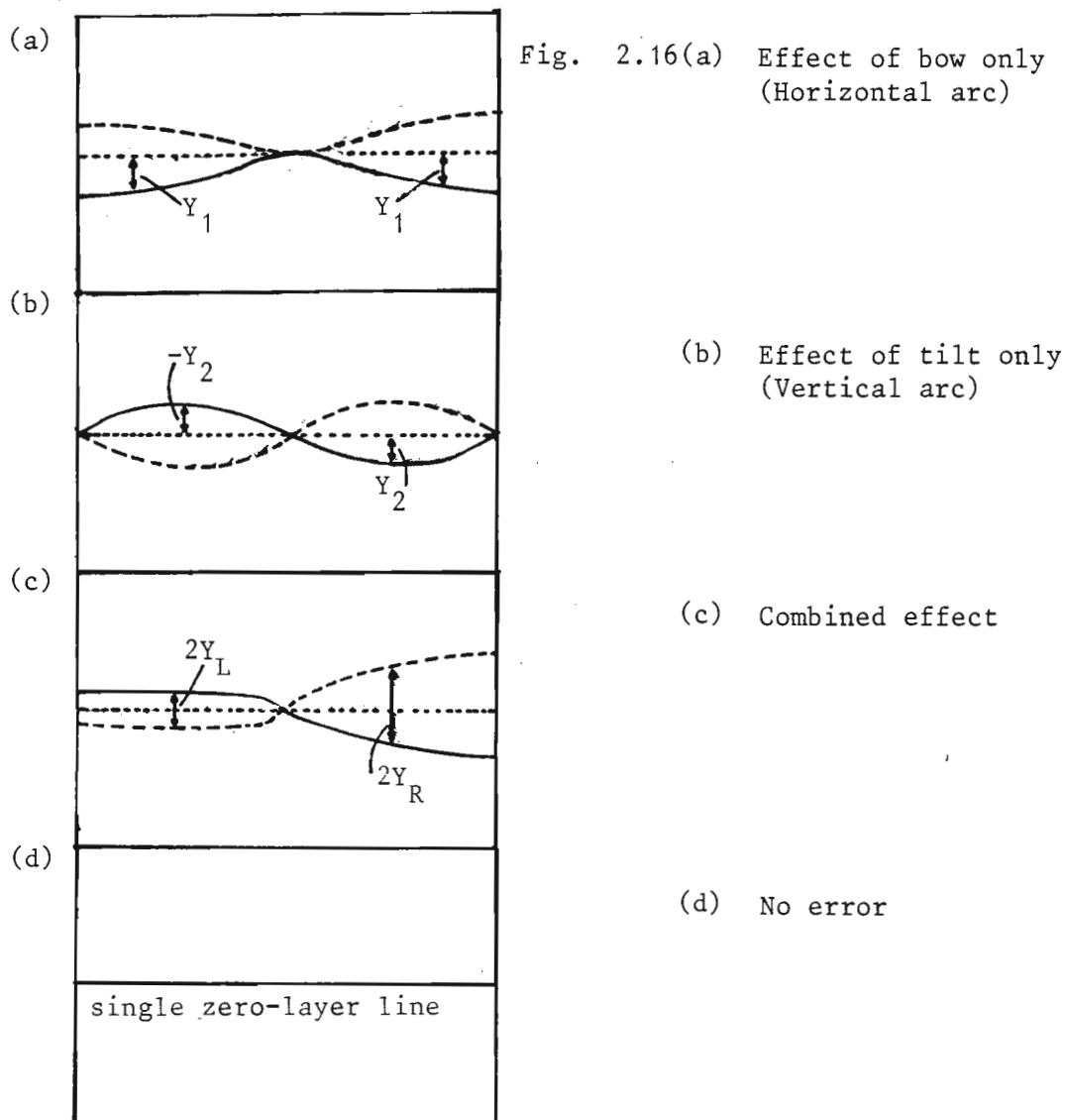
Y_2 = half-distance between lines of spots
for tilt missetting only.

$$R' = \frac{R}{\cos(\arctan x/R)} \quad (2.9)$$

where R = shortest crystal-film distance
 x = distance along zero-layer line
at which Y_1 or Y_2 are measured

and $\frac{x}{R} = \tan 2\theta$.

In the practical case both arcs are misset and the displacement Y depends on both ϵ and δ . These effects are shown in Fig. 2.16.



It can be seen that on one side of the film (say the right side) the displacements add while on the other they tend to neutralize each other:

$$Y_1 + Y_2 = Y_R \quad (2.10)$$

$$Y_1 - Y_2 = Y_L$$

where

Y_R = larger (additive) separation of the two
zero layer lines

Y_L = smaller (subtractive) separation of the
two zero layer lines

Solving these two equations gives

$$\begin{aligned} \tan \epsilon &= \frac{Y_R + Y_L}{2R'(1 - \cos 2\theta)} \\ \tan \delta &= \frac{Y_R - Y_L}{2R' \sin 2\theta} \end{aligned} \quad (2.11)$$

By measuring Y_R and Y_L and x on the film, the correction angles ϵ and δ can be determined using equation (2.11).

When the two layer lines cross Y_R and Y_L have opposite sign; if not they have the same sign. For convenience Y_R is always taken positive and the direction of adjustment is determined by inspection.

Equations (2.10) hold only when the displacements Y_R and Y_L are measurable. When $Y_L = 0$ i.e. the combined effect of bow and tilt error cancel each other out and the zero layer appears as a single line, it may be that there is a finite separation between the lines but that it is not measurable as the lines are not resolved. In that case the following alternate method is used to determine the correction angles:

Two double exposure photographs are taken at 90° to each other. The larger i.e. non-zero separations (Y_R and Y'_R respectively) on each of the films are then used to calculate the corrections to be made on the goniometer arcs. Assuming that $Y_L = Y_1 - Y_2 \neq 0$, i.e. the error due to bow \neq error due to tilt, the following relations hold:

$$\begin{aligned} Y_1 + Y_2 &= Y_R \\ Y'_1 + Y'_2 &= Y'_R \end{aligned} \quad (2.12)$$

(Primed quantities refer to corresponding values on film when the crystal is rotated through 90°).

Let s and ℓ be the corrections to be made on the small and large arcs respectively. Then equations (2.7), (2.8) and (2.10) become

$$\begin{aligned} Y_1 &= R' (1 - \cos 2\theta) \tan s \\ Y_2 &= R' \sin 2\theta \tan \ell \\ Y'_1 &= R' (1 - \cos 2\theta) \tan \ell \\ Y'_2 &= R' \sin 2\theta \tan s \end{aligned} \quad (2.13)$$

Let

$$\begin{aligned} A &= R' (1 - \cos 2\theta) \\ B &= R' \sin 2\theta \end{aligned}$$

From equations (2.12) and (2.13)

$$\begin{aligned} \tan \ell &= \frac{BY_R - AY'_R}{B^2 - A^2} \\ \tan s &= \frac{BY'_R - AY_R}{B^2 - A^2} \end{aligned} \quad (2.14)$$

(The correction angles s and ℓ are thus determined from the resolved separations Y_R and Y'_R , without requiring the inaccurate (unresolved) Y_L and Y'_L).

2.3 THE deJONG-BOUMAN TECHNIQUE

The discussion in this section is based on descriptions found in the book by P. Luger: *Modern X-ray Analysis on Single Crystals* (Ref. 8, p. 66-71).

Fig. 2.3 (Section 2.2.1) shows the experimental conditions for the formation of layer lines. The vector \underline{c} is aligned perpendicular to the primary beam and the crystal rotates about this vector. With this set-up the $r.l.$ layers $hk0$, $hk1$, etc., remain in the same plane during rotation and give rise to reflections on the Laue cones. The intersection of the Laue cones

with a cylindrical film when unrolled give rise to a set of straight lines (oscillation technique).

Now if a planar film is placed parallel to the reciprocal lattice layers (Fig. 2.3) and rotated about an axis parallel to the crystal rotation axis and synchronous with the crystal, an undistorted diffraction pattern is registered on the film. A circular screen of the correct size to allow only the Laue cones of one particular layer to pass through has also to be inserted between the crystal and the film. This is the concept of the deJong-Bouman technique. This technique is realized in a slightly different way in practice because with the experimental set up of Fig. 2.3 i.e. with the primary beam parallel to the r.l. layers, it would be impossible to photograph the zero layer as the primary beam would travel in the plane of the film.

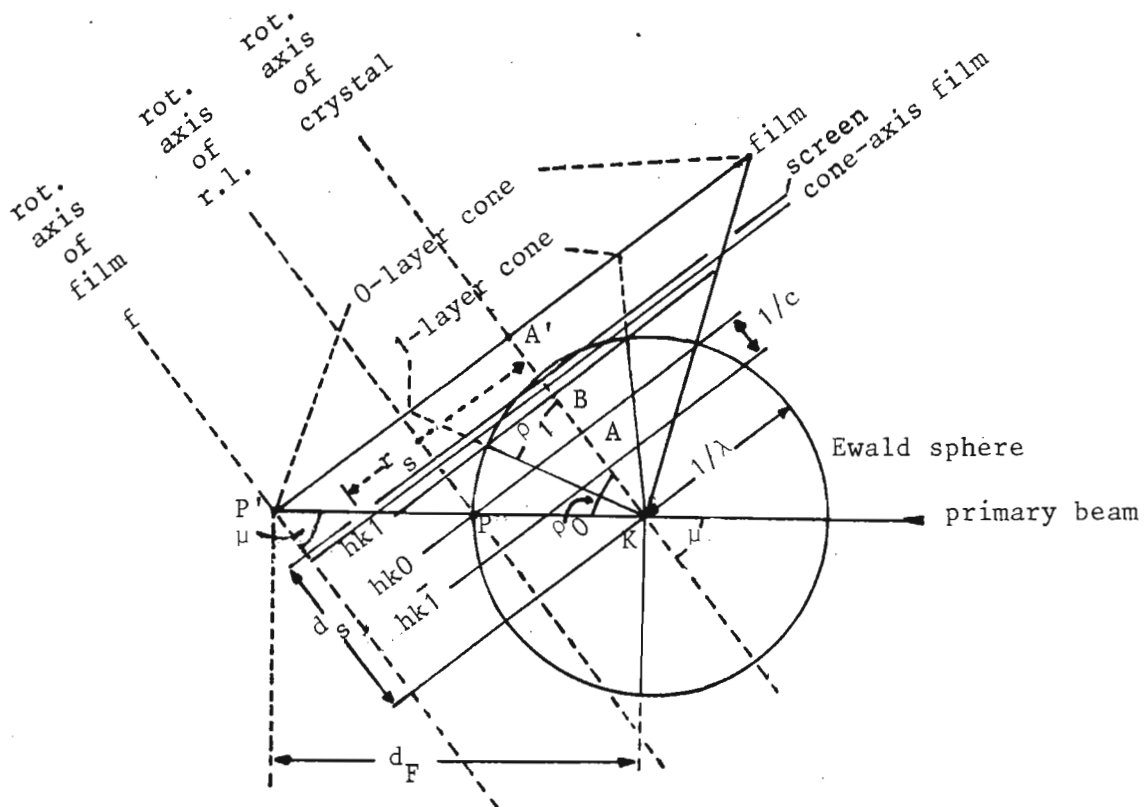


Fig. 2.17 deJong-Bouman geometry, zero layer. (Ref. 8, p. 67, Fig. 2.11).

Fig. 2.17 illustrates the arrangement for the deJong-Bouman technique. The crystal rotation axis is inclined at an angle μ ($\neq 90^\circ$) with respect to the primary beam. The angles subtended by the Laue cones are designated $2\rho_0, 2\rho_1, \dots$. The cone angle for the zero layer is $2\rho_0 = \mu$. The axis \underline{f} about which the film is rotated is parallel to the crystal rotation axis. In order to photograph the zero layer a screen with an annular opening of radius r_s is placed between the film cassette and the crystal at a distance d_s from the crystal given by

$$d_s = \frac{r_s}{\tan \rho_0} \quad (2.15)$$

Now with the crystal and film rotating synchronously, an undistorted image of the zero layer will appear on the film.

The magnification is obtained by comparing similar triangles, KAP and KA'P':

$$\frac{A'P'}{AP} = \frac{KP'}{KP}$$

i.e. $\frac{x}{d^*} = \frac{d_F}{1/\lambda}$,

so that $\frac{1}{d^*} = \frac{d_F \lambda}{x} \text{ (\AA)} \quad (2.16)$

x - distance from centre of film to a particular reflection (in mm)

d^* - " " origin of r.l. " " " r.l. point on zero layer (in \AA^{-1})

d_F - crystal to film distance

$1/\lambda$ - radius of Ewald sphere

All the Laue cones shown in Fig. 2.17 may be photographed together by placing a stationary film between the screen and the crystal. An exposure of this type is called a "cone-axis exposure" and the cones appear as circles on the film. The lattice constant c in the rotation direction can now be determined.

From Fig. 2.17

$$\frac{(AK)}{1/\lambda} = \cos \rho_0$$

$$\frac{BK}{1/\lambda} = \cos \rho_1$$

$$\text{Then } \frac{1}{c} = BK - AK = \frac{\cos \rho_1}{\lambda} - \frac{\cos \rho_0}{\lambda}$$

$$\text{or } \frac{1}{c} = \frac{\cos \rho_1}{\lambda} - \frac{\cos \mu}{\lambda}$$

And in general

$$\frac{n}{c} = \frac{\cos \rho_n}{\lambda} - \frac{\cos \mu}{\lambda} \quad (2.17)$$

Let r_0 and r_1 be the radii of the zero and first layer circle on the cone-axis photograph. Then

$$\tan \rho_i = \frac{r_i}{\Delta} \quad i = 0, 1$$

(Δ is the film to crystal distance)

From the experimental condition

$$\Delta = r_0 / \tan \rho_0$$

and

$$\tan \rho_1 = r_1 / \Delta = \frac{r_1}{r_0} \tan \rho_0 \quad (2.18)$$

By measuring r_0 and r_1 on the cone-axis photograph and using the experimental value for $\rho_0 = \mu$, ρ_1 may be obtained from (2.18). Then $1/c$ and hence c may be obtained from (2.17).

In order to photograph the first and higher layers it appears that the only modification of the experimental arrangement is a changing of the screen radius to let through the desired layer. But as the cone angle $2\rho_1$ for the first layer is not the same as $2\rho_0$ the magnification of the two layers are quite different from each other. The same magnification can be obtained for each layer if equal cone angles

r.l. the film has to be displaced by a shift t_1 , away from the crystal given by

$$t_1 = \frac{\lambda d_F}{c} \quad (2.20)$$

As the same cone angle is used the position of the annular screen remains the same for higher layer deJong-Bouman photographs once d_s is calculated from (2.15). For practical reasons the manufacturer of the Lattice Explorer recommends a cone angle of 45° for the zero layer with the screen support located in a fixed position with respect to the crystal.

2.4.1 THE BUERGER PRECESSION TECHNIQUE

A more detailed discussion of this technique can be found in the books by Luger (Ref. 8, p. 72-79) and Buerger⁽⁹⁾. In this technique a crystal axis, say \underline{a} , is aligned parallel to the primary beam and the reciprocal lattice planes which are perpendicular to \underline{a} may be photographed (Fig. 2.19a).

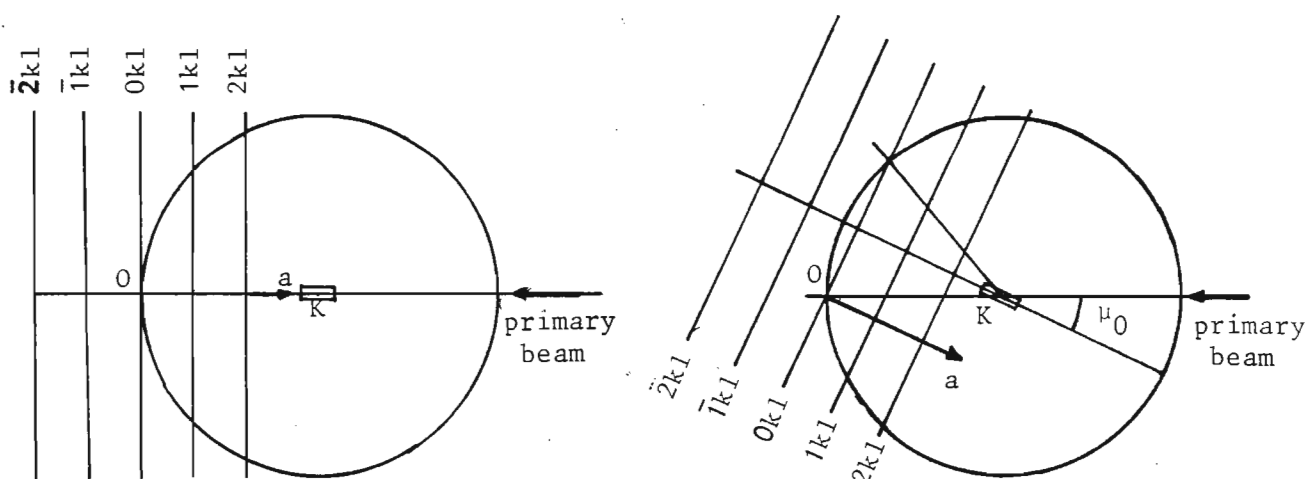


Fig. 2.19 Crystal setting by the precession method
 (a) inclination angle $\mu_0 = 0^\circ$: (b) $\mu_0 > 0^\circ$
 (Ref. 8, p. 71, Fig. 2.13).

The reciprocal lattice planes $0k\ell$, $1k\ell$, $2k\ell$, are therefore perpendicular to the X-ray beam and parallel to the crystal rotation axis, the $0k\ell$ -plane being the tangent plane to the Ewald sphere.

In order to obtain an undistorted picture of the $0k\ell$ reflections, the crystal rotation axis together with the $0k\ell$ plane, has to be tilted by μ_0 to the incident X-ray beam (Fig. 2.19b). In this tilted position the $0k\ell$ -reciprocal lattice plane intersects the Ewald sphere in a circle. In order to allow every reciprocal lattice point within this circle to pass the Ewald sphere, the tilting angle μ_0 is kept constant and a precession motion around the incident beam with precession angle μ_0 is described by the normal to the $0k\ell$ -reciprocal lattice plane.

In contrast to the deJong-Bouman method, the crystal does not rotate while precession photographs are taken, but is kept fixed in its azimuthal position so that the \underline{a} -axis coincides with the X-ray beam at $\mu_0 = 0$.

In order to obtain undistorted Buerger precession photographs, the film plate has to be kept parallel to the reciprocal lattice plane during the precession. Fig. 2.20 shows the geometry in the case of a zero layer precession exposure.

The arrangement is similar to that shown in Fig. 2.17 and nearly the same geometrical properties are obtained.

The relationship between the crystal to screen distance d_s and the screen radius r_s is

$$d_s = \frac{r_s}{\tan \mu_0} \quad (2.15)'$$

and the magnification:

$$\frac{1}{d^*} = \frac{d_F \lambda}{x} \quad (\text{\AA}) \quad (2.16)'$$

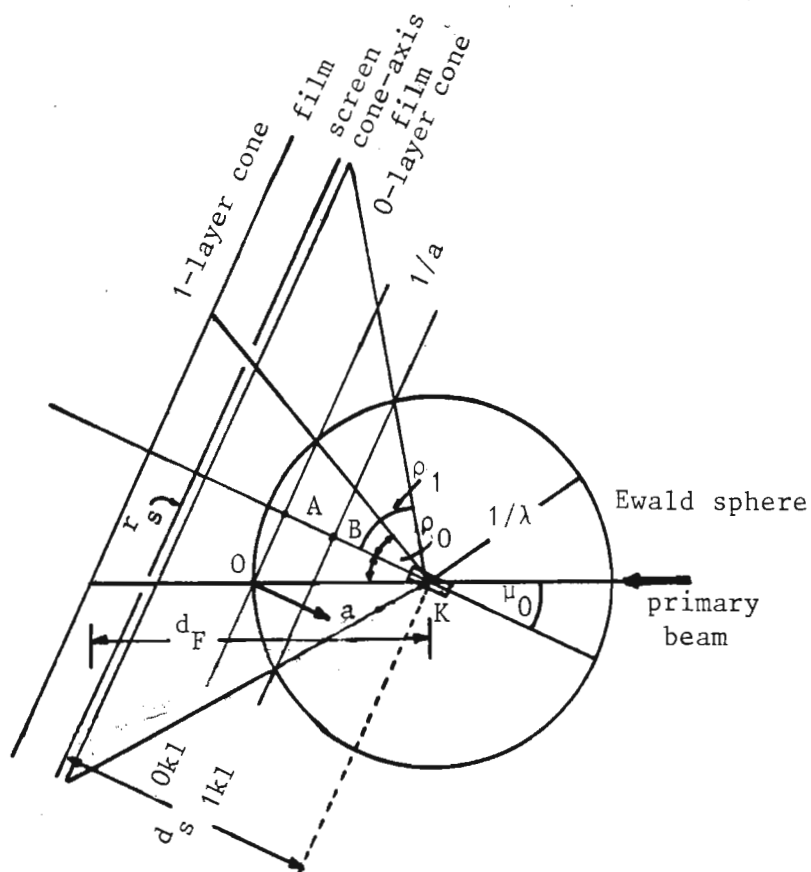


Fig. 2.20 Geometrical situation for taking a zero-layer precession exposure (Ref. 8, p. 75, Fig. 2.16).

A cone-axis photograph can also be obtained for the precession method by placing a stationary film between the crystal and the film cassette. From Fig. 2.20 it can be seen that the cone angle ρ_1 for the first layer is greater than the cone angle ρ_0 for the zero layer (for the deJong-Bouman technique $\rho_1 < \rho_0$). The lattice constant a can now be determined from

$$\frac{1}{a} = AK - BK = \frac{\cos \mu_0}{\lambda} - \frac{\cos \rho_1}{\lambda} \quad (2.21)$$

Just as for the deJong-Bouman technique, $\rho_0 = \mu_0$. ρ_1 is obtained from (2.18) and then a from (2.21).

An n^{th} layer precession photograph can be taken as follows: A precession angle μ_n is chosen to be smaller than μ_0 in order to avoid collision of the moving parts of the Lattice Explorer. The crystal to

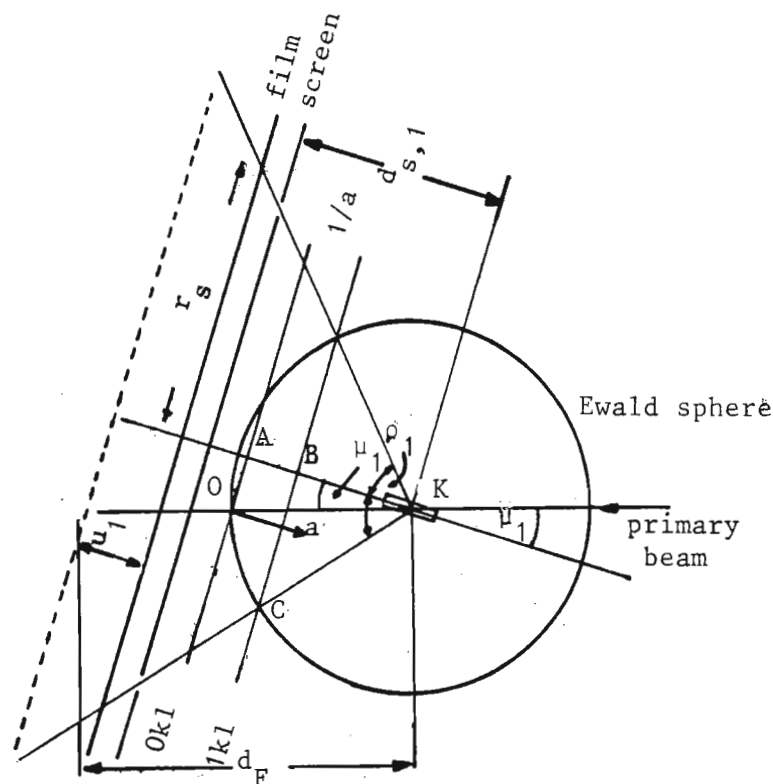


Fig. 2.21 Geometrical conditions for a first-layer precession exposure (Ref. 8, p. 76, Fig. 2.17).

screen distance is given by

$$d_{s,n} = \frac{r_s}{\tan \rho_n} \quad n = 1, 2, \dots \quad (2.22)$$

where the cone angle ρ_n is obtained from

$$\cos \rho_n = \cos \mu_n - (n\lambda)/a \quad (2.23)$$

As in the case of the deJong-Bouman technique, for the scale of the zero- and first-level photographs to be the same, the film has to be moved an amount u_1 towards the crystal. u_1 is identical in magnitude to t_1 (equation (2.20)) and is given by

$$u_1 = \frac{\lambda d_F}{a} \quad (2.24)$$

2.4.2 BUERGER PRECESSION ALIGNMENT PHOTOGRAPHS

For precession photograph the desired axis, the \underline{a} axis, has to be made parallel to the primary beam when $\mu = 0^\circ$. Stout and Jensen (Ref. 3, p. 128-133) discuss this alignment procedure in much detail. A precession adjustment photograph is taken using unfiltered radiation, no screen and a small precession angle μ_0 of about 7° . Furthermore the goniometer arcs are assumed to be approximately parallel and perpendicular to the X-ray beam.

The geometry of an approximately oriented r.l. is illustrated in Fig. 2.22. The r.l. plane is misset in the horizontal plane by angle ϵ_H , in the vertical plane by ϵ_V , and by ψ around the X-ray beam.

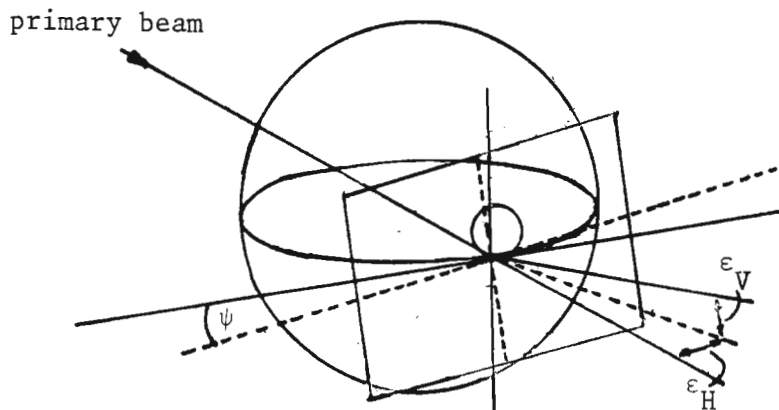


Fig. 2.22 Reciprocal lattice plane misset by ϵ_H in horizontal plane, ϵ_V in vertical plane, and ψ around the X-ray beam. (Ref. 3, p. 131, Fig. 5.64).

A precession adjustment photograph shows a small circular portion of the zero layer. If the axis is correctly aligned the centre of the circle will be at the centre of the film. If the axis is not aligned the circle will be distorted and displaced (Fig. 2.23).

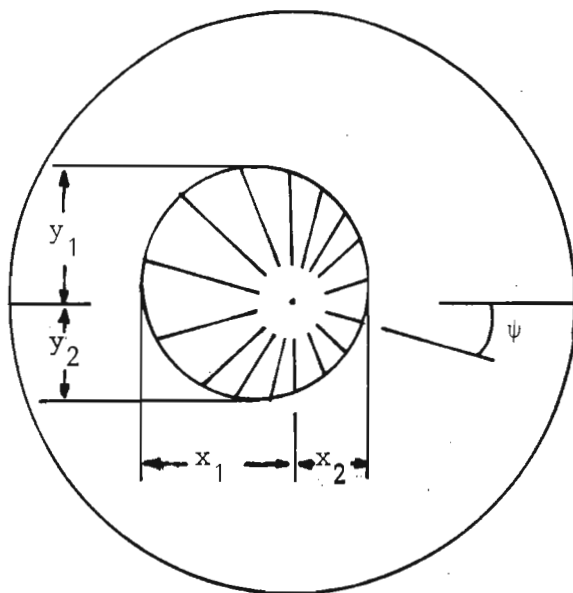


Fig. 2.23 Precession photograph showing misalignment corresponding to Fig. 2.22 (Ref. 3, p. 132, Fig. 5.65).

Let x_1 , x_2 and y_1 , y_2 respectively be distances measured on the film in two horizontal and vertical directions. The measurements are made from the central hole to the edge of the circle. The following relations hold for the differences $\Delta\xi$ (in r.l. units) between the edges of the circle:

$$\Delta\xi_H = \frac{||x_1| - |x_2||}{2R} \quad (2.25)$$

$$\Delta\xi_V = \frac{||y_1| - |y_2||}{2R}$$

where R is the crystal to film distance.

The vertical angular correction

$$\epsilon_V \sim \frac{1}{2} \tan^{-1} \Delta\xi_V \quad (2.26a)$$

is made to the azimuth and the horizontal angular correction

$$\epsilon_H \sim \frac{1}{2} \tan^{-1} \Delta\xi_H \quad (2.26b)$$

is made to the horizontal arc. The approximation is valid for small μ .

The correction ϵ_H is applied to a single arc only if one arc is exactly horizontal. In practice this arrangement is not always possible. In that case adjustments have to be made to both goniometer arcs to make the horizontal correction (see Section 4.1).

If it is required to bring a r.l. axis on the film onto the spindle axis, the correction ψ is measured directly on the film and applied to the vertical arc.

CHAPTER THREEDETAILS OF APPARATUS USED

The X-ray generator used was a Siemens Kristalloflex 4 with a horizontal tube shield. The X-ray tube was a 750 watt copper anode tube (type AG 3ö Cu) with a normal focus and was operated at 23 kV and 26 mA.

Photographs were taken on a STOE Reciprocal Lattice Explorer with X-rays which were either unfiltered or filtered through a nickel foil to remove the $\text{CuK}\beta$ radiation. Rotation, deJong-Bouman and Buerger precession techniques were utilized.

A collimator of aperture 0,5 mm was used for the incident beam. The wavelength of the $\text{CuK}\alpha$ radiation used for the photography was taken as 1,5418 Å.

The crystal was mounted at the end of a very fine glass fibre with 'Blitz Stik', an instant-bonding cyanoacrylate glue. The glass fibre was supported on a metal pin inserted into a Nonius goniometer head.

Intensity measurements were done on a Philips PW1100 computer-controlled, single crystal X-ray diffractometer using $\text{MoK}\alpha$ radiation, the wavelength being taken as 0,7107 Å. This service was performed by Mr Jon Albain of the Council for Scientific and Industrial Research (CSIR). Milburn (Ref. 10, p. 105-108) discusses the operation of this diffractometer in much detail.

The density of a RUCOPNP crystal was determined by the flotation method. A single crystal was placed in a saturated solution of cesium chloride.

Water was added dropwise into the solution until the crystal just remained suspended in the medium. The density of the solution of CsCl was then the density of the crystal. The density of the CsCl solution was determined using a 10 ml specific gravity bottle.

CHAPTER FOUR

DETERMINATION OF UNIT CELL CONSTANTS OF RUCOPNP

In this chapter crystal data of RUCOPNP are determined.

In Section 4.1 the photographic techniques which were discussed in Chapter 2 are utilized in order to determine the r.l. parameters. The length of the crystal needle axis was determined from a rotation photograph. Precession and deJong-Bouman photographs were taken of several r.l. planes. As the crystal was triclinic, further photographs were found to be necessary to determine all r.l. parameters accurately. To aid the choice of suitable crystal orientations for further photography, a model of the r.l. was constructed. The best triclinic r.l. unit cell was chosen from the model and as it had not been possible to photograph these r.l. vectors directly, the parameters were calculated from the observed ones (Sections 4.2.1 and 4.2.2).

In Section 4.2.3 the related direct lattice parameters are calculated. In Sections 4.3 the number of molecules in the unit cell is calculated from the unit cell volume, the density (measured by flotation) and the formula mass of the complex. The absorption coefficient and optimum crystal thickness for intensity measurement are calculated in Sections 4.3 and 4.4.

4.1 PHOTOGRAPHY OF RECIPROCAL LATTICE

The crystal was mounted on the goniometer head with its needle axis in the direction of the rotation axis. Using unfiltered radiation and an arbitrarily chosen azimuth, an oscillation photograph was taken. The

TABLE 4.1 Calculation of arc corrections from oscillation photographs. Experimental details: oscillation range 13° ; filter - none; film displacement reading 0,36 mm (i.e. film to crystal distance $R = 60,00$ mm); reflection coordinate $x = 59,7$ mm, ω - azimuth setting for long exposure - the setting $\omega + 180$ was given an exposure of half the time. α_L (α_S) setting angle of large (small) arc; $2Y_R$ and $2Y_L$ reflection separation defined in section 2.3; ϵ and δ -setting corrections defined in section 2.3; t - exposure time. For clarity the following values are given $R' = 84,64$ mm (equation 2.9), $\sin 2\theta = 0,7053$. For photograph 93 $Y_R - Y_L = 0,9$ mm giving $\tan \delta = 0,00754$ (equation 2.11) and $Y_R + Y_L = 0,0$ mm giving $\tan \epsilon = 0$ (equation 2.11). Note that, assuming the values of ϵ and δ namely $0,00$ and $0,43^\circ$ to be reasonably accurate, the values of $2Y_R$ and $2Y_L$ would have been expected to be not zero but $0,37$ mm and $0,37$ mm for film 92. This separation was therefore apparently too small to measure. Film 94 taken after the corrections were applied shows no separation.

Film No.	ω ($^\circ$)	α_L ($^\circ$)	α_S ($^\circ$)	$2Y_R$ (mm)	$2Y_L$ (mm)	ϵ ($^\circ$)	δ ($^\circ$)	t (h)
92	87,6	7,6	3,7	0,0	0,0	0,00	0,00	3
93	177,6	7,6	3,7	0,9	- 0,9	0,00	0,43	3
94	177,6	7,6	3,3	0,0	0,0	0,00	0,00	3

pattern of the layer lines on the photograph confirmed that the needle axis was a real axis, designated the c-axis. (The photograph showed no symmetry about the zero-layer line - hence no mirror planes m_x and m_y . This indicates that there is no direct symmetry axis coincident with the X-ray beam. The c-axis (rotation axis) is not a symmetry axis).

TABLE 4.2 Calculation of c from rotation photograph (film 95).
 Experimental details: filter - Ni; film displacement reading 0,36 mm. n , $2X$ and Y_n are defined in 2.2.3.
 $R/R' = y_n/Y_n$ (equation (2.4)') where $R' = R/\cos(\tan^{-1}(X/R))$
 (equation (2.4)') and $c = n\lambda/\cos \tan^{-1}(R/y_n)$ (equation (2.3)'). Note that measurements on lines $n \leq 3$ were considered inaccurate and neglected when calculating a mean value of c . The values used were given equal weight.

Spot No.	n	$2X(\text{mm})$	$2Y_n(\text{mm})$	R/R' $= \cos(\tan^{-1} R/y_n)$	$c(\text{\AA})$
1	7	42,5	93,0	0,5899	18,296
2	7	32,7	91,0	0,5905	18,277
3	6	34,8	73,0	0,5045	18,337
4	5	67,6	64,2	0,4225	18,246
5	5	41,6	59,0	0,4227	18,237
6	5	27,4	57,1	0,4208	18,321
7	4	78,5	51,5	0,3380	18,214
8	4	50,9	46,9	0,3363	18,339
9	4	21,0	43,5	0,3362	18,343
10	3	70,5	36,5	0,2537	(18,228)
11	7	54,1	96,3	0,5904	(18,280)
12	2	83,4	25,0	0,1686	(18,294)
13	1	105,5	13,6	0,0849	(18,168)
14	1	77,5	12,0	0,0837	(18,419)

The c -axis was made exactly parallel to the rotation axis by means of double exposure oscillation adjustment photographs. The procedure has been described in section 2.2.4. The details of the photographs (films 92, 93 and 94) are given in Table 4.1.

A rotation photograph (film 95) was then taken. A summary of the setting parameters (crystal, film and screen) for all aligned photographs (rotation, precession, deJong-Bouman, cone-axis) is given in Table 4.6. Measurements done on the photograph gave a c -value

$$c = 18,290 \pm 0,016 \text{ \AA}$$

Details of the measurement and calculations are shown in Table 4.2.

The crystal was rotated about the azimuth until a bright maltese cross was seen in the microscope-telescope system, i.e. with a prismatic face of the crystal parallel to the X-ray beam. An axis, designated the \underline{a} -axis was assumed to be parallel to this face. By means of precession adjustment photographs, the \underline{a} -axis was made parallel to the X-ray beam

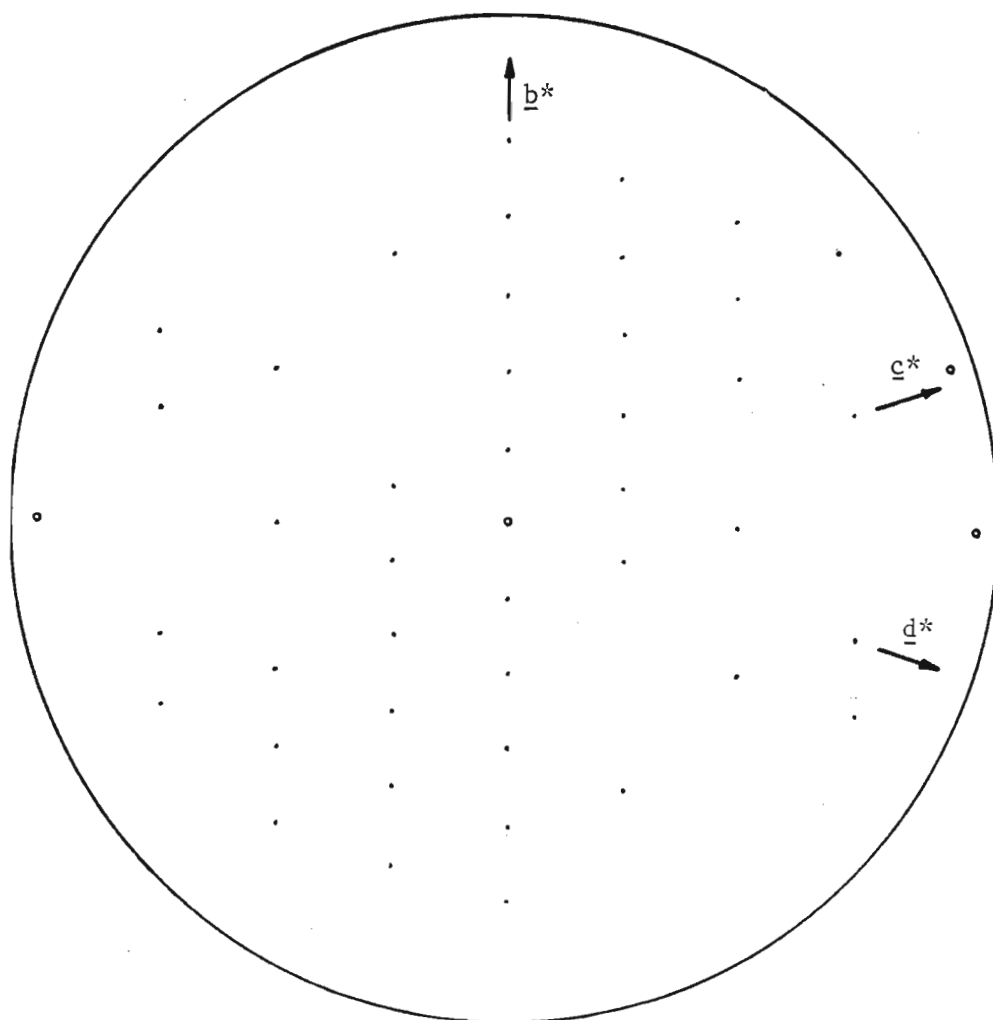


Fig. 4.1 (Film 100) 0-layer Buerger precession photograph - $\underline{b}^*\underline{c}^*\underline{d}^*$ plane.

TABLE 4.3 Calculation of arc corrections for precession photographs. ω , α_L and α_S are the crystal setting angles as defined in the caption to Table 4.1 and y_1 , y_2 , x_1 and x_2 are illustrated in Fig. 2.23. ϵ_V and ϵ_H are the arc corrections calculated using equations 2.25 and 2.26 with $R = 60,0$ mm. The values given in brackets are the corrections (ϵ_ℓ and ϵ_s) applied to each arc.

Film No.	ω	α_L	α_S	y_1 (mm)	y_2 (mm)	x_1 (mm)	x_2 (mm)	$\epsilon_V(^{\circ})$	$\epsilon_H(^{\circ})$
96	84,1	- 1,4	- 5,3	13,6	15,1	10,0	19,0	0,36	2,14
	(+ 0,4)	(+ 0,0)	(- 2,1)						
98	84,5	- 1,4	- 7,4	14,4	14,5	14,6	14,4	0,02	0,05
110	29,0	- 1,4	- 5,3	15,2	14,0	14,0	11,0	0,28	1,52
	(- 0,3)	(- 1,3)	(- 0,8)						
111	28,7	- 2,7	- 6,1	14,8	14,0	14,8	15,1	0,20	0,07
	(- 0,2)	(- 0,1)	(0,0)						
120	117,5	- 20,8	- 7,4	16,0	13,2	16,0	13,0	0,67	0,72
	(- 0,7)	(+ 2,7)	(+ 1,9)						
132	116,8	18,1	- 5,5	14,5	14,5	14,6	14,6	-	-

(see Table 4.3). A zero-layer precession photograph (film 100 - Fig. 4.1) as described in section 2.4.1, was taken of the $\underline{b}^* \underline{c}^*$ plane perpendicular to the \underline{a} -axis.

Two axes were designated \underline{b}^* and \underline{c}^* , \underline{b}^* being perpendicular to the needle axis. The lengths of \underline{b}^* and \underline{c}^* were calculated. The individual read-

TABLE 4.4 Calculation of \underline{b}^* from precession photograph (film 100). d is the distance between spots along the axis, whose indices differ by n . b_1^* is in units of mm measured on the film.

d^* (mm)	n	b_1^* (mm)	$\bar{b}^* - b_1^*$ (mm)
98,1	10	9,810	- 0,009
78,4	8	9,800	0,001
58,8	6	9,800	0,001
78,5	8	9,812	- 0,011
58,7	6	9,783	0,018
		\bar{b}^* 9,801	

ings and calculations for \underline{b}^* are shown in Table 4.4 giving a mean value of $b^* = 9,801$ mm. The standard error of the mean is calculated as follows:

$$\begin{aligned}\sigma &= \left[\frac{\sum_i (b_1^* - \bar{b}^*)^2}{N(N-1)} \right]^{\frac{1}{2}} \\ &= \left[\frac{0,000528}{5 \cdot 4} \right]^{\frac{1}{2}} \\ &= 0,005 \text{ mm.}\end{aligned}$$

Therefore $b^* = 9,801 \pm 0,005$ mm.

The values of all r.l. vectors measured on precession and deJong-Bouman films are summarised in Table 4.7.

The \underline{a} -axis was also determined from measurements on the related cone-axis photograph (film 101) (see Table 4.5).

The $\underline{b^*c^*}$ 1- and 2-layers were then photographed (films 107 and 108). These layers when compared with the zero layer were found to be shifted with respect to the origin. This 'origin shift' is caused by the third reciprocal lattice vector making an oblique angle with one (or both) of the two in the plane of the zero layer. This vector was labelled $\underline{a^*}$. The origin shift is illustrated in Fig. 4.2.

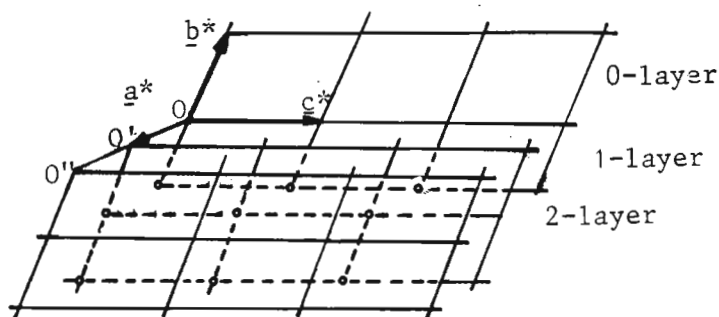


Fig. 4.2 Illustration of origin shift.

With the same goniometer arc settings as for the rotation photograph used to measure \underline{c} , a zero-layer de-Jong-Bouman photograph was taken of the plane perpendicular to the \underline{c} -axis (film 105 - Fig. 4.3).

The length of the \underline{c} -axis of $18,3 \text{ \AA}$ determined from the cone-axis photograph (Table 4.5, film 104) is in good agreement with the value of $18,290 \pm 0,016 \text{ \AA}$ from the rotation photograph (Table 4.2, film 95). Again the origin of the r.l. net on the 1-layer deJong-Bouman photograph appeared shifted with respect to the 0-layer photograph showing that the third vector was oblique. This vector was designated the $\underline{f^*}$ -axis. (Several r.l. vectors were designated as axes and labelled alphabetically for later choice of the best unit cell). It should be noted that the precession (film 100) and the deJong-Bouman (film 105) photographs contain the common axis $\underline{b^*}$.

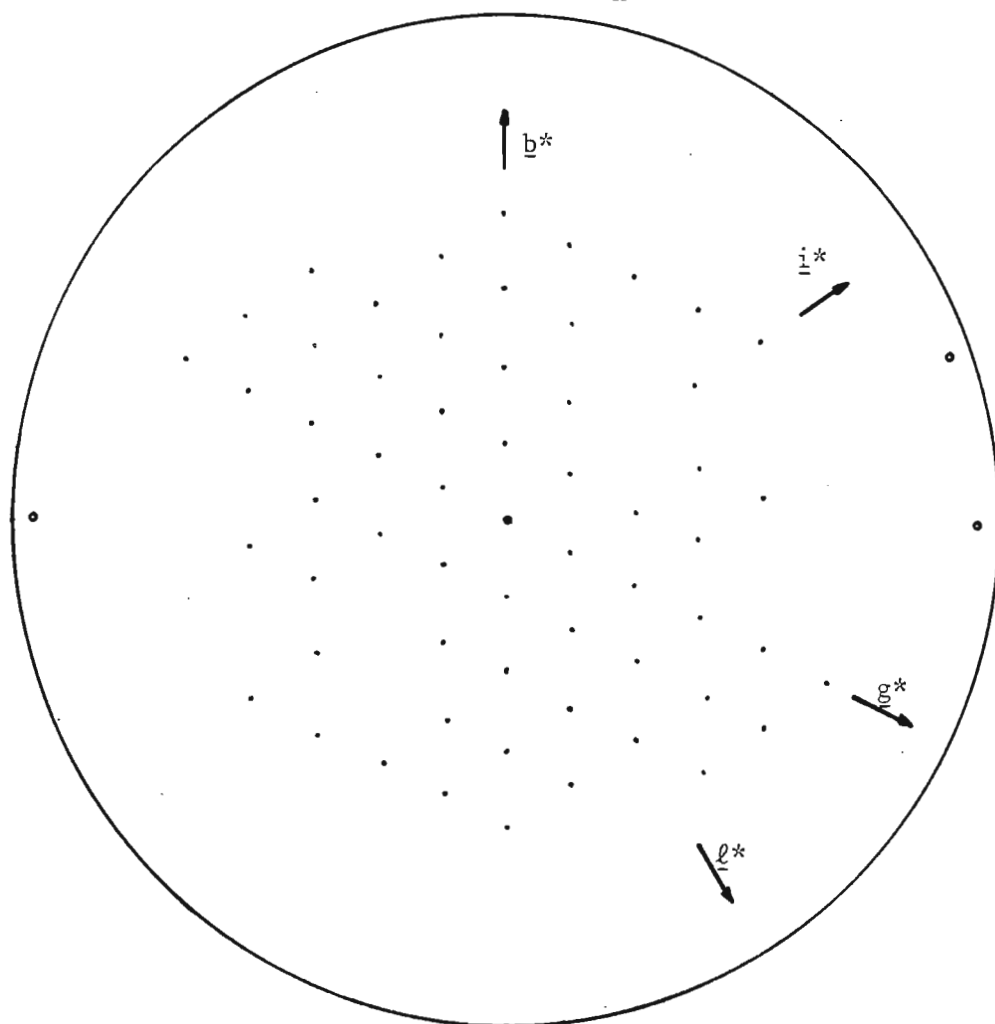


Fig. 4.3 (Film 105) 0-layer deJong-Bouman photograph - $\underline{b}^* \underline{i}^* \underline{g}^* \underline{l}^*$ plane.

In order to aid further photography and the choice of the best unit cell, a three-dimensional wire model of the reciprocal lattice was constructed as follows. The vectors \underline{b}^* , \underline{c}^* and the angle $\underline{b}^* \hat{ } \underline{c}^*$ from the zero-layer precession photograph (film 100) were used as a basis. The relative shift of the 1- and 2-layers with respect to the origin of the zero-layer was measured by superimposing exactly the reflection spots from the 0- and 1-layers. The origin shift was then determined as the distance between the centre holes of the two films. The spacing of the layers was calculated from the details required for 1-layer precession photography. The scale used for the model was 1 mm (on film) = 100 mm (on model). A third layer (photograph not taken) was also included in the

TABLE 4.5 Evaluation of the length of the direct axis from cone-axis photographs. r_0 , r_1 are the radii of the 0- and 1-layer Laue circles, ρ_0 and ρ_1 the cone half-angles. ρ_0 is equal to the precession angle μ_0 used, ρ_1 is calculated from equation 2.18 and the length of the direct axis d calculated from equation 2.17. Note that the zero layer can be identified as the layer interrupted by the shadow of the beam stop. It is also the one on which the spots have no white radiation streaks.

Film No.	Axis	r_0 (mm)	r_1 (mm)	μ_0 (°) (= ρ_0)	ρ_1 (°)	d (Å)
101	<u>a</u>	13,5	16,8	26,0	31,26	35,1
104	<u>c</u>	28,1	21,7	45,0	37,68	18,3
112	<u>b</u>	13,3	18,4	26,0	34,01	22,1

model - to account for those reciprocal vectors that may be seen on other photographs. Fig. 4.4 shows a projection of the reciprocal lattice with some vectors chosen from the model.

Buerger precession photographs were taken of the planes containing the vectors \underline{i}^* , \underline{e}^* , \underline{k}^* and the vectors \underline{a}^* , \underline{l}^* , \underline{m}^* , \underline{n}^* , \underline{d}^* (\underline{a}^* was identified from the model as being the shortest r.l. axis).

In order to photograph the \underline{i}^* \underline{e}^* \underline{h}^* plane, the \underline{i}^* axis was first set perpendicular to the X-ray beam by rotating the crystal azimuth by $55,5^\circ$. This was the angle between the \underline{i}^* and \underline{b}^* axes as measured on the deJong-Bouman photograph (film 105). A bright reflection from a crystal face was also seen in this position in the microscope-telescope. An alignment photograph (film 100) was taken and gave $\varepsilon_V = 0,3^\circ$ (azimuthal adjustment) and $\varepsilon_H = 1,5^\circ$ (horizontal adjustment). The

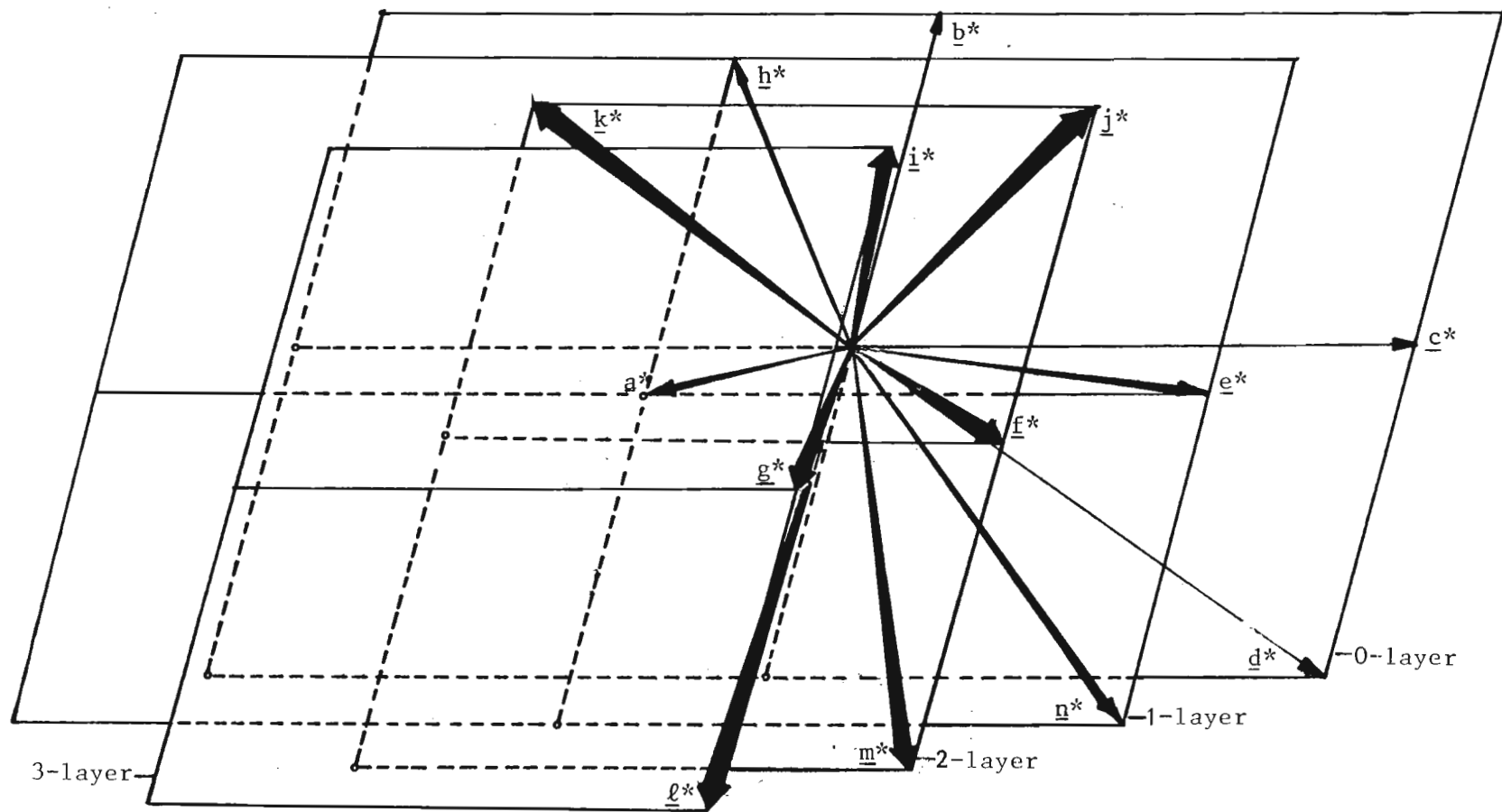


Fig. 4.4 Two-dimensional projection of the reciprocal lattice model onto the "b*c*" plane.

azimuthal correction is simply ϵ_V but the horizontal adjustment which was required to make these planes exactly perpendicular to the X-ray beam was not as easy to calculate as that for the $\underline{b}^* \underline{c}^*$ plane because the goniometer arcs were now far from being parallel and perpendicular to the X-ray beam.

The horizontal adjustment was made as follows: With the azimuthal setting at $29,0^\circ$ the arcs were positioned as shown in Fig. 4.5a (looking down the crystal rotation axis).

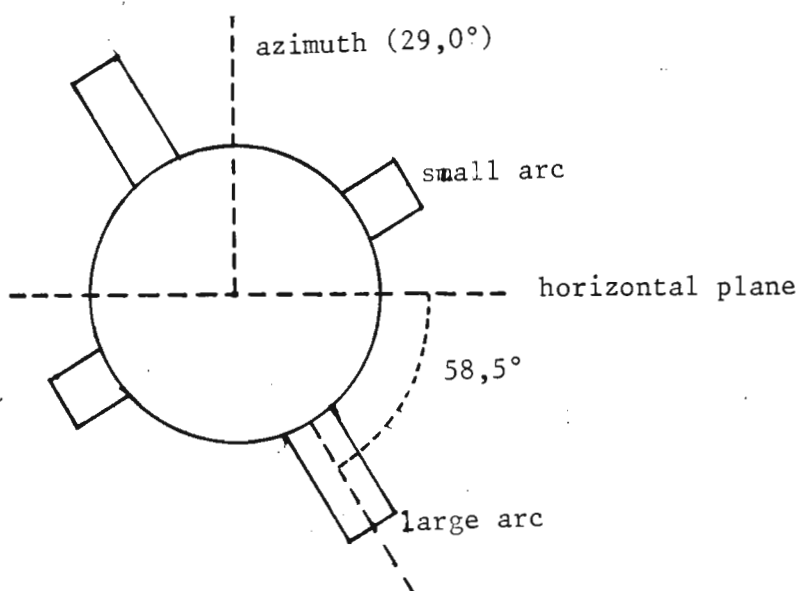


Fig. 4.5a Position of arcs at an azimuth setting of $29,0^\circ$.

When the large arc was vertical, the azimuth was $87,5^\circ$. At the $29,0^\circ$ position, the angle between the horizontal and the large arc is therefore $\phi = 87,5^\circ - 29,0^\circ = 58,5^\circ$. Assuming that for small angles the adjustments on the arcs are linear then for a horizontal adjustment of $\epsilon_H = 1,5^\circ$ the small and large arc adjustments ϵ_s and ϵ_l can be visualized as shown in Fig. 4.5b; the components of the correction in the directions of the two arcs are $\epsilon_l = 1,5 \cos 58,5^\circ = 0,78^\circ$; $\epsilon_s = 1,5 \sin 58,5^\circ = 1,3^\circ$.

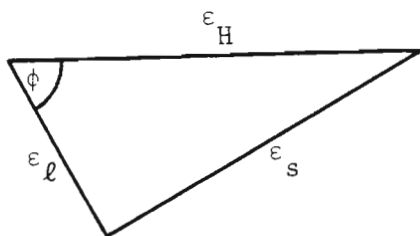


Fig. 4.5b Relationship between horizontal alignment error ϵ_H and corrections ϵ_l and ϵ_s required to adjust the large and small goniometer arcs.

The corrections were made on the arcs and a good alignment reached after taking several photographs. Table 4.3 gives the details of the alignment photographs (films 120-132). The 0-layer \underline{i}^* , \underline{e}^* , \underline{k}^* plane was photographed (film 113, Fig. 4.6). 1- and 2-layer precession photographs (films 114 and 115) again revealed the presence of a third oblique reciprocal lattice vector.

The plane containing the vectors \underline{a}^* , \underline{l}^* , \underline{m}^* , \underline{n}^* and \underline{d}^* was now aligned for precession photograph as follows. In the setting of film 100 the reciprocal lattice plane perpendicular to the X-ray beam contains the vectors \underline{b}^* , \underline{c}^* and \underline{d}^* . The \underline{d}^* axis which is common to both planes under consideration was first made horizontal i.e. made to coincide with the 3 horizontal holes on the film by rotating the crystal through $17,9^\circ$ (measured on film 100), the correction being applied to the (vertical) large arc. Upon checking the adjustment by repeating the precession photograph (film 119) of the $\underline{b}^*\underline{c}^*\underline{d}^*$ plane, it was found that a further adjustment of $1,5^\circ$ was required. Finally, from the model it was estimated that a rotation of the reciprocal lattice of 33° about the azimuth would make the $\underline{a}^*\underline{d}^*$ plane perpendicular to the X-ray beam.

With the adjustments described above, an alignment photograph (film 120) was taken. The large arc was now $\phi = 60,0^\circ$ from the horizontal. Table

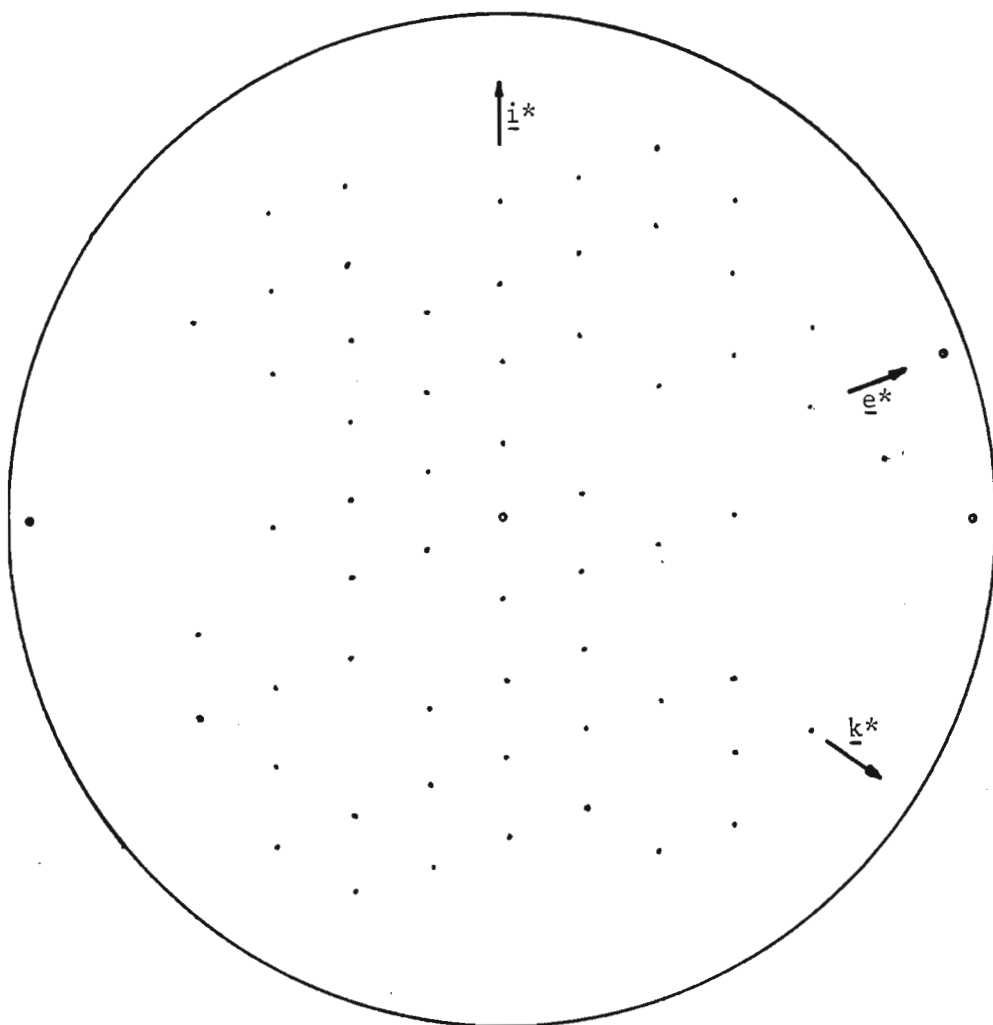


Fig. 4.6 (Film 113) Buerger precession photograph - $\underline{i}^*\underline{e}^*\underline{k}^*$ plane.

4.3 gives details of the settings. The required vertical and horizontal corrections were $\epsilon_V = 0,67^\circ$ and $\epsilon_H = 0,72^\circ$ and the corrections to the goniometer arcs were

$$\epsilon_s = \epsilon_H \cos \phi = 0,72 \cos 60^\circ = 0,36^\circ$$

$$\epsilon_\rho = \epsilon_H \sin \phi = 0,72 \sin 60^\circ = 0,62^\circ$$

The corrections actually applied between films 120 and 132 (Table 4.3) differ from those calculated due to the following circumstances.

Through a series of errors incorrect adjustments were made to the arcs and this resulted in an unnecessary rotation of the r.l. plane about an axis perpendicular to it. Errors were made in assigning values ϵ_ρ and

ϵ_s (Fig. 4.5b) and this shows that great care must be taken if the arcs are not set horizontal and vertical. Errors were also made in attempting to define the centre of the alignment circle accurately by extending the white radiation streaks. Such errors can be avoided if strong spots are visible just inside the edge of the circle. In such a case the misalignment can be estimated from the distances between these spots and the edge of the circle. The error also affects the correction to film 110 but the effect is not so marked.

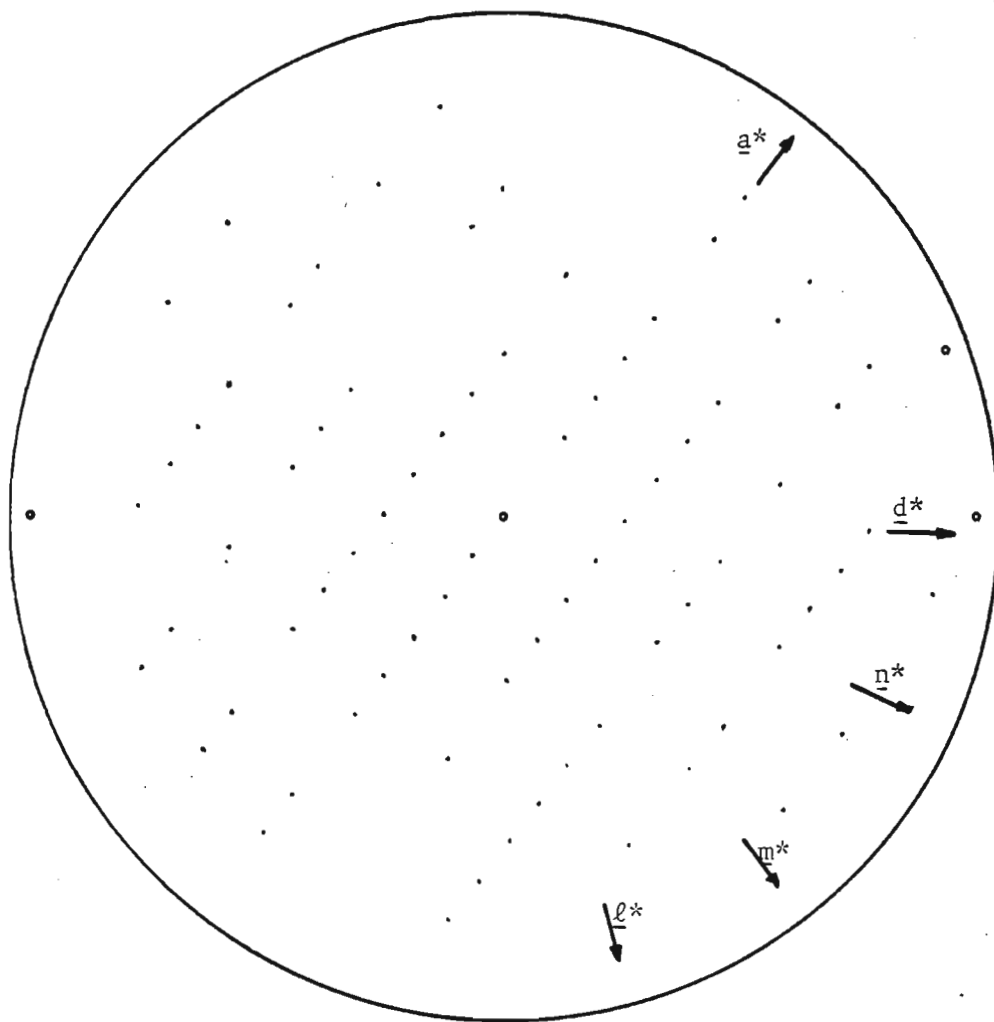


Fig. 4.7 (Film 133) Buerger precession photograph - $\underline{a^*d^*n^*m^*l^*}$ plane.

TABLE 4.6 Details of setting parameters for all aligned photographs.
 Technique: ROT - rotation photograph; PRE0, PRE1, PRE2 are 0-, 1-, 2-layer Buerger precession photographs respectively; dJB0, dJB1, dJB2 are deJong-Bouman 0-, 1-, 2-layer photographs respectively; μ - inclination (precession) angle; r_s - screen radius; d_s - crystal to screen distance (fixed at 30,00 mm for deJong-Bouman photography).

Film No.	Technique	Goniometer arcs		Azimuth ($^{\circ}$)	$\mu(^{\circ})$	r_s (mm)	Film Disp. (mm)	Exposure Time (h)	d_s (mm)
		α_L	α_S						
95	ROT	+7,6	-5,3	-	-	-	0,36	6,5	-
100	PRE0	-1,4	-7,4	84,5	26	15	"	16	30,75
101	PRE0 (cone axis)	"	"	"	"	-	"	"	-
104	dJB0 (cone axis)	"	-5,3	84,1	45	-	5,20	16	-
105	dJB0	"	"	"	"	30	5,20	"	30,00
106	dJB1	"	"	"	38,5	"	5,06	"	30,00
107	PRE1	"	-7,4	84,5	20	15	3,00	"	30,22
108	PRE2	"	"	"	"	"	5,27	"	24,34
109	dJB2	"	-5,3	84,1	32,6	30	10,12	"	30,00
112	PRE0 (cone axis)	-2,7	-6,1	28,7	26,0	-	0,36	4	-
113	PRE0	"	"	"	"	30	"	16	30,75
114	PRE1	"	"	"	20,0	15	4,55	"	26,45
115	PRE2	"	"	"	"	20	8,74	"	26,67
133	PRE0	-18,1	-5,5	116,8	26,0	15	0,36	32	30,75

TABLE 4.7 Reciprocal Lattice vectors measured on deJong-Bouman and Buerger Precession films

Film No.	r.l. Vector	Length (mm)	Error (mm)
100	\underline{b}^*	9,801	0,005
	\underline{c}^*	15,957	0,007
	\underline{d}^*	16,029	0,004
105	\underline{b}^*	9,832	0,005
	\underline{g}^*	9,379	0,009
	\underline{l}^*	16,325	0,008
113	\underline{i}^*	10,107	0,006
	\underline{e}^*	10,761	0,004
	\underline{k}^*	12,036	0,005
133	\underline{a}^*	6,431	0,003
	\underline{l}^*	16,325	0,010
	\underline{m}^*	13,418	0,007
	\underline{n}^*	13,316	0,007
	\underline{d}^*	16,019	0,008

The r.l. vectors designated \underline{a}^* to \underline{n}^* were carefully measured on the zero layer deJong-Bouman and three precession photographs. The values are shown in Table 4.7.

4.2.1 BEST RECIPROCAL UNIT CELL

The best unit cell must be chosen so that its axes are of shortest lengths and that the angles between the axes are as close as possible to being right angles. By inspection of the model, it was found that the best unit cell satisfying these conditions was the cell with axes labelled \underline{a}^* , \underline{f}^* and \underline{h}^* . The parameters, based on the unit cell $\underline{a}^*\underline{f}^*\underline{h}^*$, were determined from those axial lengths measured on the photographs (see Table 4.7, p. 51). The calculation of the unit cell parameters is done in the next section.

4.2.2 RECIPROCAL UNIT CELL PARAMETERS

From the reciprocal lattice model (Fig. 4.4), relations between the various lattice vectors labelled are deduced. The * denoting reciprocal lattice vectors is omitted for convenience in this section. All length calculations are in mm units as measured on the films and are converted to \AA^{-1} only when the direct lattice cell is calculated. The reciprocal lattice vectors \underline{a} , \underline{b} , \underline{c} , \underline{d} , \underline{e} , \underline{g} , \underline{i} , \underline{k} , \underline{l} , \underline{m} , \underline{n} were measured on the films and the parameters required were \underline{a} , \underline{f} , \underline{h} and the angles between them. These parameters are calculated below and the calculation of their errors is shown in Appendix 1.

The following parameters were used in the calculations:

$$a = 6,431 \pm 0,003 \text{ mm}$$

$$b = 9,801 \pm 0,003 \text{ mm}$$

$$c = 15,957 \pm 0,007 \text{ mm}$$

$$g = 9,379 \pm 0,009 \text{ mm}$$

$$i = 10,107 \pm 0,006 \text{ mm}$$

$$k = 12,036 \pm 0,005 \text{ mm}$$

Calculation of f and $\hat{a}f$

The vectors \underline{g} , \underline{c} , \underline{a} and \underline{f} are in the same plane. Therefore f and $\hat{a}f$ can be calculated given the lengths of \underline{g} , \underline{c} and \underline{a} .

The following relations are deduced from the model:

$$\underline{g} = \underline{c} + 3\underline{a} \quad \text{so that} \quad g^2 = c^2 + 6\underline{c} \cdot \underline{a} + 9a^2 \quad (\text{A})$$

$$\underline{f} = \underline{c} + 2\underline{a} \quad " \quad " \quad f^2 = c^2 + 4\underline{c} \cdot \underline{a} + 4a^2 \quad (\text{B})$$

$$(\underline{g} = \underline{a} + \underline{f} \quad " \quad " \quad g^2 = a^2 + 2\underline{a} \cdot \underline{f} + f^2) \quad (\text{C})$$

From equations (A) and (B)

$$f^2 = c^2 + \frac{4}{6}(g^2 - c^2 - 9a^2) + 4a^2$$

$$\text{i.e. } Y = 3f^2 = c^2 + 2g^2 - 6a^2 \quad (\text{D})$$

$$= (15,957)^2 + 2(9,379)^2 - 6(6,431)^2$$

$$= 182,411 \text{ mm}^2$$

$$\therefore f = 7,798 \text{ mm}$$

From equations (C) and (D)

$$\underline{a} \cdot \underline{f} = \frac{1}{2}[g^2 - \frac{1}{3}(c^2 + 2g^2 - 6a^2) - a^2]$$

$$\text{i.e. } 6\underline{a} \cdot \underline{f} = g^2 - c^2 + 3a^2 \quad (\text{E})$$

$$= (9,379)^2 - (15,957)^2 + 3(6,431)^2$$

$$= -42,586 \text{ mm}^2$$

Hence

$$\cos \hat{a}f = \frac{\underline{a} \cdot \underline{f}}{|\underline{a}| |\underline{f}|} = \frac{\frac{1}{6}(g^2 - c^2 + 3a^2)}{a[\frac{1}{3}(c^2 + 2g^2 - 6a^2)]^{\frac{1}{2}}}$$

$$\text{i.e. } 2(3)^{\frac{1}{2}} \cos \hat{a}f = \frac{(g^2 - c^2 + 3a^2)}{a(c^2 + 2g^2 - 6a^2)^{\frac{1}{2}}}$$

$$= \frac{-42,586}{6,431 (182,411)^{\frac{1}{2}}}$$

$$= -0,49030$$

Therefore $\cos \hat{a}f = -0,141538$, and

$$\hat{a}f = 98,14^\circ$$

The values including errors calculated in Appendix 1 are:

$$f = 7,798 \pm 0,010 \text{ mm}$$

$$\cos \hat{a}f = -0,1415 \pm 0,0010, \text{ and}$$

$$\hat{a}f = 98,14 \pm 0,06^\circ$$

Calculation of h and $\hat{f}h$

From the model, the following relations are deduced:

$$\underline{i} = \underline{f} + \underline{h} \quad \text{so that} \quad 2\underline{f} \cdot \underline{h} = i^2 - f^2 - h^2 \quad (\text{F})$$

$$\underline{f} = \underline{c} + 2\underline{a} \quad " \quad " \quad f^2 = c^2 + 4\underline{c} \cdot \underline{a} + 4a^2 \quad (\text{B})$$

$$\underline{h} = \underline{a} + \underline{b} \quad " \quad " \quad h^2 = a^2 + 2\underline{a} \cdot \underline{b} + b^2 \quad (\text{G})$$

Therefore substituting (B) and (G) into (F)

$$2\underline{f} \cdot \underline{h} = i^2 - (c^2 + 4\underline{c} \cdot \underline{a} + 4a^2) - (a^2 + 2\underline{a} \cdot \underline{b} + b^2) \quad (\text{H})$$

But from the model $\underline{g} = \underline{c} + 3\underline{a}$ so that $6\underline{a} \cdot \underline{c} = g^2 - c^2 - 9a^2$, and (A)

$$\underline{k} = \underline{b} + 2\underline{a} \quad " \quad " \quad 4\underline{a} \cdot \underline{b} = k^2 - b^2 - 4a^2 \quad (\text{I})$$

Therefore substituting (A) and (I) into (H)

$$2\underline{f} \cdot \underline{h} = i^2 - [c^2 + 4(\frac{1}{6}(g^2 - c^2 - 9a^2)) + 4a^2] - [a^2 + 2(\frac{1}{4}(k^2 - b^2 - 4a^2)) + b^2]$$

so that

$$12\underline{f} \cdot \underline{h} = 18a^2 - 3b^2 - 2c^2 - 4g^2 + 6i^2 - 3k^2 \quad (\text{J})$$

Now

$$3f^2 = c^2 + 2g^2 - 6a^2, \text{ and} \quad (\text{D})$$

$$2h^2 = -2a^2 + b^2 + k^2 \quad (\text{K}) \text{ (substituting (I) into (G))}$$

so that

$$\cos \hat{f}h = \frac{\underline{f} \cdot \underline{h}}{|\underline{f}| |\underline{h}|} = \frac{\frac{1}{12}(18a^2 - 3b^2 - 2c^2 - 4g^2 + 6i^2 - 3k^2)}{[\frac{1}{3}(-6a^2 + c^2 + 2g^2)]^{\frac{1}{2}} \cdot [\frac{1}{2}(-2a^2 + b^2 + k^2)]^{\frac{1}{2}}}$$

$$\text{i.e. } Z = 2(6)^{\frac{1}{2}} \cos \hat{f}h = \frac{(18a^2 - 3b^2 - 2c^2 - 4g^2 + 6i^2 - 3k^2)}{(-6a^2 + c^2 + 2g^2)^{\frac{1}{2}} (-2a^2 + b^2 + k^2)^{\frac{1}{2}}}$$

$$= p q r.$$

Now $h^2 = \frac{1}{2}(-2a^2 + b^2 + k^2) = 79,1046$ so that

$$h = (79,1046)^{\frac{1}{2}} = 8,894 \text{ mm.}$$

Furthermore

$$\begin{aligned} p &= 18a^2 - 3b^2 - 2c^2 - 4g^2 + 6i^2 - 3k^2 \\ &= 18(6,431)^2 - 3(9,801)^2 - 2(15,957)^2 - 4(9,379)^2 + 6(10,107)^2 - 3(12,036)^2 \\ &= -226,541 \text{ mm}^2 \end{aligned}$$

$$\begin{aligned} q &= (-6a^2 + c^2 + 2g^2)^{-\frac{1}{2}} = [-6(6,431)^2 + (15,957)^2 + 2(9,379)^2]^{-\frac{1}{2}} \\ &= (182,411)^{-\frac{1}{2}} = 0,074041 \end{aligned}$$

$$\begin{aligned} r &= (-2a^2 + b^2 - k^2)^{-\frac{1}{2}} = [-2(6,431)^2 + (9,801)^2 - (12,036)^2]^{-\frac{1}{2}} \\ &= (158,209)^{-\frac{1}{2}} = 0,079503 \end{aligned}$$

Hence

$$Z = p q r = \frac{-226,541}{(182,411)^{\frac{1}{2}} (158,209)^{\frac{1}{2}}} = -1,33354$$

$$\text{and } \cos \underline{f}^{\underline{h}} = Z/2(6)^{\frac{1}{2}} = -0,272208$$

$$\text{i.e. } \underline{f}^{\underline{h}} = 105,796^\circ$$

Finally, including errors calculated in Appendix 1

$$h = 8,894 \pm 0,005 \text{ mm}$$

$$\underline{f}^{\underline{h}} = 105,80 \pm 0,08^\circ$$

Calculation of $\underline{a}^{\underline{h}}$

$$\underline{h} = \underline{a} + \underline{b} \quad (\text{G})$$

$$\underline{k} = \underline{b} + 2\underline{a} \quad (\text{I})$$

$$(\underline{k} = \underline{a} + \underline{h})$$

$$\text{so that } k^2 = a^2 + 2\underline{a} \cdot \underline{h} + h^2 \quad (\text{L})$$

Substituting (K) into (L) gives

$$4\underline{a} \cdot \underline{h} = k^2 - b^2 \quad (\text{M})$$

Now

$$\cos \underline{a}^{\underline{h}} = \frac{\underline{a} \cdot \underline{h}}{|\underline{a}| |\underline{h}|} = \frac{\frac{1}{4}(k^2 - b^2)}{a \left[\frac{1}{2}(k^2 - 2a^2 + b^2) \right]^{\frac{1}{2}}}$$

$$\text{i.e. } U = 2(2)^{\frac{1}{2}} \cos \underline{a}^{\underline{h}} = \frac{(k^2 - b^2)}{a(k^2 - 2a^2 + b^2)^{\frac{1}{2}}} = v t w$$

$$\text{Therefore } v = k^2 - b^2 = (12,036)^2 - (9,801)^2 = 48,8057$$

$$t = a^{-1} = (6,431)^{-1} = 0,155497$$

$$w = (k^2 - 2a^2 + b^2)^{-\frac{1}{2}} = [(12,036)^2 - 2(6,431)^2 + (9,801)^2]^{-\frac{1}{2}}$$

$$= (158,209)^{-\frac{1}{2}} = 0,079503$$

Hence

$$U = v t w = \frac{-48,8057}{6,431 (158,209)^{\frac{1}{2}}} = 0,603359$$

$$\text{and } \cos \underline{a^*h} = U/2(2)^{\frac{1}{2}} = 0,213320$$

$$\underline{a^*h} = 77,68 \pm 0,04^\circ.$$

The reciprocal cell lengths can now be converted from mm (on film) to \AA^{-1}) using

$$d^*(\text{\AA}^{-1}) = x(\text{mm})/R\lambda$$

$$= x(\text{mm})/60,00 \times 1,5418$$

$$= x(\text{mm})/92,508$$

$$\text{e.g. } a^* = 6,431 \pm 0,003 \text{ mm} = \frac{6,431}{92,508} \pm \frac{0,003}{92,508} \text{\AA}^{-1}$$

$$= 0,06952 \pm 0,00003 \text{\AA}^{-1}.$$

TABLE 4.8 Comparison of r.l. parameters (photography and diffractometry)

Parameter	Value from		Difference
	Photography	Diffractometry	
$a^*(\text{\AA}^{-1})$	$0,06952 \pm 0,00003$	0,06974	-0,00022
$b^*(\text{\AA}^{-1})$	$0,08430 \pm 0,00006$	0,08421	0,00009
$c^*(\text{\AA}^{-1})$	$0,09614 \pm 0,00004$	0,09629	-0,00015
$\alpha^*(^\circ)$	$74,20 \pm 0,08$	74,20	0,00
$\beta^*(^\circ)$	$77,68 \pm 0,04$	77,66	0,02
$\gamma^*(^\circ)$	$81,86 \pm 0,06$	82,05	-0,19

In Table 4.8 the reciprocal lattice parameters calculated from the photographs are compared with values obtained on the CSIR diffractometer. The agreement is good. The largest difference of angles is $0,19^\circ$ for γ^* and the largest difference in lengths is $0,00022 \text{ \AA}^{-1}$ for a^* . These differences are larger than the estimated errors. If we assume that the diffractometer values are more accurate, then the estimated errors appear to be too low by a factor of about 3. Unfortunately no errors were supplied with the diffractometer values.

The volume V^* of the reciprocal unit cell was found to be

$$V^* = a^*b^*c^*(1 - \cos^2\alpha^* - \cos^2\beta^* - \cos^2\gamma^* + 2\cos\alpha^*\cos\beta^*\cos\gamma^*)^{\frac{1}{2}}$$

$$= 5,2756 \times 10^{-4} \text{ \AA}^{-3}$$

4.2.3 REAL (DIRECT SPACE) UNIT CELL PARAMETERS

Direct lattice parameters were calculated from the reciprocal lattice parameters as follows (diffractometer values in parentheses):

$$a = b^*c^* \sin \alpha^*/V^* = 14,782 \text{ \AA} \quad (14,732 \text{ \AA})$$

$$b = a^*c^* \sin \beta^*/V^* = 12,376 \text{ \AA} \quad (12,386 \text{ \AA})$$

$$c = a^*b^* \sin \gamma^*/V^* = 10,995 \text{ \AA} \quad (10,982 \text{ \AA})$$

$$\alpha = \cos^{-1} \left[\frac{\cos \beta^* \cos \gamma^* - \cos \alpha^*}{\sin \beta^* \sin \gamma^*} \right] = 104,49^\circ \quad (104,52^\circ)$$

$$\beta = \cos^{-1} \left[\frac{\cos \alpha^* \cos \gamma^* - \cos \beta^*}{\sin \alpha^* \sin \gamma^*} \right] = 100,57^\circ \quad (100,64^\circ)$$

$$\gamma = \cos^{-1} \left[\frac{\cos \alpha^* \cos \beta^* - \cos \gamma^*}{\sin \alpha^* \sin \beta^*} \right] = 95,10^\circ \quad (94,89^\circ)$$

$$V = 1/V^* = 1896,6 \text{ \AA}^3.$$

The parameters obtained using the diffractometer were however used in preference to the above values for the structure determination.

4.3 DETERMINATION OF THE NUMBER OF MOLECULES IN THE UNIT CELL

The density of the crystal was determined as described in Chapter 3.

Table 4.9 gives details of the measurement.

TABLE 4.9 Specific gravity determination. m_b is the mass of bottle + stopper, m_c the mass of the bottle + stopper + CsCl solution, m_w the mass of the bottle + stopper + H_2O . (The masses are given in g). S.G. - specific gravity.

m_b	m_c	m_w	$m_c - m_b$	$m_w - m_b$	S.G. $= \frac{m_c - m_b}{m_w - m_b}$
10,0483	27,1396	19,9593	17,0913	9,9110	1,724
10,0462	27,2809	19,9519	17,2347	9,9057	1,740

The determination was done at about 25°C for which the density of H_2O is 0,997 g/cm³. The average value of the specific gravity of the crystal is thus 1,732 ± 0,020. The density of the crystal is $\rho = 0,997 \times 1,732 = 1,727 \pm 0,020$ gm/cm³.

The molecular mass of RUCOPNP was calculated to be 996,76 u. The mass absorption coefficients ($\frac{\mu}{\rho}$) for RUCOPNP for $CuK\alpha$ and $MoK\alpha$ radiation are 63,51 cm²g⁻¹ and 7,414 cm²g⁻¹ respectively. Table 4.10 shows the details for the calculations. The mass absorption coefficients for the elements Ru, C, O, H, P, N, are listed in International Tables for X-ray Crystallography, Vol. IV (Ref. 11, p. 61-66).

TABLE 4.10 Calculation of molecular mass and mass absorption coefficients for RUCOPNP. For radiation of wavelength λ the mass absorption coefficient for a substance consisting of n elements is defined as $(\frac{\mu}{\rho})_{\lambda} = \frac{\sum_{i=1}^n x_i (\frac{\mu}{\rho})_{i,\lambda}}{\sum_{i=1}^n x_i}$ where x_i is the mass fraction and $(\frac{\mu}{\rho})_{i,\lambda}$ is the mass absorption coefficient for each element i of the substance.

Element	No. of atoms	Atomic mass A (u)	nA = M (u)	$x_i = \frac{nA}{\sum nA}$	$(\frac{\mu}{\rho})_{i,CuK\alpha}$ (cm ² /g)	$x_i (\frac{\mu}{\rho})_{i,CuK\alpha}$ (cm ² /g)	$(\frac{\mu}{\rho})_{i,MoK\alpha}$ (cm ² /g)	$x_i (\frac{\mu}{\rho})_{i,MoK\alpha}$ (cm ² /g)
Ru	3	101,07	303,21	0,30420	180,8	54,999	21,33	6,4886
C	36	12,01115	432,4014	0,433807	4,219	1,8302	0,5348	0,2320
O	10	15,9994	159,994	0,160514	11,03	1,770	1,147	0,1841
H	25	1,00797	25,19925	0,025281	0,3912	0,0099	0,3737	0,0094
P	2	30,9738	61,9476	0,062149	77,28	4,8029	7,870	0,4887
N	1	14,0067	14,0067	0,014052	7,142	0,1004	0,7898	0,0111
			<u>Σ 996,76</u>			<u>Σ 63,51</u>		<u>Σ 7,414</u>

The volume V of the unit cell is $V = 1896,6 \text{ \AA}^3$.

The number of molecules, Z , in the unit cell is

$$Z = \frac{0,60226 \times \rho(\text{g/cm}^3) \times V(\text{\AA}^3)}{M(\text{u})}$$

$$= \frac{0,60226 \times 1,727 \times 1896,6}{996,758}$$

$$= 1,979.$$

$$\sim 2.$$

Using $Z = 2$, the density can be calculated as

$$\rho_{\text{calc}} = \frac{ZM}{0,60226 V} = 1,745 \text{ g cm}^{-3}$$

4.4 OPTIMUM THICKNESS OF CRYSTAL FOR INTENSITY MEASUREMENT (Ref. 3, p. 68)

The so-called optimum thickness t_{opt} of the crystal is the thickness for which the reflected intensity is a maximum, and is given by the formula

$$t_{\text{opt}} = \frac{2}{\mu} = \frac{2}{\rho \cdot \left(\frac{\mu}{\rho}\right)}$$

For $\text{CuK}\alpha$, $t_{\text{opt}} = 0,018 \text{ cm} \sim 0,2 \text{ mm}$

$\text{MoK}\alpha$, $t_{\text{opt}} = 0,155 \text{ cm} \sim 1,6 \text{ mm}.$

4.5 SUMMARY OF CRYSTAL DATA

The crystal data are summarized in Table 4.11

TABLE 4.11. Crystal data determined by photography

System	: Triclinic $a = 14,732 \text{ \AA}$, $b = 12,386 \text{ \AA}$, $c = 10,982 \text{ \AA}$		
	: $\alpha = 104,53^\circ$, $\beta = 100,64^\circ$, $\gamma = 99,89^\circ$		
Formula	: $\text{Ru}_3(\text{CO})_{10}(\text{C}_6\text{H}_5)_2\text{PN}(\text{C}_2\text{H}_5)\text{P}(\text{C}_6\text{H}_5)_2$		
V	: $1888,13 \text{ \AA}^3$		
ρ_{meas}	: 1,727	ρ_{calc}	: 1,745
M	: 996,76 u		
Z	: 2		
Space group:	P1 or $\bar{P}1$		
$\left(\frac{\mu}{\rho}\right)_{\text{CuK}\alpha}$: 63,51 cm^2/g	$t_{\text{opt}}(\text{CuK}\alpha)$	= 0,2 mm
$\left(\frac{\mu}{\rho}\right)_{\text{MoK}\alpha}$: 7,414 cm^2/g	$t_{\text{opt}}(\text{MoK}\alpha)$	= 1,6 mm

CHAPTER FIVE

INTENSITY MEASUREMENT

5.1 IDENTIFICATION OF CRYSTAL HABIT

The original r.l. vectors \underline{a} , \underline{f} , \underline{h} were renamed $-\underline{a}^*$, \underline{b}^* , $-\underline{c}^*$ respectively. The crystals formed needles and the needle axis was perpendicular to the r.l. plane observed in the deJong-Bouman photograph (film 105 - Fig. 4.3). The r.l. vectors visible on this film \underline{b} , \underline{i} and \underline{g} were normal to the real lattice planes which formed the prismatic faces of the crystal. In order to identify these planes \underline{b} , \underline{i} and \underline{g} had to be written in terms of the unit vectors chosen:

$$\begin{aligned} \underline{b} &= \underline{h} - \underline{a} = -\underline{c}^* + \underline{a}^* & \text{i.e. } \underline{b} & \text{ is a r.l. vector } 10\bar{1} \\ \underline{i} &= \underline{h} + \underline{f} = -\underline{c}^* + \underline{b}^* & \text{" } \underline{i} & \text{ " " " " } 01\bar{1} \\ \underline{g} &= \underline{a} + \underline{f} = -\underline{a}^* + \underline{b}^* & \text{" } \underline{g} & \text{ " " " " } \bar{1}10 \end{aligned}$$

The r.l. vector $10\bar{1}$ is perpendicular to a real lattice plane i.e. to a face of the crystal, viz. the $10\bar{1}$ plane and this is the plane that is horizontal when \underline{b} is vertical, i.e. for azimuth 84° .

In Table 5.1, the angles between the vectors on the film are compared with the angles between the crystal faces as measured by observing optical reflections in the microscope. The agreement is good.

The needle axis is a real lattice vector, $\underline{n} = x\underline{a} + y\underline{b} + z\underline{c}$ such that \underline{n} is normal to the reciprocal lattice vectors describing the zone of planes making up the prismatic faces of the crystal. \underline{n} is the zone axis of the planes $(10\bar{1})$, $(01\bar{1})$, $(\bar{1}10)$. Therefore

$$\underline{n} \cdot (\text{r.l. vector } 10\bar{1}) = 0 \quad \text{i.e.} \quad (x\underline{a} + y\underline{b} + z\underline{c}) \cdot (1\underline{a}^* + 0\underline{b}^* - 1\underline{c}^*) = 0.$$

Using the relationships $\underline{a} \cdot \underline{a}^* = 1$ and $\underline{a} \cdot \underline{b}^* = 0$, etc. this reduces to

Table 5.1 Comparison of angles on deJong-Bouman (film 105) and angles between crystal surfaces

Angle between vectors from deJong Bouman (film 105) (°)	Angle between planes (from Maltese cross positions) (°)	Difference $\Delta\theta$ (°)
$\underline{b}^* \wedge \underline{i}^* = 55,8$	$\angle(10\bar{1}, 01\bar{1}) = 55,1$	0,7
$\underline{i}^* \wedge \underline{g}^* = 60,5$	$\angle(01\bar{1}, \bar{1}10) = 60,8$	0,3
$\underline{b}^* \wedge \underline{g}^* = 63,4$	$\angle(10\bar{1}, \bar{1}10) = 63,8$	0,4

$$x(\underline{a} \cdot \underline{a}^*) - z(\underline{c} \cdot \underline{c}^*) = x - z = 0 \quad \text{i.e.} \quad x = z.$$

Similarly

$$\underline{n} \cdot (01\bar{1}) = 0 \quad \text{i.e.} \quad y - z = 0 \quad \text{and} \quad y = z$$

$$\underline{n} \cdot (\bar{1}10) = 0 \quad \text{i.e.} \quad -x + y = 0 \quad \text{and} \quad x = y.$$

Thus the needle axis is a vector $k(\underline{a} + \underline{b} + \underline{c})$ where k is a constant, i.e. it is in the direction (111) of the real lattice.

Hence the habit of crystals can be described as follows: the crystals form needles with the (111) direction as the needle axis and the side faces are the planes $(10\bar{1})$, $(01\bar{1})$ and $(\bar{1}10)$.

5.2 CHOICE OF CRYSTAL FOR INTENSITY MEASUREMENT

Two crystals RUCOPNP(6) and RUCOPNP(8) with maximum length 0,375 mm were each attached to the ends of fine glass rods and mounted on special holders (of shape and size prescribed by the CSIR). These were sent for intensity measurement. Fig. 5.1 shows a diagram of RUCOPNP(6) not exactly drawn to scale. Also shown in the figure are normals to the prismatic faces identified as vectors in the related reciprocal lattice.

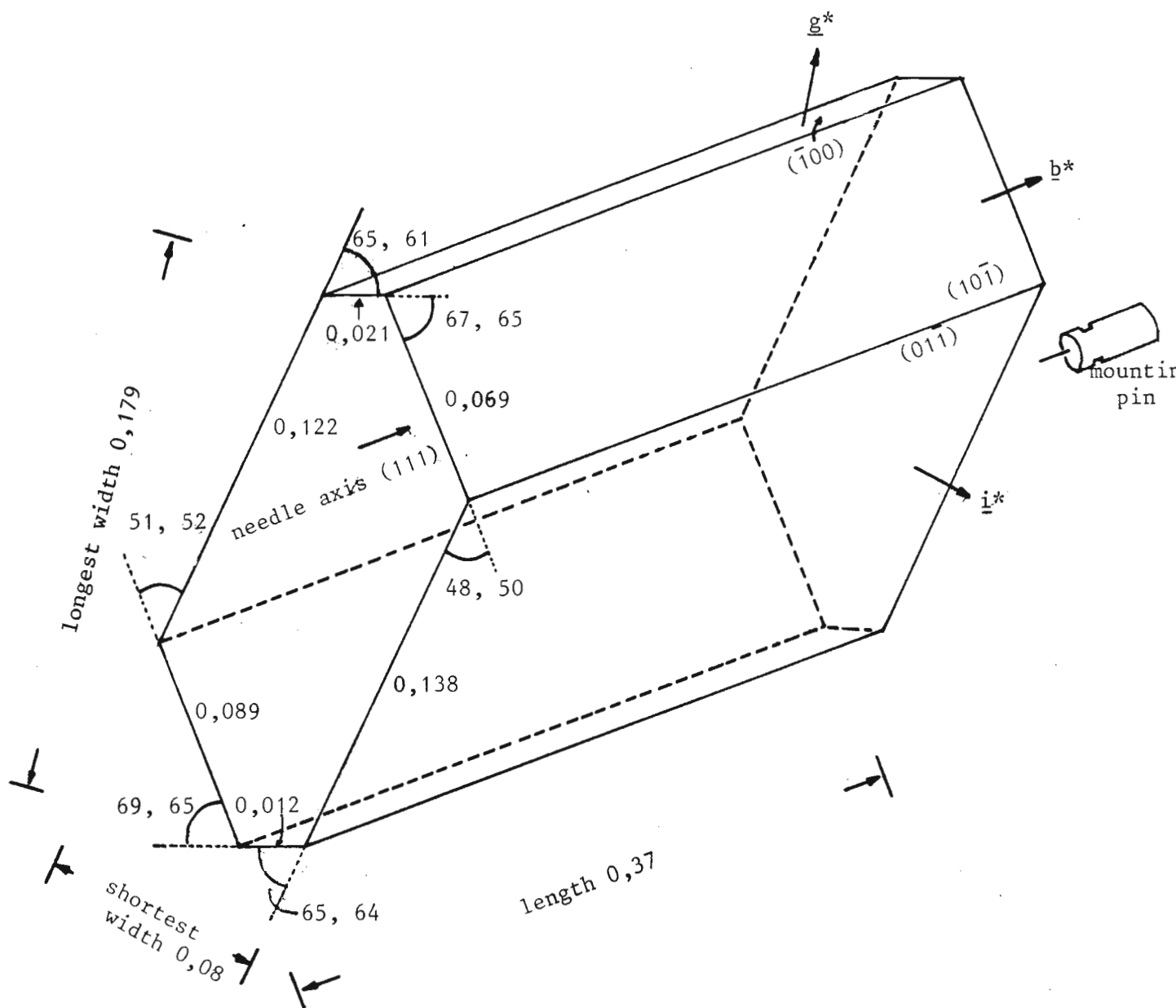


Fig. 5.1 Diagram of crystal RUCOPNP(6). All lengths are in mm and angles in $^{\circ}$. Each angle was measured twice independently and both values are given.

5.3 INTENSITY DATA FROM CSIR

Crystal RUCOPNP(6) of dimensions 0,370 x 0,179 x 0,080 mm was used to collect intensities and measure accurate cell parameters. 5295 reflections were measured by the ω scan technique between 3° and $23^{\circ} 2\theta$. A scan speed of $0,5^{\circ} 2\theta \text{ s}^{-1}$ and a scan width of $1,3^{\circ}$ were employed. The background was counted for half the scanning time on both sides of each reflection. There were 1365 unobserved reflections according to

the criterion $I < 1,65 \sigma(I)$ where $\sigma(I) = \left[(0,02)^2 + S + B \right]^{\frac{1}{2}}$ where S is the scan count and B the background count. Corrections for Lorentz and polarization effects were applied, but no absorption correction was made. Three strong reference reflections - (6 1 1), (-7 -1 2) and (-1 -1 3) - measured periodically throughout the data collection indicated no crystal decomposition.

A sample calculation on the intensity data for reflection 300 to illustrate how the various quantities in the computer list were determined is shown below.

The corrected intensity I is given by

$$I = P - B1 - B2 = 3200 - 282 - 236 = 2682$$

where P is the intensity count of the 300 reflection. B1, B2 are two background counts taken at angles $2\Delta \sim 1,5^\circ$ about the peak position.

The error in I due to counting statistics is $\sigma(I)_{\text{stat.}} = \left[(\sigma(P))^2 + (\sigma(B1))^2 + (\sigma(B2))^2 \right]^{\frac{1}{2}}$ where the statistical error is $\sigma(N) = N^{\frac{1}{2}}$ on the number of counts N.

$$\begin{aligned} \text{Therefore } \sigma(I)_{\text{stat}} &= (3200 + 282 + 236)^{\frac{1}{2}} \\ &= 60,98 \end{aligned}$$

The error in I is made up of two parts: 1) the statistical error due to counting, $\sigma(I)_{\text{stat}}$, above; 2) the error due to the count of the primary X-ray beam not being constant at all times: this is taken as 2% of I.

$$\begin{aligned} \text{Therefore } \sigma(I) &= \left[(\sigma(I)_{\text{stat}})^2 + (0,02 I)^2 \right]^{\frac{1}{2}} \\ &= \left[(60,98)^2 + (0,02 \times 2682)^2 \right]^{\frac{1}{2}} \\ &= 81. \end{aligned}$$

$$\text{Hence } I = 2682 \pm 81,2$$

Now the observed intensity $I_o = I_{rel} = \frac{I}{Lp}$ = where Lp is the Lorentz polarization factor.

$$\text{Hence } I_{rel} = I_o = \frac{I}{Lp} = \frac{2682}{6,759} \pm \frac{81,2}{6,759} = 396,8 \pm 12,02$$

The observed structure factor $F_o = F_{rel} = (I_{rel})^{\frac{1}{2}} = 396,8^{\frac{1}{2}} = 19,92$,

$$\text{and } \sigma(F_{rel}) = \frac{1}{2} \sigma(I_{rel}) / I_{rel}^{\frac{1}{2}} = \frac{1}{2} \times 12,02 / 19,92 = 0,30.$$

CHAPTER SIX

STRUCTURE DETERMINATION - THEORY

6.1 RELATIONSHIP BETWEEN ELECTRON DENSITY FUNCTION AND STRUCTURE FACTORS

A crystal contains atoms arranged in a repetitive three-dimensional pattern. The solution of a crystal structure depends upon recombining, mathematically, the diffracted X-ray beams to synthesize an image of the molecular structure producing the diffraction.

The 3-dimensional periodic electron density $\rho(x,y,z)$ in a crystal can be represented by the three-dimensional Fourier series (see Ref. 12, p. 11):

$$\rho(x,y,z) = \sum_{h'} \sum_{k'} \sum_{l'} C(h'k'l') \exp 2\pi i(h'x + k'y + l'z) \quad (6.1)$$

where h' , k' , l' are integers with values from $-\infty$ to $+\infty$, and x , y , z are fractions of the period related to a set of axes. $C(h'k'l')$ are the Fourier coefficients.

Diffraction theory shows that the scattering amplitude due to the contents of the unit cell of a crystal depends on a factor:

$$F(hk\ell) = \int_V \rho(x,y,z) \exp 2\pi i(hx + ky + \ell z) \, dV, \quad (6.2)$$

the integral being taken over the volume of one unit cell. This is called the structure factor of the reflection with Miller indices $hk\ell$.

Combination of equations (6.1) and (6.2) leads to an expression which contains a periodic exponential:

$$F(hk\ell) = \int_V \sum_{h'} \sum_{k'} \sum_{l'} C(h'h'l') \exp 2\pi i[(h + h')x + (k + k')y + (\ell + \ell')z] \, dV \quad (6.3)$$

It can be shown that the integral over one unit cell is zero (Réf. 12, p. 11) except when $h' = -h$, $k' = -k$ and $l' = -l$, when the periodicity disappears.

$$\text{Then} \quad F(hk\ell) = V C(\overline{h\overline{k}\overline{\ell}}) \quad (6.4)$$

$$\text{i.e.} \quad C(\overline{h\overline{k}\overline{\ell}}) = \frac{1}{V} F(hk\ell).$$

Equation (6.1) then becomes

$$\rho(x,y,z) = \frac{1}{V} \sum_h \sum_k \sum_\ell F(hk\ell) \exp[-2\pi i (hx + ky + lz)] \quad (6.5)$$

Equations (6.2) and (6.5) describe the reciprocal relationship of the Fourier transforms. Equation (6.2) gives the structure factors in reciprocal space in terms of the electron density in real space. Equation (6.5) gives the electron density in real space in terms of the structure factors in reciprocal space. The structure factors are described as the Fourier transform of the electron density, and the converse is also true.

The calculation of the integral in (6.2) can be abbreviated by considering the electron density to be made up of discrete atoms each with a spherically symmetric distribution of electron density. The integral of electron density over the volume of an atom is available in tables (Ref. 11, p. 71) for each type of atom and is called the atomic scattering factor f :

$$f = \int_V \rho(x'y'z') \exp 2\pi i (hx' + ky' + lz') \, dV \quad (6.6)$$

where $x'y'z'$ are positional co-ordinates relative to the centre of the atom.

Now the integral for the structure factor simplifies to a sum over the atoms in the unit cell:

$$F(hk\ell) = \sum_j f_j \exp 2\pi i (hx_j + ky_j + lz_j) \quad (6.7)$$

where x_j , y_j and z_j are the co-ordinates of the centre of the j^{th} atom.

6.2 THE PHASE PROBLEM

Consider equation (6.5):

$$\rho(x,y,z) = \frac{1}{V} \sum_h \sum_k \sum_\ell F(hk\ell) \exp[-2\pi i(hx + ky + lz)] \quad (6.5)$$

The solution of crystal structures, i.e. the determination of ρ , requires a knowledge of $F(hk\ell)$. The structure factor $F = |F| e^{i\phi}$ consists of the amplitude of F and a phase angle ϕ . To calculate ρ we need both $|F|$ and ϕ . $|F|$ is obtained from the observed intensity ($|F| = kI^{\frac{1}{2}}$). The phase however is not an observable quantity. The phase problem of crystal structure analysis is to find methods to deduce the phases.

6.3 THE FOURIER METHOD

In order to apply the Fourier method, some trial structure is needed to begin with, i.e. the co-ordinates of some of the atoms (partial structure) must be located by some other means, e.g. a Patterson synthesis as described in section 6.4.1).

A structure factor calculation using the atom co-ordinates of the partial structure yields structure factor amplitudes $|F(hk\ell)|_{\text{calc}}$ and phases ϕ_{calc} for the partial structure. A Fourier synthesis is now done using the observed structure factor magnitudes $|F_o|$ and the calculated phases ϕ_{calc} - this yields an improved structure giving the positions of other atoms in the structure which may be identified by the chemistry of the structure. A second structure factor calculation using the positions of the new atoms and the original atoms yields improved phases and again using $|F_o|$ and ϕ_{calc} more atoms are found. This procedure is repeated until all the atoms in the structure are found.

6.4.1 THE PATTERSON SYNTHESIS

A solution for the phase problem was put forward by Patterson. Instead of the structure factors F , the squares of the $|F|$'s are used as the coefficients of the Fourier series. These $|F|$'s are phaseless and readily measurable since they are proportional to the observed intensities. A Patterson synthesis calculated using the observed intensities may not solve the structure completely but is very useful in providing a starting point in the form of a partial structure leading to the solution of the structure.

Patterson defined a function $P(uvw)$:

$$P(uvw) = V \int_0^1 \int_0^1 \int_0^1 \rho(xyz) \rho(x+u, y+v, z+w) dx dy dz \quad (6.8)$$

- a product of two electron densities at a pair of points a vector u, v, w apart, and the integral is taken over all pairs of points in the unit cell. As ρ is large at positions occupied by atoms, peaks in this function will be related to vectors between atoms in the unit cell.

Recall, the Fourier expression for the electron distribution

$$\rho(x,y,z) = \frac{1}{V} \sum_h \sum_k \sum_l F(hk\ell) \exp[-2\pi i(hx + ky + \ell z)] \quad (6.5)$$

From equations (6.8) and (6.5), it can be shown (Ref. 12, p. 13) that

$$P(uvw) = \frac{1}{V} \sum_h \sum_k \sum_{\ell=-\infty}^{\infty} |F(hk\ell)|^2 \exp 2\pi i(hx + ky + \ell z) \quad (6.9)$$

The quantities $|F|^2$ are directly derivable from the X-ray intensities and so the series can be summed. There are no phases involved. Furthermore, it can be shown (Ref. 12, p. 14) that $P(uvw)$ is real for all values of u, v and w :

$$P(uvw) = \frac{1}{V} \sum_h \sum_k \sum_{\ell=-\infty}^{\infty} |F(hk\ell)|^2 \cos 2\pi(hu + kv + \ell w). \quad (6.10)$$

6.4.2 CHARACTERISTICS OF A PATTERSON VECTOR MAP

A three-dimensional synthesis provides a vector map of the contents of the unit cell of the crystal. The function will have peaks where uvw represents a vector between two atoms. The following characteristics are displayed by a Patterson vector map:

1. Every pair of atoms in the unit cell will produce a peak in the vector map. Therefore, if there are N atoms in the unit cell there will be N^2 peaks in the vector map, corresponding to the N possible vectors which can be drawn from each of the N atoms.
2. N of these peaks will be of zero length corresponding to the vector between each atom and itself and these occur as a very large peak at the origin of the vector map. There are therefore, $N^2 - N = N(N - 1)$ non-origin peaks.
3. The unit cell of the Patterson function has the same dimensions as that of the crystal and the peaks will be obviously much more densely packed in the unit cell and there is generally a good deal of overlap among them. The overlapping is further enhanced by the fact that the peaks in the Patterson function are wider than in the the electron density function. This is illustrated in Fig. 6.1. The distribution of vector density over the Patterson peak P corresponds to a summation of all vectors between elements of electron density in the two atomic peaks. S_1 and S_2 (of same length) contribute to the maximum of P . S_3 and S_4 (difference twice atomic width) determine its outer limits. Therefore the maximum width of P is twice that of A .

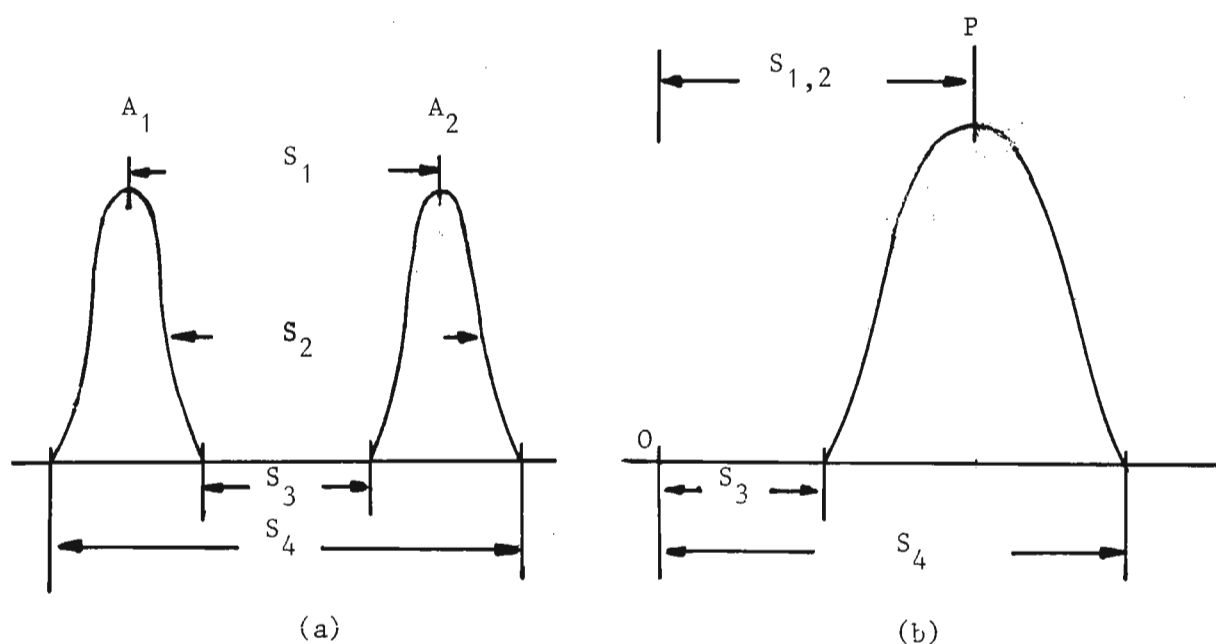


Fig. 6.2 The electron density function of two atoms.

(a) Two atoms.

(b) Patterson peak resulting from atoms in (a). The origin peak is not shown.

4. The symmetry of the unit cell of a crystal can be described by one of the 230 space groups. Only 24 space groups are needed to describe the possible symmetry of a vector map.
5. A peak in the Patterson function between atoms of atomic numbers Z_1 and Z_2 will have a weight $Z_1 \cdot Z_2$. (The weight is the volume integral inside the peak, i.e. $\int_V \rho_{12}(r) dV = Z_1 Z_2$). As the weight of the Patterson peak is $Z_1 \cdot Z_2$, peaks between two heavy atoms will be much larger than heavy-light and light-light atom vectors. It is this fact which allows the heavy atom vectors to be recognised in the Patterson, usually without difficulty, as a start to solving the crystal structure. This is the basis of the so-called "heavy atom method".
6. The Patterson function is centro-symmetric. The vector from atom 1 to atom 2 is related to the vector from 2 to 1 by a centre of symmetry.

CHAPTER SEVENSTRUCTURE DETERMINATION OF RUCOPNP

7.1.1 APPLICATION OF HEAVY ATOM METHOD

The proposed structure of the molecule has 3 heavy atoms, namely Ru with $Z = 44$. The heavy atom method was used to determine the positions of the three Ru atoms. (The next heaviest atom is phosphorus, $Z = 15$).

7.1.2 CALCULATION OF PATTERSON SYNTHESIS

A Patterson synthesis was calculated using the crystal data for RUCOPNP with the help of the program SHELX77 by George Sheldrick⁽¹³⁾. The program and the instruction cards used in this project are described in Appendix 3. The FMAP subroutine was used to calculate the Patterson function for a grid of points and search the grid for peaks giving an output of Patterson peak positions in order of height. The MERG subroutine (MERG -1) was used to put the reflections on an absolute scale. The scale factor obtained was 2,89913 and the overall temperature factor 0,100. The Patterson function was mapped with the FMAP -1 option. The function was calculated for half the unit cell, $x: 0 - 1$, $y: 0 - 0,5$, $z: 0 - 1$. The grid increments were chosen as 0,02 in all directions. The input was similar to that for Fourier 1 shown in Table 7.4. Of 5295 reflections that were supplied 125 were rejected by the program. No further reflections were omitted. The program found 131 independent peaks.

7.1.3 TRANSFORMATION MATRIX - SKEW TO ORTHOGONAL

The unit cell is triclinic - therefore the peak positions are given in skew co-ordinates. In order to draw and visualize the Patterson peaks

easily, the skew co-ordinates were transformed into orthogonal co-ordinates. The transformation equations in matrix form are:

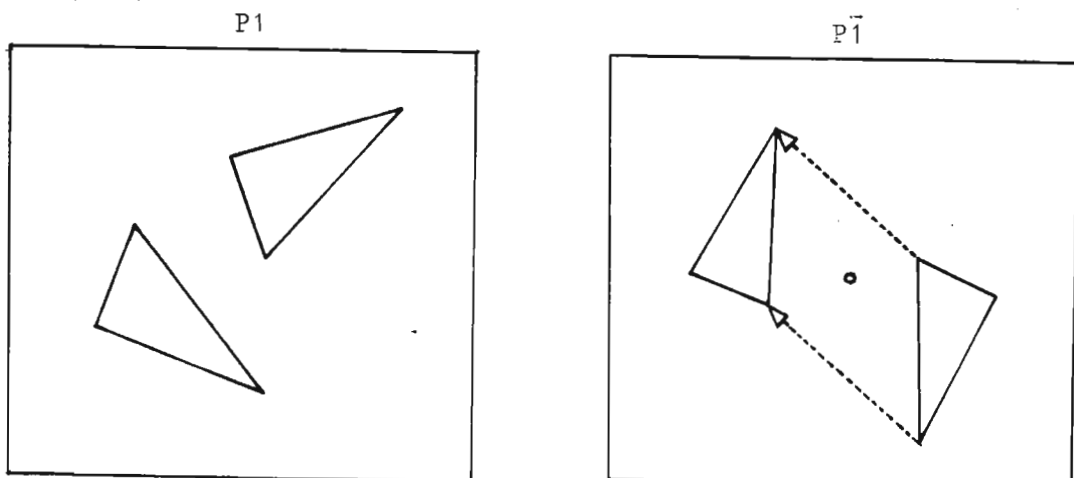
$$\begin{bmatrix} u \\ v \\ w \end{bmatrix} = \begin{bmatrix} 14,732 & -1,056 & -2,028 \\ 0 & 12,341 & -2,938 \\ 0 & 0 & 10,385 \end{bmatrix} \begin{bmatrix} x \\ y \\ z \end{bmatrix} = A \begin{bmatrix} x \\ y \\ z \end{bmatrix}$$

where x , y and z are the fractional coordinates in terms of skew axes and u , v and w the rectangular coordinates in Å. The transformation equations are deduced in Appendix 2.

7.1.3 DISTINCTION BETWEEN $P1$ AND $P\bar{1}$

Consider the heaviest atoms only. There are 6 Ru atoms at positions \underline{r}_i in the unit cell. Therefore there will be $6^2 = 36$ peaks in the Patterson at positions $\underline{r}_i - \underline{r}_j$. 6 will be at the origin ($i = j$). Of the other 30 non-origin peaks, 15 will be independent, equal weight peaks and the other 15 will be related by a centre of symmetry, $(\underline{r}_i - \underline{r}_j, \underline{r}_j - \underline{r}_i)$. This will be the case for a non-centric structure.

If the structure is centro-symmetric, some of the 15 peaks will overlap (e.g. the two identical vectors in the $P\bar{1}$ diagram of Fig. 7.1) and there will be 9 distinct peaks (6 double and 3 single).



6 heavy atoms
15 Patterson peaks
(all equal weight)

6 heavy atoms
9 Patterson peaks
(6 double, 3 single)

Fig. 7.1 Distinction between non-centric and centro-symmetric structures.

The overlap is now investigated in more detail. Let $\underline{r}_1, \underline{r}_2, \underline{r}_3$ be the position co-ordinates of the atoms in one molecule in the centrosymmetric case. The coordinates for the other molecule are $-\underline{r}_1, -\underline{r}_2, -\underline{r}_3$ (see Fig. 7.2).

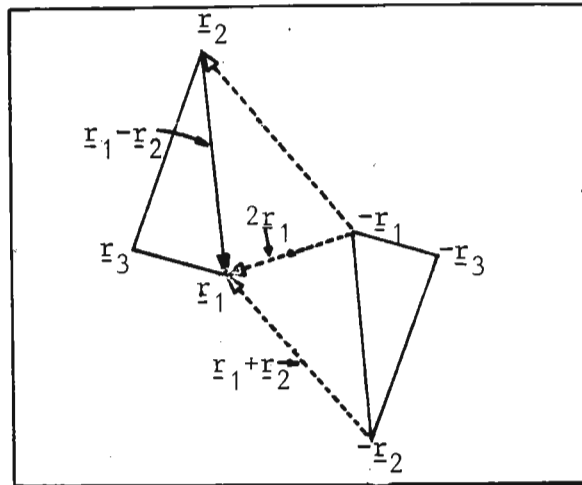


Fig. 7.2 Some representative vectors in a centrosymmetric structure.

Fig. 7.2 shows some representative vectors between atoms. The vectors from \underline{r}_2 to \underline{r}_1 and from $(-\underline{r}_1)$ to $(-\underline{r}_2)$ are identical; therefore, there is a double peak. The weights for $\underline{r}_1 - \underline{r}_2$, $\underline{r}_1 + \underline{r}_2$ and $2\underline{r}_1$ are now illustrated.

$$\begin{aligned} \underline{r}_1 - \underline{r}_2 &= (\underline{r}_1) - (\underline{r}_2) && \text{double peak — inside molecule} \\ &= (-\underline{r}_2) - (-\underline{r}_1) \end{aligned}$$

$$\begin{aligned} \underline{r}_1 + \underline{r}_2 &= (\underline{r}_1) - (-\underline{r}_2) && \text{double peak — between two molecules} \\ &= (\underline{r}_2) - (-\underline{r}_1) \end{aligned}$$

$$2\underline{r}_1 = (\underline{r}_1) - (-\underline{r}_1) \quad \text{single peak — between molecules.}$$

In this way it can be shown (Ref. 14, p. 269) that the Patterson map has

Double peaks at	$\underline{r}_1 - \underline{r}_2$	
	$\underline{r}_1 - \underline{r}_3$	(inside molecules)
	$\underline{r}_2 - \underline{r}_3$	
	$\underline{r}_1 + \underline{r}_2$	
	$\underline{r}_1 + \underline{r}_3$	(between molecules)
	$\underline{r}_2 + \underline{r}_3$	

Single peaks at $2\mathbf{r}_1$
 $2\mathbf{r}_2$ (between molecules)
 $2\mathbf{r}_3$

The problem is to find out whether the structure is $P1$ or $P\bar{1}$, i.e. whether the Patterson has 15 strongest peaks of roughly equal weight or 6 strongest peaks of roughly equal weight. It should be noted that 6 and not 9 strongest peaks are considered.

		Relative weight
A Ru - Ru vector has peak weight	$Z_1 Z_2 = 44^2$ single	1
	$= 44^2 \times 2$ double	2
A Ru - P vector has peak weight	$Z_1 Z_2 = 44 \times 15$ single	0,34
	$2 \times 44 \times 15$ double.	0,68

Therefore a double Ru-P peak is nearly as strong as a single Ru - Ru peak.

A graph of peak height vs peak number (in order of height) was drawn (Fig. 7.3). The graph shows 7 distinct peaks which stand out above the others. This strongly suggests that the structure is $P\bar{1}$. An attempt is now made to correlate 6 of the 7 peaks with the 6 double weight peaks of a centro-symmetric structure rather than the 15 single weight peaks of the acentric structure.

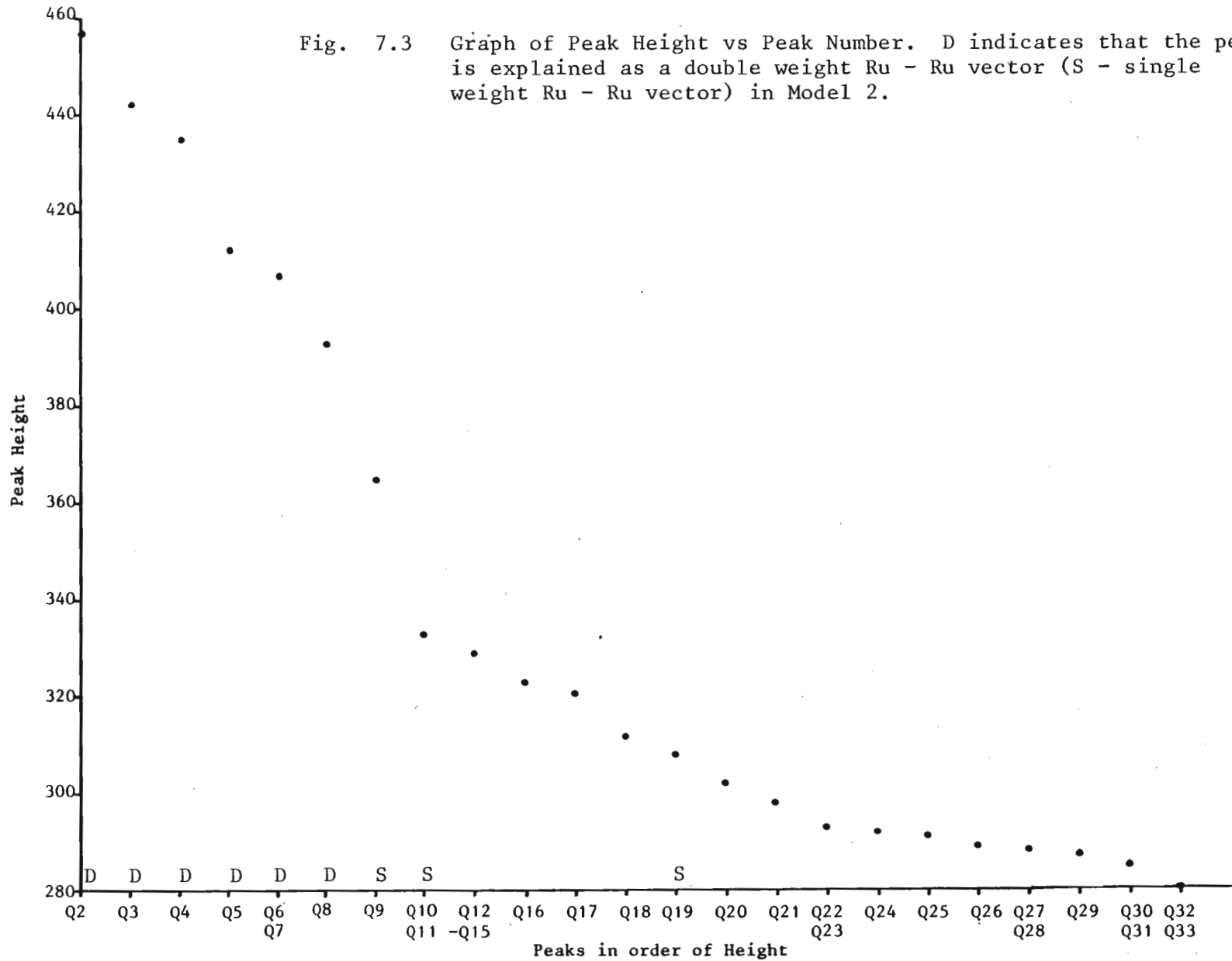
7.1.4 IDENTIFICATION OF HEAVY ATOM PEAKS INSIDE THE MOLECULE

A search was made in the Patterson map for Ru - Ru (double) peaks near the origin with bond distance $\sim 2,9\text{\AA}$. Three vectors Q2, Q4 and Q5 were found close to the origin. These three vectors can be explained as vectors between three Ru atoms at \mathbf{r}_1 , \mathbf{r}_2 and \mathbf{r}_3 as follows:

$$Q2 = \mathbf{r}_2 - \mathbf{r}_1$$

$$Q4 = \mathbf{r}_2 - \mathbf{r}_3$$

$$Q5 = \mathbf{r}_3 - \mathbf{r}_1$$



Thus $Q2 - Q4 = (\underline{r}_2 - \underline{r}_1) - (\underline{r}_2 - \underline{r}_3) = \underline{r}_3 - \underline{r}_1 = Q5$. Table 7.1 shows that the three peaks accurately obey this relationship.

TABLE 7.1 Patterson peaks near the origin. uvw fractional co-ordinates; $u'v'w'$ are rectangular co-ordinates (in \AA) and d the interatomic distance in \AA .

Peak	u	v	w	u'	v'	w'	$d(\text{\AA})$
Q2	-0,017	+0,234	+0,040	-0,578	+2,770	+0,415	2,860
Q4	+0,058	+0,117	-0,181	+1,097	+1,975	-1,879	2,938
Q5	-0,075	+0,119	+0,219	-1,674	+0,825	+2,274	2,941
Q2-Q4	-0,075	+0,117	+0,221				

The vectors Q2, Q4 and Q5 define the shape and orientation of the molecule but not its position. To illustrate the shape let $\underline{r}_1 = (0,0,0)$ (temporarily). Then $\underline{r}_2 = Q2$, $\underline{r}_3 = Q5$ (see Fig. 7.4a, b). The unit cell contains two molecules, the one shown in Fig. 7.4b and the one related to it by the centre of symmetry.

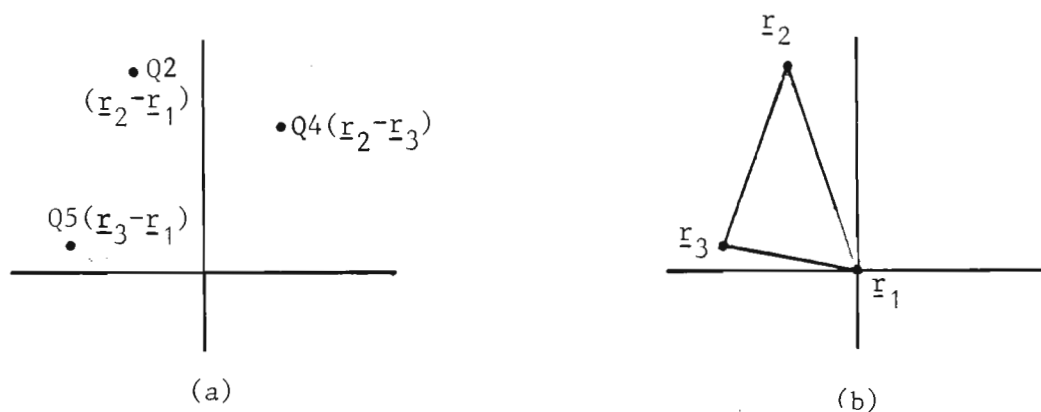


Fig. 7.4 Shape of molecule: (a) Patterson space; (b) Real space.

7.1.5 IDENTIFICATION OF HEAVY ATOM PEAKS BETWEEN MOLECULES

Figs. 7.5 and 7.6 show two possible interpretations of the intermolecular

vectors in Patterson space. The dashed triangles are the molecules in direct space superimposed on the diagram. Note that the central set of peaks (intramolecular vectors) are the same for the two models but that the outer set of vectors (intermolecular vectors) form different patterns. Both models can be adjusted to fit the Patterson peaks optimally by translation of the set of three Ru-atoms keeping their configuration and orientation constant. The co-ordinates of the Ru-atoms are deduced from the models as follows. Assigning vectors to peaks as in Fig. 7.6 gives:

$$Q6 \quad \quad \quad = \underline{r}_1 + \underline{r}_2 = (-0,434, +0,490, +0,228) \quad (a)$$

$$Q3 \quad \quad \quad = \underline{r}_2 + \underline{r}_3 = (-0,359, +0,379, +0,010) \quad (b)$$

$$Q8' = -Q8 + (0, +1,0) = \underline{r}_1 + \underline{r}_3 = (-0,376, +0,606, +0,045) \quad (c)$$

$$(a) - (b): Q6 - Q3 = \underline{r}_1 - \underline{r}_3 \quad (d)$$

$$(d) + (c): \underline{r}_1 = \frac{1}{2}(Q6 - Q3 + Q8')$$

$$\begin{aligned} \text{From (a): } \underline{r}_2 &= Q6 - \underline{r}_1 \\ &= \frac{1}{2}(Q6 + Q3 - Q8') \end{aligned}$$

$$\begin{aligned} \text{From (c): } \underline{r}_3 &= Q8' - \underline{r}_1 \\ &= \frac{1}{2}(Q8' - Q6 + Q3) \end{aligned}$$

Substituting for Q6, Q3 and Q8':

$$\underline{r}_1 = (-0,2255, +0,3585, +0,1315)$$

$$\underline{r}_2 = (-0,2085, +0,1315, +0,0965)$$

$$\underline{r}_3 = (-0,1505, +0,2475, -0,0865).$$

Table 7.3 shows the resulting interpretation of all nine vectors. A similar calculation can be done from Fig. 7.5 giving the interpretation shown in Table 7.2. Table 7.3 gives the best correlation. In this case the double weight vectors corresponding to the six highest peaks in the Patterson and the three single weight vectors correspond to the 7th, 8th and 13th peaks in order of height (i.e. Q9, Q10, Q19). It is likely that the 9th, 10th, 11th and 12th peaks may be Ru-P double weight vectors but

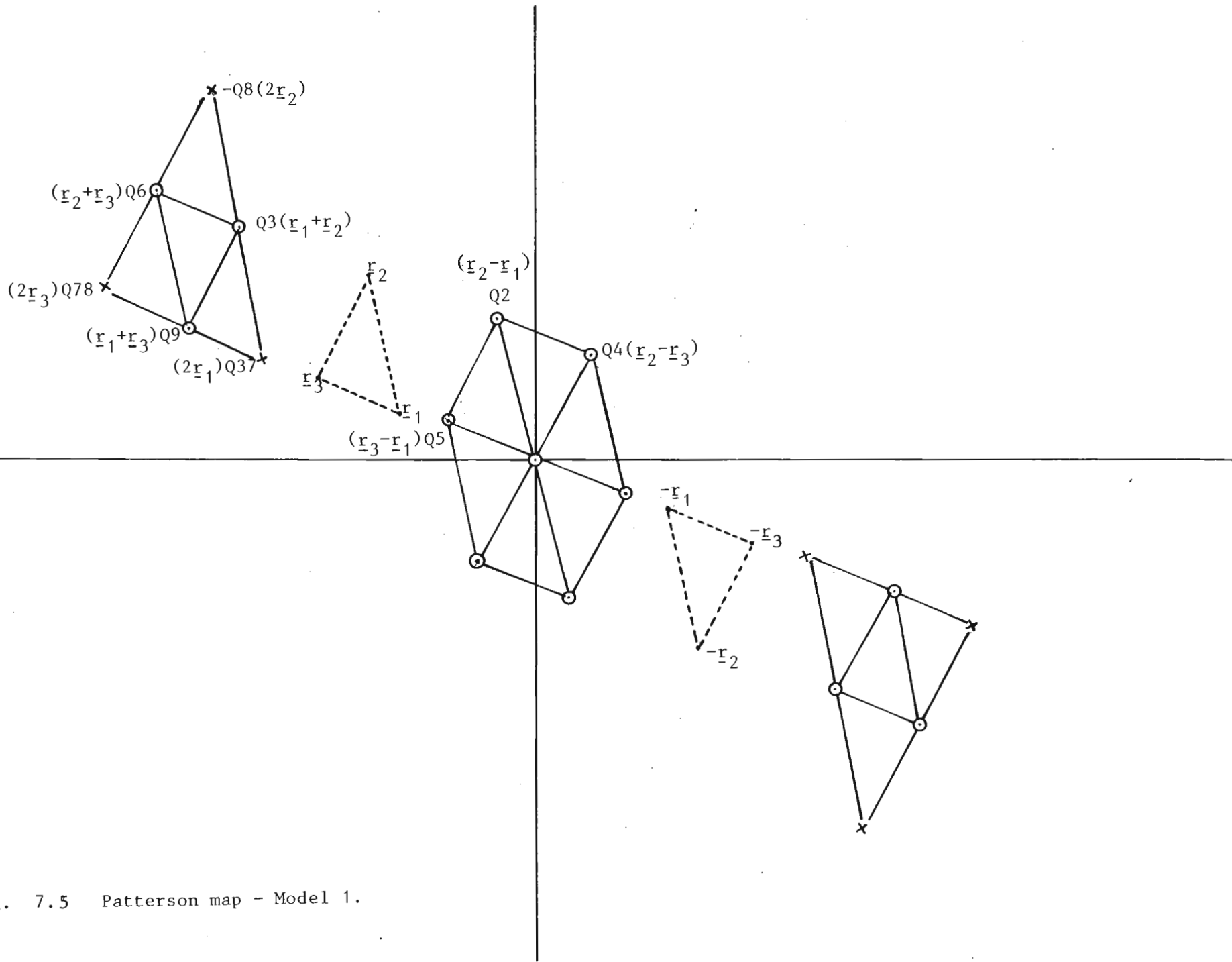


Fig. 7.5 Patterson map - Model 1.

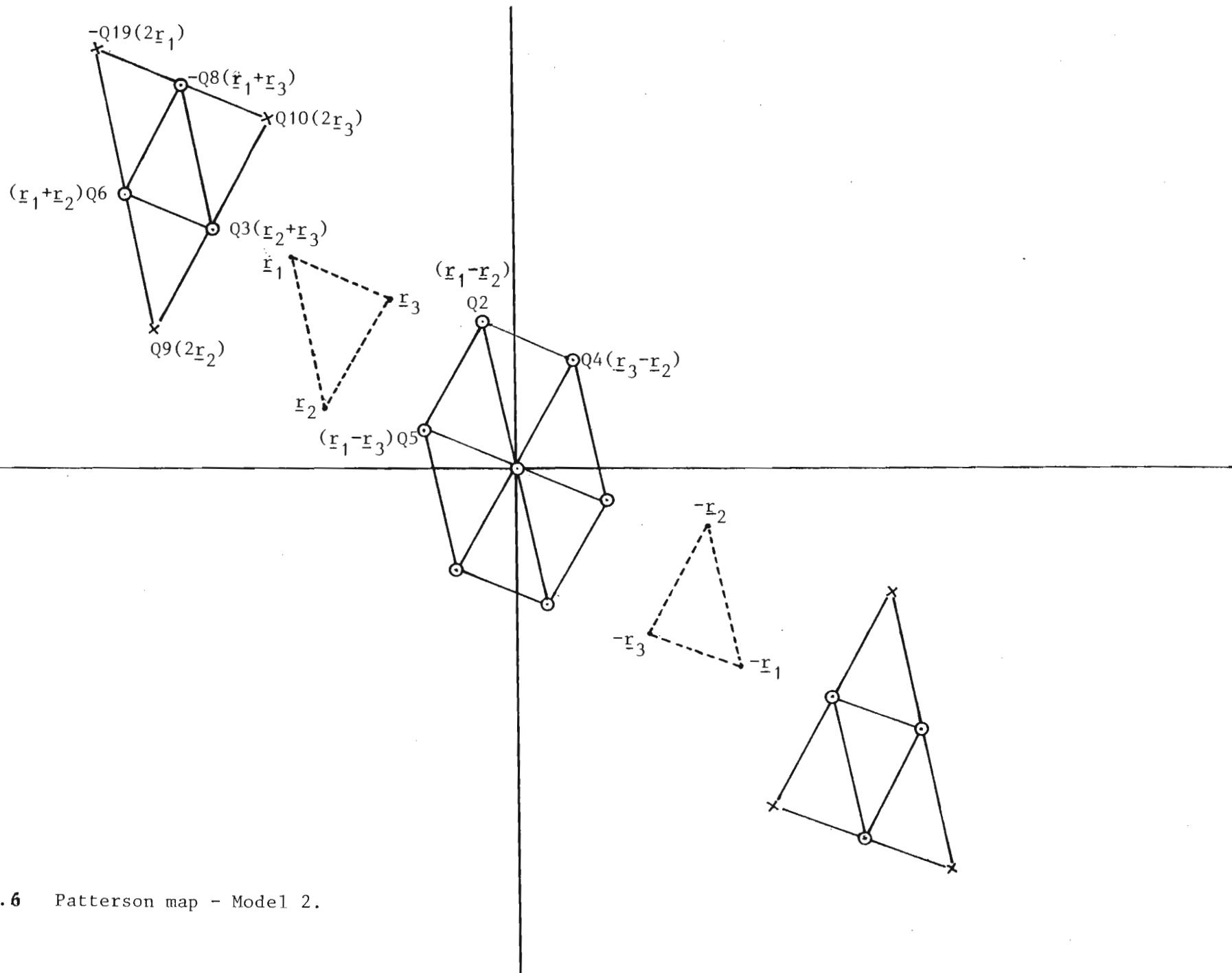


Fig. 7.6 Patterson map - Model 2.

TABLE 7.2 Ru-Ru Patterson Peaks for RUCOPNP (Model 1); D - double peak; S - single peak; r_1, r_2, r_3 are the atomic positions from which the Patterson peaks r_1-r_2 , etc. are calculated; Q2, etc. are the peaks found in the Patterson; * = +(0, +1,0); ** = +(-1,0, 0); Δ = difference between Patterson peak and calculated vector co-ordinate

	Height	x/a	Δ	y/b	Δ	z/c	Δ
r_1		-0,171		+0,075		-0,016	
r_2		-0,187		+0,304		+0,026	
r_3		-0,246		+0,186		+0,202	
D r_1-r_2		+0,016		-0,229		-0,042	
-Q2	457	+0,017	1	-0,234	5	-0,040	2
D r_1-r_3		+0,075		-0,111		-0,218	
-Q5	412	+0,075	0	-0,119	8	-0,219	1
D r_2-r_3		+0,059		+0,118		-0,176	
Q4	435	+0,058	1	+0,117	1	-0,181	5
D r_1+r_2		-0,358		+0,379		+0,010	
Q3	442	-0,359	1	+0,379	0	+0,010	0
D r_1+r_3		-0,417		+0,261		+0,186	
Q9	365	-0,418	1	+0,261	0	+0,186	0
D r_2+r_3		-0,433		+0,490		+0,228	
Q6	407	-0,434	1	+0,490	0	+0,228	0
S $2r_1$		-0,342		+0,150		-0,032	
Q37	276	-0,339	3	+0,088	62	-0,013	19
S $2r_2$		-0,374		+0,608		+0,052	
-Q8*	393	-0,376	2	+0,606	2	+0,045	7
S $2r_3$		-0,492		+0,372		+0,404	
Q78	264	-0,495	3	+0,407	35	+0,479	75
Q106**	256	-0,559	67	+0,380	8	+0,451	47

TABLE 7.3 Ru-Ru Patterson Peaks for RUCOPNP (Model 2); D - double peak; S - single peak; r_1, r_2, r_3 are the atomic positions from which the Patterson peaks $r_1 - r_2$, etc. are calculated; Q2, etc. the peaks found in the Patterson; * = +(0, +1, 0); Δ - difference between Patterson peak and calculated vector co-ordinate. Note that Δ 's are all zero for peaks Q3, Q6, -Q8 as these were used to calculate the co-ordinate r_1, r_2 and r_3 .

	Height	x/a	Δ	y/b	Δ	z/c	Δ
r_1		-0,2255		+0,3585		+0,1315	
r_2		-0,2085		+0,1315		+0,0965	
r_3		-0,1505		+0,2475		-0,0865	
D $r_1 - r_2$		-0,017		+0,227		+0,035	
Q2	457	-0,017	0	+0,234	7	+0,040	5
D $r_1 - r_3$		-0,075		+0,111		+0,217	
Q5	412	-0,075	0	+0,119	8	+0,219	2
D $r_2 - r_3$		-0,058		-0,116		+0,182	
-Q4	435	-0,058	0	-0,117	1	+0,181	1
D $r_2 + r_3$		-0,359		+0,379		+0,010	
Q3	442	-0,359	0	+0,379	0	+0,010	0
D $r_1 + r_2$		-0,434		+0,490		+0,228	
Q6	407	-0,434	0	+0,490	0	+0,228	0
D $r_1 + r_3$		-0,376		+0,606		+0,045	
-Q8*	393	-0,376	0	+0,606	0	+0,045	0
S $2r_1$		-0,451		+0,717		+0,263	
Q19	308	+0,446		+0,295		-0,263	
-Q19*		-0,446	5	+0,705	12	+0,263	0
S $2r_2$		-0,417		+0,263		+0,193	
Q9	365	-0,418	1	+0,261	2	+0,186	7
S $2r_3$		-0,301		0,495		-0,173	
Q10	333	-0,300	1	+0,492	3	-0,163	10

it was not attempted to interpret these further. In the other possible model (Table 7.2) two single weight vectors did not correspond to very high peaks in the Patterson and one of the single weight vectors corresponded to a higher Patterson peak than one of the double weight vectors (see peaks 8 and 9 in Table 7.2).

The satisfactory interpretation of the Ru - Ru interatomic vectors confirms that the space group is $P\bar{1}$.

7.2 FOURIER SYNTHESIS - IDENTIFICATION OF ATOMS IN STRUCTURE

In order to facilitate identification and discussion of the Fourier map, a convenient labelling was adopted for the proposed structure (see Fig. 7.7).

A Fourier synthesis (Fourier 1) was done using the fractional coordinates of the 3 Ru atoms found by means of the Patterson synthesis. Details of the programs called and parameters input are shown in Table 7.4 - as instruction cards. 86 independent peaks (in order of height) were found in the Fourier map. Bonds between the Ru atoms and distances between neighbouring peaks were also determined using the BOND card. The PLAN option gave a list of bond lengths between neighbouring peaks including the input atoms.

The 86 peak positions were transformed into orthogonal coordinates as described in Appendix 2 using the Departmental Wang computer (model 2200T) and a model built. Several further peaks in symmetry-related positions were added for clarity. The x-y coordinates were drawn on graph paper and fixed onto a flat wooden base. The z-coordinates were represented as the ends of 3,2 mm steel welding rods inserted into the

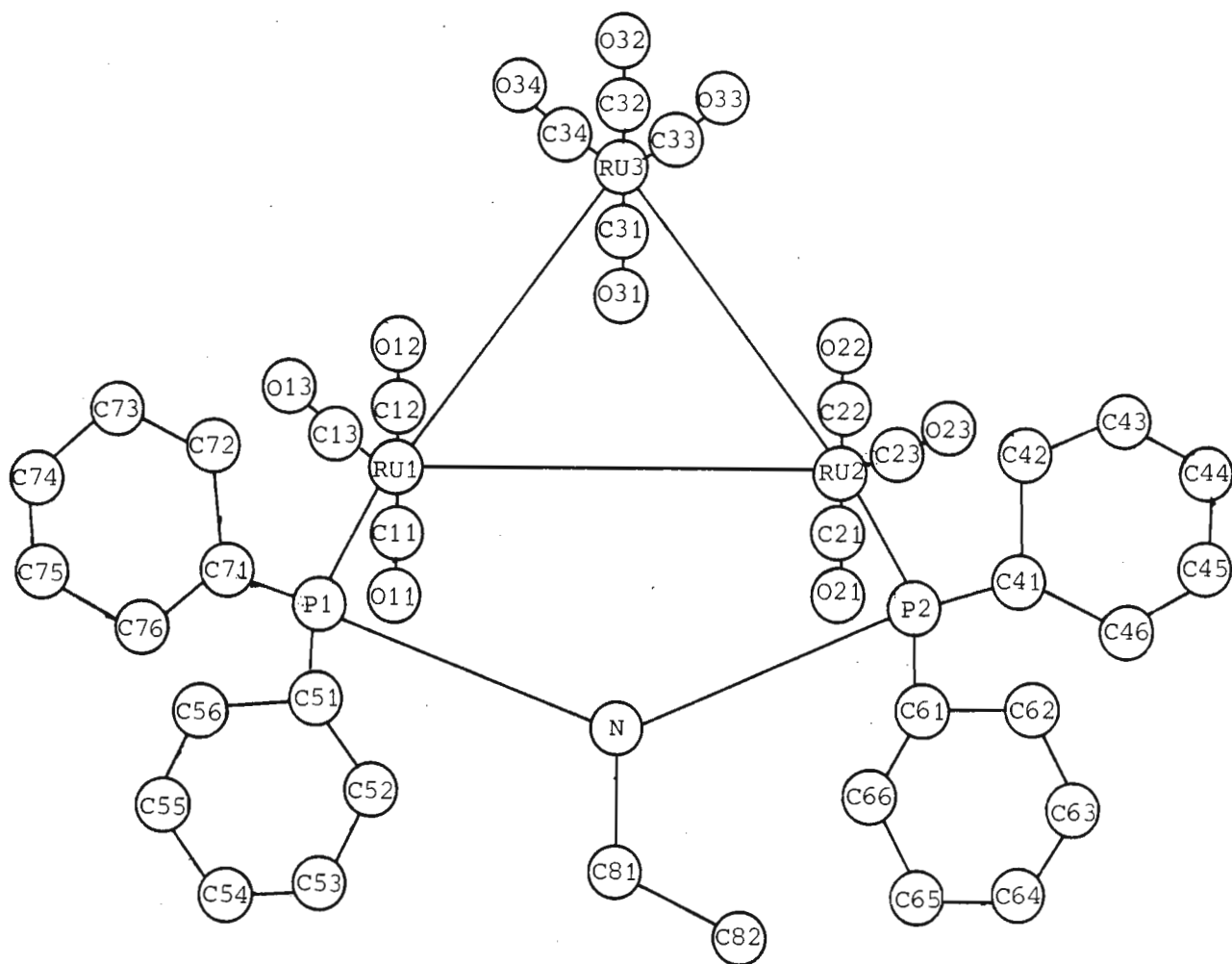


Fig. 7.7 Labelling scheme adopted for proposed structure of RUCOPNP.

base. A scale of $20 \text{ mm} \equiv 1 \text{ \AA}$ was used for the x, y and z coordinates. This model gave a 3-dimensional picture of the peaks of the Fourier map. Small balls of plasticine were placed on the ends of the rods for clarity. From the geometry of the peaks in the model and a comparison of distances between peaks listed by the program with typical bonds between atoms, a further 19 atoms were located in the structure.

TABLE 7.4 Instruction cards for Fourier 1

TITL RUCOPNP	REFLDATA
CELL 0.7107 14.732 12.386 10.982 104.525 100.644 94.893	
SYMM -X,-Y,-Z	
SFAC C O H P N	
SFAC 19.2674 0.808520 12.9182 8.43467 4.86337 24.7997 1.56756 =	
94.2928 5.37874 -1.420 0.836 3579.6 1.25	
UNIT 72 20 50 4 2 6	
FMAP -3 1 53 180 0	
GRID -52 -2 -52 2 2 2	
HKLF -3	
(read reflections)	
(Blank card)	
END 4	

MERG -1	ATOMDATA
OMIT 5	
RU1 6 -.171 .075 -.016	
RU2 6 -.187 .304 .026	
RU3 6 -.246 .186 .202	
LIST 5	
END	

The two phosphorus atoms (P1 and P2) and the nitrogen (N) were easily found in relation to the triangle formed by the 3 Ru atoms and their peak heights.

Consider the ethyl group bonded to the nitrogen. There were two possible peaks for C81 (viz. Q14 and Q29) and one peak for C82 (Q41). The geometry was best using Q14 and gave $N - C81 = 1,92\text{\AA}$, $C81 - C82 = 1,06\text{\AA}$ and $N - \widehat{C81} - C82 = 128^\circ$. However, this was considered too inaccurate (both $N - C$ and $C - C$ distances should be $1,54\text{\AA}$) and C81 and C82 were not input at this stage.

Consider atom P2. Peaks Q35 (C61), Q44 (C66) and Q36 (C65) were suitably situated with respect to P2 to form part of the C6 benzene ring. Peaks $Q18 + (0,0,+1)$ and $Q17 + (0,0,+1)$ (i.e. peaks Q18 and Q17 1 unit away in z-direction) were in favourable positions to form part of the second (C4) benzene ring attached to P2. They would be C42 and C43 with the linking atom C41 missing. Consider now atom P1. Peaks Q54, Q27, Q28 and Q19 could be identified as the carbon atoms C51, C52, C54 and C55 of the benzene ring C5 bonded to P1. Other peaks were visible to complete the benzene ring but they were weak and there were extra peaks in the vicinity. These were therefore omitted. Peaks Q25, Q12 and Q46 (identified as C71, C72 and C73) form part of the second benzene ring bonded to P2.

Five of the six C-O groups perpendicular to the plane of the Ru atoms were recognisable. However, only two groups were input. Peaks Q8 and Q16 could be identified as the lower C21 - O21 group bonded to RU2. The matching C - O group situated above RU2 could be seen as the peaks Q81 and Q42, but Q81 was a very weak peak - so this C - O was neglected. The lower (C11 - O11) group attached to RU1 could be identified as peaks Q30 and Q6. The upper one was omitted because of the presence of a further peak.

A total of 22 atoms were thus identified. Table 7.5 shows these atoms and their coordinates.

A second Fourier synthesis (Fourier 2) was done using the 22 atoms found thus far. The program found 103 independent peaks in the Fourier map. A model was again built using the 86 highest peaks. In the model all 52 atoms (excluding hydrogens) of the structure were identified. However, several spurious peaks were found and in some cases the peaks exhibited poor geometry and so could not be correctly identified. All the 52 atoms could be explained by the 66 highest peaks, i.e. 14 spurious peaks were found to be higher than the weakest atom peak. The heights of peaks corresponding to atoms not input into the Fourier synthesis ranged from 46 to 23. The height of the largest spurious peak, labelled Q39, was 33 and 15 of the 30 peaks corresponding to new atoms were higher than Q39. Table 7.6 shows these 52 atoms and their co-ordinates.

Using now, all the 52 atoms of the structure, Fourier 3 was calculated. Fig. 7.8 shows part of the graph of peak height vs peak number for the output of Fourier 3. The kink in the graph indicates clearly the point where the peaks corresponding to the input atoms end and the spurious peaks begin. Two spurious peaks were still higher than the weakest atoms. One spurious peak had a height of 38 and was larger than 12 of the atoms peaks; the other had height 34 and was larger than 3 atom peaks. The weakest atom peak had a height of 33.

TABLE 7.5 Fractional coordinates of the 22 atoms found in Fourier 1
and input into Fourier 2

ATOM	PEAK		x/a(Å)	y/b(Å)	z/c(Å)
	LABEL	HEIGHT			
C11	Q30	35	-0.3571	0.3420	-0.0278
C21	Q16	41	-0.3402	0.0960	0.0117
C42	Q18	40	-0.0860	0.3010	0.5202
C43	Q17	41	-0.0213	0.3246	0.6025
C61	Q35	33	-0.2721	0.0202	0.3408
C65	Q36	32	-0.3913	-0.1366	0.2596
C66	Q44	31	-0.3370	-0.0376	0.2450
C71	Q25	37	-0.2981	0.4711	0.4389
C72	Q12	43	-0.3677	0.5024	0.4872
C73	Q46	31	-0.3680	0.5950	0.5829
C51	Q54	29	-0.4242	0.3288	0.2240
C52	Q27	36	-0.4852	0.2277	0.1807
C54	Q28	36	-0.6203	0.3318	0.0854
C55	Q19	40	-0.5642	0.4202	0.1160
O11	Q6	59	-0.4170	0.2853	-0.1278
O21	Q8	48	-0.4081	0.0758	-0.0218
P1	Q5	96	-0.3036	0.3552	0.2951
P2	Q4	100	-0.2226	0.1437	0.3006
N	Q7	56	-0.2833	0.2345	0.3427
RU1	Q1	469	-0.2238	0.3693	0.1326
RU2	Q2	428	-0.2046	0.1316	0.0998
RU3	Q3	413	-0.1566	0.2434	-0.0900

TABLE 7.6 Fractional coordinates of the 52 atoms found in Fourier 2 and input into the first least squares refinement

ATOM	PEAK		x/a(Å)	y/b(Å)	z/c(Å)
	LABEL	HEIGHT			
C11	Q28	40	-0.3593	0.3251	-0.0382
C12	Q41	31	-0.0972	0.3921	0.2631
C13	Q63	24	-0.2312	0.5278	0.1336
C21	Q17	47	-0.3397	0.1007	0.0164
C22	Q33	36	-0.0760	0.1626	0.1404
C23	Q35	35	-0.1955	-0.0387	0.0331
C31	Q47	29	-0.2768	0.1384	-0.2006
C32	Q50	28	-0.0219	0.3590	0.0368
C33	Q36	33	-0.0757	0.1336	-0.1918
C34	Q70	23	-0.1616	0.3779	-0.1696
C41	Q46	29	-0.1383	0.1908	0.4167
C42	Q13	50	-0.0889	0.2857	0.5220
C43	Q14	49	-0.0204	0.3115	0.6089
C44	Q31	38	0.0521	0.2358	0.6039
C45	Q68	23	0.0441	0.1468	0.5029
C46	Q53	26	-0.0685	0.1054	0.4077
C61	Q24	43	-0.2755	0.0205	0.3350
C62	Q25	43	-0.2602	-0.0130	0.4403
C63	Q56	25	-0.3196	-0.1164	0.4412
C64	Q61	24	-0.3806	-0.1751	0.3575
C65	Q16	48	-0.3894	-0.1414	0.2612
C66	Q23	43	-0.3402	-0.0464	0.2551
C71	Q12	50	-0.2966	0.4722	0.4354
C72	Q10	51	-0.3666	0.5062	0.4840
C73	Q22	45	-0.3648	0.5944	0.5872
C74	Q37	33	-0.2514	0.6639	0.6402

TABLE 7.6 Continued

ATOM	PEAK LABEL	HEIGHT	x/a(Å)	y/b(Å)	z/c(Å)
C75	Q30	38	-0.1819	0.6283	0.5825
C76	Q49	28	-0.2202	0.5428	0.4792
C51	Q20	45	-0.4259	0.3375	0.2217
C52	Q15	49	-0.4856	0.2334	0.1844
C53	Q43	30	-0.5973	0.2154	0.1112
C54	Q18	47	-0.6199	0.3235	0.0768
C55	Q8	53	-0.5628	0.4166	0.1132
C56	Q45	29	-0.4898	0.4305	0.1800
C81	Q38	33	-0.3412	0.2255	0.4648
C82	Q34	35	-0.4181	0.1965	0.4667
O11	Q7	55	-0.4138	0.2986	-0.0971
O12	Q21	45	-0.0315	0.4070	0.3238
O13	Q26	41	-0.2386	0.6003	0.1548
O21	Q6	64	-0.4077	0.0744	-0.0240
O22	Q29	39	-0.0018	0.1592	0.1697
O23	Q27	40	-0.1870	-0.1172	0.0359
O31	Q19	46	-0.3379	0.0902	-0.2541
O32	Q32	37	0.0372	0.3895	0.0628
O33	Q44	30	-0.0618	0.0699	-0.2473
O34	Q42	30	-0.1681	0.4387	-0.2224
P1	Q5	146	-0.3042	0.3586	0.2934
P2	Q4	158	-0.2234	0.1475	0.3010
N	Q9	51	-0.2860	0.2361	0.3481
RU1	Q1	486	-0.2233	0.3621	0.1339
RU2	Q2	479	-0.2033	0.1320	0.0997
RU3	Q3	425	-0.1548	0.2459	-0.0883

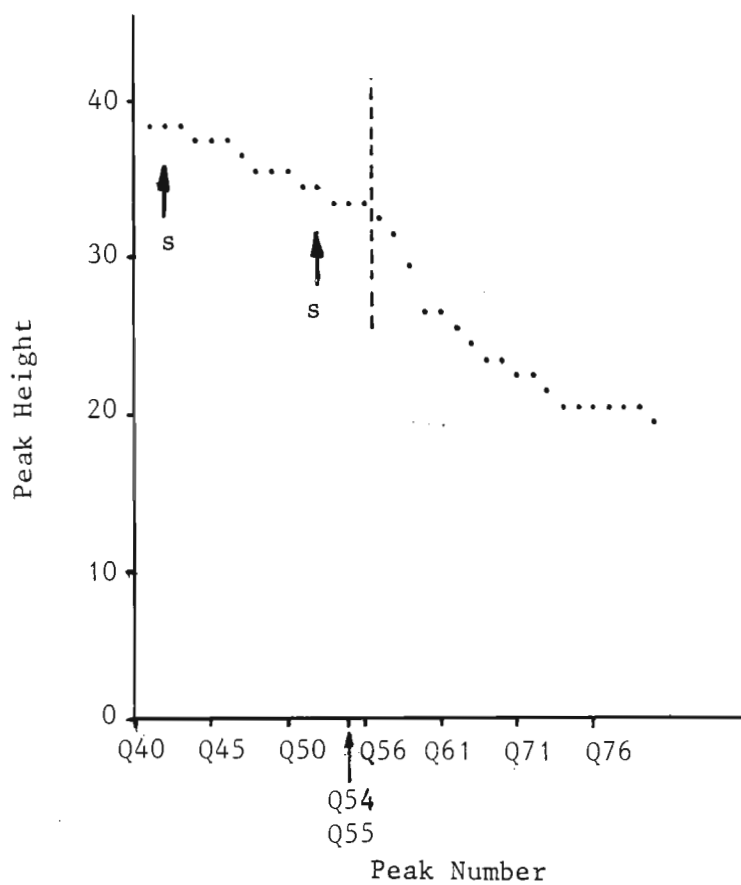


Fig. 7.8 Graph of Peak Height vs Peak Number. Only part of the full set is shown. The vertical dotted line separates the peaks corresponding to input atoms from the spurious peaks. Two spurious peaks which are larger than the smallest atom peak are indicated by the letter s.

7.3 REFINEMENT OF THE STRUCTURE

The structure of 52 atoms was refined using the full-matrix least squares procedure (which minimizes the function $\sum w(|F_o|^2 - |kF_c|^2)$, w = weight, k = scale factor) incorporated in the SHELX program. 1631 reflections were suppressed out of 5170 by the condition $I < 5\sigma(I)$. Unit weights were used for all reflections. The atomic scattering factors used were those of Cromer and Mann⁽¹⁵⁾ for C, N, P, O; Cromer⁽¹⁶⁾ for anomalous contributions and Stewart *et al.*⁽¹⁷⁾ for H (supplied by the program); and International Tables, Vol. IV⁽¹¹⁾ for Ru.

The first refinement of 3 cycles (Jobs 30, 31) was calculated with individual isotropic thermal parameters for all 52 atoms, and an R index of 0,1549 was obtained. (R is defined as $R = (\sum ||F_o| - |F_c||) / \sum |F_o|$). The benzene rings were now made rigid (regular hexagons including H-atoms with constant isotropic factor $U = 0,05$) by use of the AFIX card in order to reduce the number of parameters to be refined. This change in input parameters reduced R to 0,1473 and one cycle of refinement (Job 40) yielded $R = 0,1416$. R was further reduced to 0,0650 on refinement with anisotropic thermal parameters for the three Ru, two P and N atoms (Job 41). The isotropic thermal parameters of the H atoms in the benzene rings were allowed to vary but the values for H atoms in each group were linked together with the aid of the FVAR (free-variable) card. H atoms were also added as rigid groups for $-CH_2-$ and $-CH_3$, the U-values being allowed to vary but linked together in each group. (The 15 1 0 reflection was omitted at this stage as the observed intensity was obviously incorrect. This reflection had the highest intensity as it was 16 times larger than the next highest reflection, and for this reflection $F_o \sim 19 F_c$. Thus this omission may have been responsible for a considerable part of the large drop in R).

TABLE 7.7 Details of least squares refinement

Job No.	Refinement No.	Cycle No.	R	No. of parameters	Constraints on atoms
30,31	1	0	0,7100	-	52 atoms isotropic
		1	0,1661	209	
		2	0,1542	"	
		3	0,1549	"	
40	2	0	0,1473	-	52 atoms isotropic, benzene rings rigid, H atoms included in benzene rings with fixed isotropic U = 0,05.
		1	0,1416	166	
41	3	0	0,1387	-	Only Ru, P and N atoms anisotropic, H atoms added to -CH ₂ - and -CH ₃ . U-values for all H refined but linked in groups. Reflection (15 1 0) omitted.
		1	0,0650	200	
43	4	0	0,0651	-	Carbonyl atoms made anisotropic and refined in cycle 1, all other atoms in cycle 2.
		1	0,0574	120	
		2	0,0537	187	

In the next and final refinement of 2 cycles (Job 43), the atoms in the C-O groups were made anisotropic. By making use of the BLOC card, to limit the number of parameters to be refined in each cycle, the carbonyl atoms were refined in the first cycle, and all other atoms in the second cycle. R was finally reduced to 0,0537. Table 7.7 gives the refinement details.

The final position co-ordinates (fractional) of the 52 atoms are given in Table 7.8. In Table 7.9, the final anisotropic thermal parameters are listed; the thermal parameters are in the form:

$$T = \exp \left[-2\pi^2 (a^2 h^2 U_{11} + b^2 k^2 U_{22} + c^2 \ell^2 U_{33} + 2b^*c^*k\ell U_{23} + 2a^*c^*h\ell U_{13} + 2a^*b^*hk U_{12}) \times 10^{-4} \right]$$

In Table 7.10 the isotropic temperature factors for the atoms in the benzene rings and $-\text{CH}_2-\text{CH}_3$ groups are listed.

A difference Fourier map was calculated for the 52 refined atoms. The hydrogen atoms could be identified in the list of peak heights as they had not been put into the structure factor calculation. The highest H-atom peak had a height of 78. There were 8 (spurious) peaks present in the map which were larger than the highest H-atom peak of 78 of heights ranging from 140 to 86. The fact that the highest spurious peak is only twice the size of an H-atom peak means that it does not appear that any atoms have been missed out in the determination of the trial structure of 52 atoms.

The refinement should be continued for several more cycles to reach convergence. However, an absorption correction has still to be applied and final refinement should be delayed until this has been done.

A table of observed and calculated structure factors was printed with the LIST 0 option after the final refinement (Job 43) and is shown in Appendix 4.

TABLE 7.8 Final atomic positions - fractional co-ordinates (standard deviations in parentheses)

Atom	x/a	y/b	z/c
C11	-0.3341(12)	0.3213(13)	-0.0070(16)
C12	-0.1059(10)	0.3839(11)	0.2492(13)
C13	-0.2203(11)	0.5129(14)	0.1353(15)
C21	-0.3356(10)	0,0977(10)	0.0169(12)
C22	-0.0691(10)	0,1640(10)	0.1444(12)
C23	-0.1898(10)	-0.0230(13)	0.0435(14)
C31	-0.2697(11)	0.1473(13)	-0.1827(15)
C32	-0.0416(15)	0.3390(18)	0.0200(20)
C33	-0.0857(13)	0.1425(15)	-0.1767(17)
C34	-0.1792(13)	0.3556(17)	-0.1729(19)
C41	-0.1195(4)	0.1867(6)	0.4228(6)
C42	-0.1008(4)	0.2853(6)	0.5237(6)
C43	-0.0157(4)	0.3103(6)	0.6122(6)
C44	0.0507(4)	0.2368(6)	0.5998(6)
C45	0.0320(4)	0.1382(6)	0.4990(6)
C46	-0.0531(4)	0.1131(6)	0.4105(6)
C61	-0.2794(5)	0.0210(5)	0.3320(7)
C62	-0.2493(5)	-0.0060(5)	0.4475(7)
C63	-0.2895(5)	-0.1047(5)	0.4669(7)
C64	-0.3598(5)	-0.1766(5)	0.3707(7)
C65	-0.3899(5)	-0.1496(5)	0.2553(7)
C66	-0.3497(5)	-0.0509(5)	0.2359(7)
C71	-0.2951(5)	0.4791(5)	0.4229(6)
C72	-0.3686(5)	0.5094(5)	0.4823(6)
C73	-0.3532(5)	0.6009(5)	0.5913(6)

TABLE 7.8 Continued

Atom	x/a	y/b	z/c
C74	-0.2643(5)	0.6621(5)	0.6410(6)
C75	-0.1908(5)	0.6318(5)	0.5816(6)
C76	-0.2062(5)	0.5403(5)	0.4726(6)
C51	-0.4361(3)	0.3401(5)	0.2159(6)
C52	-0.4926(3)	0.2363(5)	0.1823(6)
C53	-0.5846(3)	0.2244(5)	0.1149(6)
C54	-0.6201(3)	0.3162(5)	0.0811(6)
C55	-0.5636(3)	0.4199(5)	0.1147(6)
C56	-0.4716(3)	0.4319(5)	0.1821(6)
C81	-0.3261(9)	0.2461(12)	0.4803(13)
C82	-0.4248(10)	0.1946(13)	0.4686(15)
O11	-0.3995(9)	0.3090(9)	-0.0842(11)
O12	-0.0373(8)	0.4061(8)	0.3211(10)
O13	-0.2179(9)	0.6047(12)	0.1390(13)
O21	-0.4127(8)	0.0716(8)	-0.0270(10)
O22	0.0102(8)	0.1728(9)	0.1753(11)
O23	-0.1815(9)	-0.1160(11)	0.0150(12)
O31	-0.3306(10)	0.0909(11)	-0.2537(13)
O32	0.0284(11)	0.3915(13)	0.0698(15)
O33	-0.0465(12)	0.0808(14)	-0.2299(16)
O34	-0.1975(9)	0.4223(12)	-0.2278(13)
P1	-0.3114(2)	0.3537(2)	0.2863(3)
P2	-0.2274(2)	0.1487(2)	0.3016(3)
N	-0.2983(6)	0.2451(8)	0.3557(9)
RU1	-0.22510(7)	0.35816(8)	0.13191(9)
RU2	-0.20438(7)	0.13050(8)	0.09536(9)
RU3	-0.15591(8)	0.24518(9)	-0.08444(10)

TABLE 7.9 Final anisotropic thermal parameters in ($\text{\AA}^2 \times 10^{-3}$) (standard deviations in parentheses)

Atom	U11	U22	U33	U23	U13	U12
C11	72(10)	36(10)	57(10)	16(8)	19(8)	6(8)
C12	52(9)	38(8)	59(8)	19(7)	17(7)	13(7)
C13	70(10)	44(10)	57(10)	21(8)	4(8)	6(8)
C21	49(8)	44(7)	47(7)	13(6)	9(6)	9(6)
C22	60(8)	34(8)	50(7)	8(6)	25(6)	14(6)
C23	45(9)	47(10)	83(9)	2(8)	15(7)	0(8)
C31	76(10)	73(10)	53(10)	0(8)	19(8)	-5(8)
C32	104(15)	80(15)	66(15)	22(12)	29(12)	8(12)
C33	97(12)	63(12)	74(12)	27(10)	34(9)	29(10)
C34	98(13)	71(13)	48(13)	6(10)	36(10)	3(11)
O11	65(8)	68(8)	59(8)	12(6)	-11(7)	6(6)
O12	48(7)	59(7)	79(7)	17(6)	11(6)	10(6)
O13	116(10)	34(11)	115(10)	34(9)	-17(8)	2(9)
O21	48(7)	58(7)	80(7)	21(5)	8(6)	11(6)
O22	29(8)	85(8)	90(8)	25(6)	15(6)	5(6)
O23	79(9)	38(9)	147(9)	-2(7)	32(7)	14(7)
O31	111(10)	102(10)	62(9)	5(8)	26(8)	-20(8)
O32	87(12)	119(12)	107(12)	24(9)	21(10)	-30(10)
O33	153(13)	92(14)	138(13)	14(11)	98(10)	77(11)
O34	131(10)	74(10)	91(10)	36(8)	27(8)	16(8)
P1	31(2)	36(2)	45(2)	9(1)	10(1)	10(1)
P2	34(2)	37(2)	42(2)	12(1)	11(1)	11(1)
N	30(6)	47(6)	46(6)	14(5)	15(5)	18(5)
RU1	40,3(6)	38,3(5)	46,4(6)	10,2(4)	13,3(5)	6,3(4)
RU2	41,5(6)	38,3(5)	44,8(6)	7,7(4)	14,2(5)	6,8(4)
RU3	75,8(8)	53,0(7)	52,4(7)	13,3(5)	31,3(6)	9,7(6)

TABLE 7.10 Isotropic temperature factors ($\text{\AA}^2 \times 10^{-3}$) for the atoms in the benzene rings and $-\text{CH}_2-\text{CH}_3$ groups

Atom	U	Atom	U
C41	41(3)	C73	66(3)
C42	47(3)	C74	61(3)
C43	60(3)	C75	52(3)
C44	60(3)	C76	49(3)
C45	62(4)	H72-H76	114(21)
C46	54(3)	C51	41(2)
H42-H46	88(18)	C52	42(2)
C61	42(3)	C53	60(3)
C62	50(3)	C54	65(3)
C63	68(5)	C55	62(3)
C64	76(5)	C56	55(3)
C65	83(4)	H52-H56	90(18)
C66	67(4)	C81	57(4)
H62-H66	113(25)	H81, H83	65(28)
C71	42(3)	C82	83(4)
C72	53(3)	H82, H84, H86	76(21)

CHAPTER EIGHT

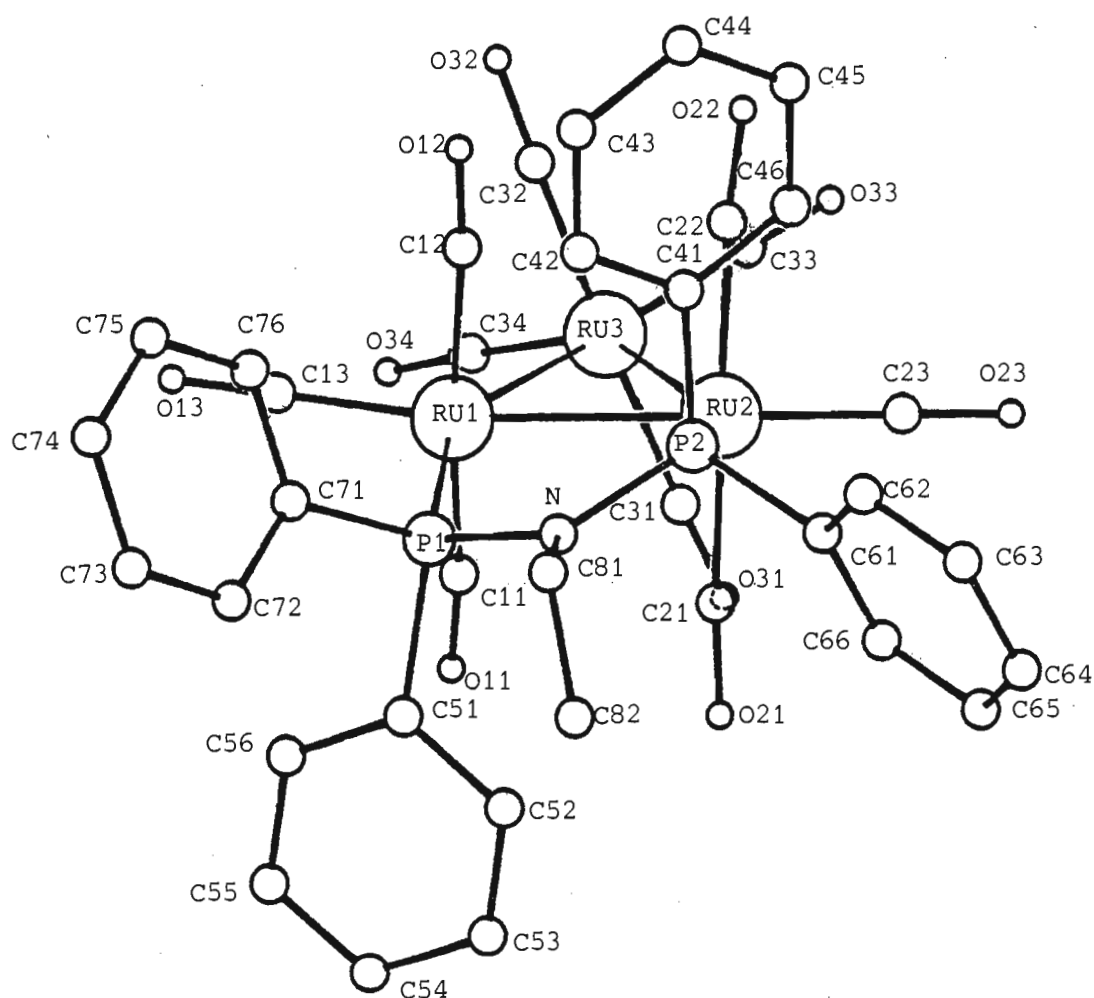
DISCUSSION OF STRUCTURE8.1 EFFECT OF THE LIGAND ON THE Ru₃ CORE

Fig. 8.1 A view of the RUCOPNP molecule from a direction approximately 75° from the normal to the Ru₃ plane. The diagram was drawn on the HP 1000 computer using the program CRYSTEP⁽¹⁸⁾.

Two views of the molecule are shown (Figs. 8.1 and 8.2). In the former the molecule is viewed from a direction approximately 75° from the normal to the Ru₃ plane and in the latter from above and along the normal to the plane. (Selected interatomic distances and bond angles

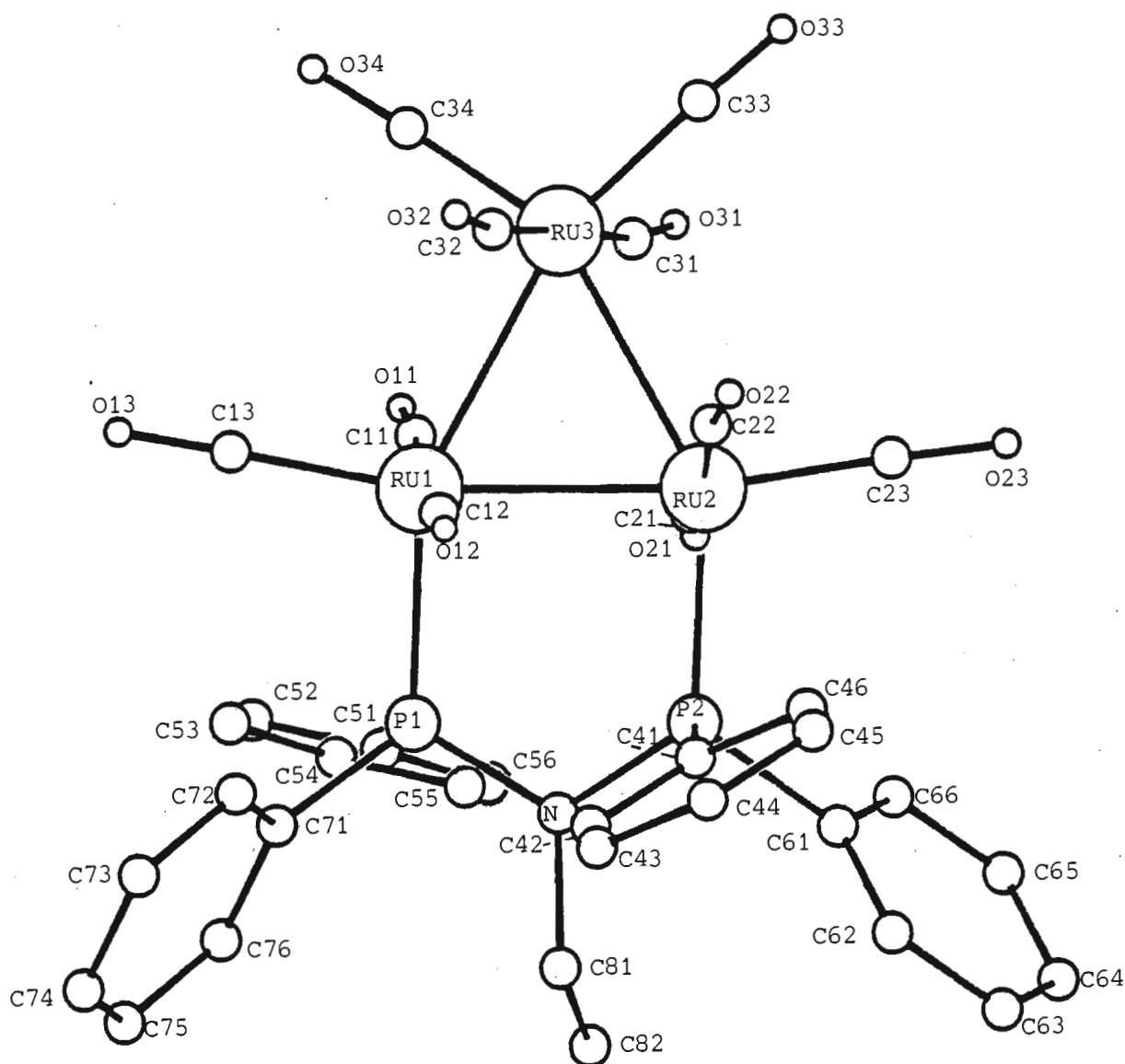


Fig. 8.2 A view of the RUCOPNP molecule from above and along the normal to the Ru_3 plane (Drawn by CRYSTEP).

for the structure are given in Table 8.1 and Table 8.2 respectively).

In the parent carbonyl $Ru_3(CO)_{12}$ the Ru-Ru bonds are 2,8595(4), 2,8518(4) and 2,8512(4) Å, average 2,854(7) Å (Churchill⁽¹⁹⁾). In RUCOPNP, the Ru atoms form a nearly isosceles triangle, with each Ru atom exhibiting a distorted octahedral co-ordination geometry. The $(C_6H_5)_2PN(C_2H_5)P(C_6H_5)_2$ ligand (PNP) does not chelate but bridges equatorially, by substitution of two carbonyl ligands, resulting in a significant shortening of the RU1-RU2

TABLE 8.1 Selected interatomic distances (\AA) for RUCOPNP

(A) Ru-Ru			
RU1-RU2	2,798(1)	RU2-RU3	2,860(2)
RU1-RU3	2,848(2)		
(B) Ru-C			
Axial		Equatorial	
RU1-C11	1,933(15)	RU1-C13	1,903(18)
RU1-C12	1,926(14)	RU2-C23	1,886(16)
RU2-C21	1,928(13)	RU3-C33	1,918(19)
RU2-C22	1,945(14)	RU3-C34	1,885(23)
RU3-C31	1,943(14)	Mean	1,898(8)
RU3-C32	1,946(19)		
Mean	1,937(4)		
(C) C-O			
Axial		Equatorial	
C11-O11	1,130(19)	C13-O13	1,125(24)
C12-O12	1,126(17)	C23-O23	1,139(21)
C21-O21	1,133(17)	C33-O33	1,111(26)
C22-O22	1,143(18)	C34-O34	1,161(28)
C31-O31	1,124(18)	Mean	1,134(10)
C32-O32	1,133(25)		
Mean	1,131(3)		
(D) Non-bonded contacts (for axial carbonyls)			
C...C		O...O	
C11...C31	2,864	O11...O31	3,231
C31...C21	2,736	O31...O21	3,013
C21...C11	2,845	O21...O11	3,155
C12...C32	2,795	O12...O32	3,058
C32...C22	2,877	O32...O22	3,211
C22...C12	2,819	O22...O12	3,136
Mean	2,822(21)	Mean	3,134(35)
(E) Other interatomic distances			
RU1-P1	2,309(3)	N-P1	1,711(11)
RU2-P2	2,311(3)	N-P2	1,725(10)
P1-C71	1,831(6)	N-C81	1,493(18)
P1-C51	1,832(6)	C81-C82	1,506(21)
P2-C41	1,815(6)		
P2-C61	1,831(8)		

TABLE 8.2 Selected bond angles ($^{\circ}$) for RUCOPNP

(A) Within Ru ₃ triangle			
RU3-RU1-RU2	60,9(0)	RU2-RU3-RU1	58,7(0)
RU1-RU2-RU3	60,4(0)		
(B) Ru-Ru-Co			
Axial			
RU2-RU1-C11	91,3(5)	RU1-RU3-C31	98,5(5)
RU2-RU1-C12	84,3(4)	RU1-RU3-C32	80,5(7)
RU3-RU1-C11	76,9(5)	RU1-RU2-C21	86,8(4)
RU3-RU1-C12	93,8(5)	RU1-RU2-C22	92,4(4)
RU2-RU3-C31	77,6(5)	RU3-RU2-C21	95,0(4)
RU2-RU3-C32	99,8(7)	RU3-RU2-C22	76,0(4)
Equatorial			
RU3-RU1-C13	108,0(5)	RU1-RU2-C23	170,5(5)
RU1-RU3-C34	94,2(6)	RU1-RU3-C33	156,4(6)
RU2-RU3-C33	101,8(6)	RU2-RU1-C13	168,0(5)
RU3-RU2-C23	110,8(5)	RU2-RU3-C34	148,6(6)
(C) OC-Ru-OC			
Axial-Equatorial		Axial-Axial	
C11-RU1-C13	90,2(6)	C11-RU1-C12	170,7(7)
C12-RU1-C13	92,4(6)	C21-RU2-C22	169,9(6)
C21-RU2-C23	91,5(6)	C31-RU3-C32	177,3(9)
C22-RU2-C23	87,6(6)		
C31-RU3-C34	92,7(7)	(Equatorial-Equatorial)	
C31-RU3-C33	89,0(7)	C34-RU3-C33	107,9(9)
C32-RU3-C33	90,9(8)		
C32-RU3-C34	90,0(9)		
(D) Ru-C-O			
Axial		Equatorial	
RU1-C11-O11	174,0(14)	RU1-C13-O13	179,0(16)
RU1-C12-O12	175,4(12)	RU2-C23-O23	178,3(15)
RU2-C21-O21	175,3(13)	RU3-C34-O34	177,1(17)
RU2-C22-O22	172,9(12)	RU3-C33-O33	178,2(19)
RU3-C31-O31	170,6(17)	Mean	178,1(4)
RU3-C32-O32	173,1(21)		
Mean	173,6(7)		
(E) P environment			
P1 (environment)		P2 (environment)	
C71-P1-RU1	117,6(3)	C41-P2-RU2	113,0(3)
C51-P1-RU1	110,2(3)	C61-P2-RU2	115,9(3)
N -P1-RU1	115,3(4)	N -P2-RU2	116,7(4)

TABLE 8.2 Continued

(E) P environment (contd.)			
P1 (environment)		P2 (environment)	
C71-P1-C51	102,2(3)	C41-P2-C61	102,0(4)
C51-P1-N	105,8(4)	C61-P2-N	102,2(4)
C71-P1-N	104,3(4)	C41-P2-N	105,3(4)
(F) Ru environment			
C11-RU1-P1	93,3(6)	C21-RU2-P2	94,2(4)
C13-RU1-P1	99,9(5)	C23-RU2-P2	101,4(5)
RU2-RU1-P1	91,9(1)	RU1-RU2-P2	87,7(1)
C12-RU1-P1	95,0(5)	C22-RU2-P2	95,8(4)
RU3-RU1-P1	150,3(1)	RU3-RU2-P2	146,1(1)
(G) N environment			
	P2-N-C81	117,5(9)	
	P1-N-P2	118,1(6)	
	P1-N-C81	122,5(8)	

bond of the Ru_3 triangle. Two bonds of 2,860(2) and 2,848(2) Å are very close to the values for the parent compound, while the bridged bond length (2,798(1) Å) is shorter than that in the parent compound. The shortening could be due to steric strain in the PNP ligand and the bond angles in the ligand should therefore be inspected.

The tetrahedral arrangement round the phosphorus atoms deviates slightly from the ideal regular one with bond angles of 109,5°. This is probably due to the fact that the Ru atom is much larger than the C and N atoms bonded to P. The mean value of the six bond angles around the P atoms involving Ru is 114,3(1,0)° and the mean of the six not involving Ru is 103,6(7)°. The differences within these groups are not large and this suggests that there is no distortion of the Ru-P-N bond angles. Furthermore, the three angles about the nitrogen (118,1(6)°, 122,5(8)°, 117,5(9)°) are close to 120°, the ideal value for sp^2 hybridization. It

would appear that the PNP ligand is not severely strained so that a steric effect on the Ru-Ru distance would not be expected. Steric strain could further be taken up by puckering of the ring which does occur in RUCOPNP to a slight degree.

The shortening of the bond may, on the other hand, indicate a strengthening of the bond due to an increase in electron density between RU1 and RU2. This in turn suggests that the ligand donor atoms, viz., the phosphorus atoms have been responsible for electron donation to the metal atoms to which they are bonded. This is as expected for basic donor atoms such as phosphorus. This behaviour contrasts with the lengthening of metal-metal bonds as produced by the acidic bridging H^+ ligand (e.g., Churchill and de Boer⁽²⁰⁾).

Lavigne *et al.*⁽²¹⁾ report a similar shortening of the Ru-Ru bonds that are bridged by a bidentate ligand. They present a discussion of electronic and steric influences. Benfield *et al.*⁽²²⁾ and Forbes *et al.*⁽²³⁾ have explained a lengthening of the metal-metal bond adjacent to a bulky terminal ligand as being due to steric hindrance.

This contraction in the length of the Ru-Ru bond in comparison with the parent carbonyl thus appears more likely to be due to an electronic rather than a steric effect or a combination of both. In order to differentiate between the two effects more clearly it may be of value to study the structure of an analogous complex with a core consisting of smaller metal atoms such as iron (Fe). If the shortening is still observed this would indicate that the effect is electronic; if the shortening is not observed this would indicate that the effect is steric in the Ru_3 plane.

8.2 THE CO GROUPS

The overall geometry of the $\text{Ru}_3(\text{CO})_{10}$ skeleton is similar to that found for the parent carbonyl $\text{Ru}_3(\text{CO})_{12}$ (19, 24).

The Ru-C bond lengths range from 1,885 to 1,946 Å (mean 1,911 Å) and are in good agreement with expected values (19, 23, 25, 26). The axial bond lengths (mean 1,937(4) Å) are longer than the equatorial ones (mean 1,898(8) Å). This effect has been noted for similar compounds and the differences are shown in Table 8.3. Churchill and de Boer (20) have proposed an explanation and have suggested that there may be a significant difference between the average axial and equatorial C-O distances as well. In Table 8.3 these differences are compared for several compounds but there does not seem to be a significant trend for the C-O distances. The difference for $\text{Os}_3(\text{CO})_{11}^- \text{P}(\text{OCH}_3)_3$ does seem rather large but is opposite in sign to the difference found by Churchill and de Boer (20).

TABLE 8.3 Comparison of Ru-C and C-O bonds for various tri-nuclear carbonyl compounds. Bond lengths in Å. (* - the present study).

Compound	Metal-C			C-O		
	Axial	Eq.	Ax.-Eq.	Axial	Eq.	Ax.-Eq.
$\text{Os}_3(\text{CO})_{12}$ (20)	1,946(6)	1,912(7)	+0,034(9)	1,134(8)	1,145(5)	-0,011(9)
$\text{Ru}_3(\text{CO})_{12}$ (19)	1,942(4)	1,921(5)	+0,021(7)	1,133(2)	1,127(2)	+0,006(3)
$\text{Ru}_3(\text{CO})_{10} \text{PNP}^*$	1,937(4)	1,898(8)	+0,039(9)	1,131(3)	1,134(11)	-0,003(11)
$\text{Ru}_2(\text{CO})_{11} \text{Ph}_3\text{P}^{(22)}$	1,935(11)	1,888(10)	+0,047(15)	1,142(11)	1,146(7)	-0,004(13)
$\text{Os}_3(\text{CO})_{11} \text{P}(\text{OCH}_3)_3^{(21)}$	1,915(5)	1,903(6)	+0,012(8)	1,159(6)	1,132(5)	+0,027(8)

The non-bonded C···C and O···O contacts for the axial carbonyls range from 2,734 to 2,864 Å (mean 2,822 Å) and from 3,013 to 3,231 Å (mean 3,134 Å) respectively. The C···C contacts are all comparable to the mean Ru-Ru distances (2,854 Å) while O···O distances are greater. This relative increase of the O···O distance with respect to the C···C implies a bending of the carbonyl groups. This can be explained to be a result of van der Waals' repulsions between the axial oxygen atoms. The average value of the Ru-C-O angle for axial carbonyl ligands is 173,6(7)°, a deviation of 6,4° from the straight line. The average value for the equatorial carbonyl ligands is 178,1(4)° a deviation of only 1,9° from linearity. This strongly suggests that the axial carbonyl ligands are bent in order to increase the non-bonded distance. (The values for the equivalent means for the parent compound are 173,0(2)° and 178,9(3)° for the axial and equatorial Ru-C-O angles respectively). This bending of the axial carbonyls from each other has been observed in $\text{Os}_3(\text{CO})_{11}\text{P}(\text{OCH}_3)$ ⁽²²⁾ and $\text{Os}_3(\text{CO})_{12}$ ⁽²⁰⁾. Kettle⁽²⁷⁾ attributes the small deviations to electronic effects alone but suggests that the larger ones may have a steric component as well. Furthermore, the Ru-Ru-CO axial angles range from 76,0 to 99,8°. This large variation of Ru-Ru-CO angles coupled with the fact that the axial carbonyls bend away from each other indicate that there is gross distortion of the axial carbonyl ligands. The axial CO groups on Ru_3 deviate significantly from the normal to the Ru_3 plane. Lavigne *et al.*⁽²¹⁾ have discussed such a staggering of carbonyl ligands.

8.3 THE EQUATORIAL BOND ANGLES

The bond angles in the equatorial plane of RUCOPNP can be compared with those of the parent compound $\text{Ru}_3(\text{CO})_{12}$. The average values of the chemically equivalent bond angles are used for the comparison as it is assumed

that the differences between individual values are due to packing effects. In Table 8.4 these average values are compared for the two compounds. The nomenclature for the angles is defined in Fig. 8.3.

TABLE 8.4 Average values of chemically equivalent angles ($^{\circ}$). n is the number of individual values from which the mean is calculated (in each case).

Angle ($^{\circ}$)	RUCOPNP	n	$\text{Ru}_3(\text{CO})_{12}$	n	Δ
A	107,9	1	104,1	3	+ 3,8
B	98,0	2	98,0	6	0,0
C	109,4	2	(98,0)		+11,4
D	100,7	2	(104,1)		- 3,4
E	89,8	2	(98,0)		- 8,2
F	58,7	1	60,0	3	- 1,3
G	60,6	2	(60,0)		+ 0,6

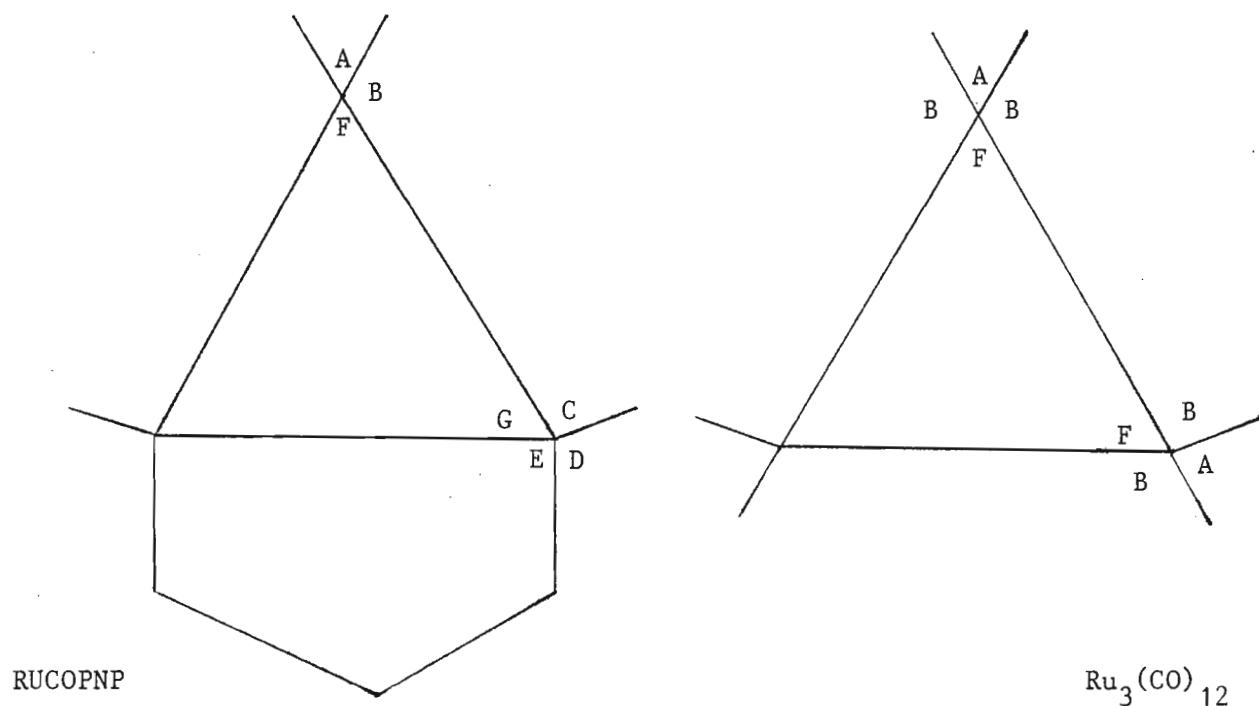


Fig. 8.3 Nomenclature for equatorial bond angles.

From the table it can be seen that all the equatorial ligand bonds have been rotated in the sense towards the nitrogen atom. This phenomenon has also been observed in $\text{Os}_3(\text{CO})_{12}$ on the addition of a μ_2 -bridging hydride ($\text{H}_2\text{Os}_3(\text{CO})_{11}$)⁽²⁰⁾. Thus the Ru-Ru-P angle E in RUCOPNP is $8,2^\circ$ smaller than the equivalent angle B in $\text{Ru}_3(\text{CO})_{12}$; the Ru-Ru-C angle C is $11,4^\circ$ larger than the equivalent angle B and the C-Ru-C angle A is $3,8^\circ$ larger than the equivalent angle A. Why the angle C should have increased to such a large extent and the angle D become $3,4^\circ$ smaller is not clear.

In summary, the addition of the PNP ligand has the following effects:

1. It causes contraction of the bond length between the bridged Ru atoms.
2. It causes the adjacent equatorial carbonyl ligands to be rotated towards the PNP ligand relative to their positions in $\text{Ru}_3(\text{CO})_{12}$.
3. It causes considerable deviations of some of the axial carbonyl ligands from the normal to the Ru_3 plane.

REFERENCES

1. G. EWART, A.P. LANE, J. McKECHNIE & D.S. PAYNE, J. Chem. Soc. (A) (1964), 1543-1547.
2. F.A. COTTON & B.E. HANSON, Inorg. Chem. 16 (1977), 3369-3371.
3. G.H. STOUT & L.H. JENSEN, 'X-ray Structure Determination, A Practical Guide', (Macmillan, New York, 1968).
4. E.W. NUFFIELD, 'X-ray Diffraction Method', (Wiley, London, 1966).
5. E.R. WÖLFEL, J. Appl. Cryst. 4 (1971), 297-302.
6. O. WEISZ & W.F. COLE, J. Sci. Instrum. 25 (1948), 213-215.
7. O.P. HENDERSHOT, Rev. Sci. Instrum. 8 (1937), 436-438.
8. P. LUGER, 'Modern X-ray Analysis of Single Crystals', (Walter de Gruyter, Berlin, 1980).
9. M.J. BUERGER, 'The Precession Method', (Wiley, New York, 1964).
10. G.W.H. MILBURN, 'X-ray Crystallography', (Butterworth, London, 1973).
11. J.A. IBERS & W.C. HAMILTON (Editors), 'International Tables for X-ray Crystallography', Vol. IV, Kynoch Press, Birmingham, England, 1974. (a) Table 2.1C, p. 61 (Mass Absorption Coefficients)
(b) Table 2.2B, p. 100 (Scattering factors for Ru).

12. H. LIPSON & W. COCHRAN, 'The Determination of Crystal Structures', (Bell, London, 1968).
13. G.M. SHELDRICK, SHELX 76. Program for crystal structure determination, (University of Cambridge, England, 1976).
14. M.M. WOOLFSON, 'An Introduction to X-ray Crystallography', (Cambridge University Press, 1970).
15. D.T. CROMER & J.B. MANN, Acta Cryst. A24 (1968), 321-324.
16. D.T. CROMER & J. LIBERMAN, J. Chem. Phys. 53 (1970), 1891-1898.
17. D.T. CROMER, R.F. STEWART, E. DAVIDSON & W. SIMPSON, J. Chem. Phys. 42 (1965), 3175-3187.
18. J.F. DE WET, CRYSTEP Desk Plotter System, J. Appl. Cryst. 13 (1980), 625-629.
19. M.R. CHURCHILL, F.J. HOLLANDER & J.P. HUTCHINSON, Inorg. Chem. 16 (1977), 2655-2659.
20. M.R. CHURCHILL & B.G. DE BOER, Inorg. Chem. 16 (1977), 878-884.
21. G. LAVIGNE, N. LUGAN & J.J. BONNET, Acta Cryst. B38 (1982), 1911-1916.
22. R.E. BENFIELD, B.F.G. JOHNSON, P.R. RAITBY & G.M. SHELDRICK, Acta Cryst. B34 (1978), 666-667.

23. E.J. FORBES, N. GOODHAND, D.L. JONES & T.A. HAMOR, *J. Organomet. Chem.* 182 (1979), 143-154.
24. R. MASON & A.I.M. RAE, *J. Chem. Soc. (A)* (1968), 778-779.
25. K. SASVARI, P. MAIN, F.H. CANO & M. MARTINEZ-RIPOLL, *Fourth European Crystallographic Meeting*, (1977), 227.
26. R.D. WILSON, S.M. WU, R.A. LOVE & R. BAU, *Inorg. Chem.* 17 (1978), 1271-1280.
27. S.F.A. KETTLE, *Inorg. Chem.* 4 (1965), 1661-1663.

APPENDIX 1ERROR CALCULATIONS FOR RECIPROCAL LATTICE PARAMETERS

List of parameters used in calculations:

$$a = 6,431 \pm 0,003 \text{ mm}$$

$$c = 15,957 \pm 0,007 \text{ mm}$$

$$g = 9,379 \pm 0,009 \text{ mm}$$

$$b = 9,801 \pm 0,003 \text{ mm}$$

$$k = 12,036 \pm 0,005 \text{ mm}$$

$$i = 10,107 \pm 0,006 \text{ mm}$$

$$f = 7,798 \text{ mm}$$

$$h = 8,894 \text{ mm}$$

Error in f:

$$\text{Now } Y = 3f^2 = c^2 + 2g^2 - 6a^2$$

Therefore

$$\begin{aligned} [\sigma(Y)]^2 &= [\sigma(c^2)]^2 + [2\sigma(g^2)]^2 + [6\sigma(a^2)]^2 \\ &= [2c\sigma(c)]^2 + [4g\sigma(g)]^2 + [12a\sigma(a)]^2 \\ &= 4[(c\sigma(c))^2 + (2g\sigma(g))^2 + (6a\sigma(a))^2] \\ &= 4[(15,957 \times 0,007)^2 + (2 \times 9,379 \times 0,009)^2 \\ &\quad + (6 \times 6,431 \times 0,003)^2] \\ &= 4[(0,112)^2 + (0,169)^2 + (0,116)^2] \end{aligned}$$

$$\sigma(Y) = 2 \times 0,234$$

$$= 0,468 \text{ mm}^2$$

$$\text{Now } f = \left(\frac{1}{3} Y\right)^{\frac{1}{2}}, \text{ so that}$$

$$\sigma(f) = \frac{1}{2} \left(\frac{1}{3} Y\right)^{-\frac{1}{2}} \frac{1}{3} \sigma(Y)$$

$$= \frac{1}{6} \frac{1}{f} \sigma(Y)$$

$$= \frac{1}{6} \times \frac{1}{7,798} \times 0,468$$

$$= 0,010 \text{ mm.}$$

Hence

$$f = 7,798 \pm 0,010 \text{ mm.}$$

Error in \hat{a}^f

$$\text{Let } X = 2(3)^{\frac{1}{2}} \cos \hat{a}^f = \frac{(g^2 - c^2 + 3a^2)}{a(c^2 + 2g^2 - 6a^2)^{\frac{1}{2}}} = s t u.$$

Where

$$s = g^2 - c^2 + 3a^2 = -42,587$$

$$t = a^{-1} = 0,15550$$

$$u = (c^2 + 2g^2 - 6a^2)^{-\frac{1}{2}} = (182,411)^{-\frac{1}{2}} = 0,074041$$

$$X = s t u = -0,49030$$

Now

$$[\sigma(X)]^2 = \left[\frac{\partial X}{\partial a} \sigma(a) \right]^2 + \left[\frac{\partial X}{\partial c} \sigma(c) \right]^2 + \left[\frac{\partial X}{\partial g} \sigma(g) \right]^2$$

Therefore,

$$\left[\frac{1}{X} \sigma(X) \right]^2 = \left[\frac{1}{X} \frac{\partial X}{\partial a} \sigma(a) \right]^2 + \left[\frac{1}{X} \frac{\partial X}{\partial c} \sigma(c) \right]^2 + \left[\frac{1}{X} \frac{\partial X}{\partial g} \sigma(g) \right]^2$$

Also

$$\begin{aligned} \frac{1}{X} \frac{\partial X}{\partial a} &= \frac{1}{s} \frac{\partial s}{\partial a} + \frac{1}{t} \frac{\partial t}{\partial a} + \frac{1}{u} \frac{\partial u}{\partial a} \\ &= 6a/s + (-a^{-2})/a^{-1} + 6u^3 a/u \\ &= 6a/s - a^{-1} + 6u^2 a \\ &= 6(6,431)/(-42,587) - (6,431)^{-1} + 6(0,074041)^2 (6,431) \\ &= -0,90605 - 0,15550 + 0,21153 \\ &= -0,85002 \end{aligned}$$

$$\begin{aligned}
\frac{1}{X} \frac{\partial X}{\partial c} &= \frac{1}{s} \frac{\partial s}{\partial c} + \frac{1}{t} \frac{\partial t}{\partial c} + \frac{1}{u} \frac{\partial u}{\partial c} \\
&= -2c/s + 0 + (-u^3 c)/u \\
&= -2c/s + 0 - u^2 c \\
&= -2(15,957)/(-42,587) + 0 - (0,074041)^2 (15,957) \\
&= 0,74938 + 0 - 0,08747 \\
&= + 0,66191
\end{aligned}$$

$$\begin{aligned}
\frac{1}{X} \frac{\partial X}{\partial g} &= \frac{1}{s} \frac{\partial s}{\partial g} + \frac{1}{t} \frac{\partial t}{\partial g} + \frac{1}{u} \frac{\partial u}{\partial g} \\
&= 2g/s + 0 + (-2u^3 g)/u \\
&= 2g/s + 0 - 2u^2 g \\
&= 2(9,379)/(-42,587) + 0 - 2(0,074041)^2 (9,379) \\
&= -0,44046 + 0 - 0,10283 \\
&= -0,54330
\end{aligned}$$

Therefore

$$\begin{aligned}
\left[\frac{1}{X} \sigma(X) \right]^2 &= \left[\frac{1}{X} \frac{\partial X}{\partial a} \sigma(a) \right]^2 + \left[\frac{1}{X} \frac{\partial X}{\partial c} \sigma(c) \right]^2 + \left[\frac{1}{X} \frac{\partial X}{\partial g} \sigma(g) \right]^2 \\
&= [(-0,850) \sigma(a)]^2 + [0,662 \sigma(c)]^2 + [(-0,543) \sigma(g)]^2 \\
&= (0,850 \times 0,003)^2 + (0,662 \times 0,007)^2 + (0,543 \times 0,009)^2 \\
&= (0,00255)^2 + (0,00463)^2 + (0,00489)^2
\end{aligned}$$

so that

$$\frac{1}{X} \sigma(X) = 0,00720$$

and $\sigma(X) = 0,4903 \times 0,0072 = 0,0035$

i.e. $X = -0,4903 \pm 0,0035$

$$\cos \underline{a} \hat{=} \underline{f} = X/2(3)^{\frac{1}{2}} = -0,14154 \pm 0,00101$$

Now $\sigma(\underline{a} \hat{=} \underline{f}) = \sigma(\cos \underline{a} \hat{=} \underline{f}) / |\sin \underline{a} \hat{=} \underline{f}|$

$$\begin{aligned}
&= 0,00101 / |\sin 98,14^\circ| \\
&= 0,00102 \text{ rad.} \\
&= 0,058^\circ
\end{aligned}$$

Therefore $\underline{a} \hat{=} \underline{f} = 98,14 \pm 0,06^\circ$

Error in h

$$\text{Now } T = 2h^2 = -2a^2 + b^2 + k^2$$

Therefore

$$\begin{aligned} [\sigma(T)]^2 &= [2\sigma(a^2)]^2 + [\sigma(b^2)]^2 + [\sigma(k^2)]^2 \\ &= [4a\sigma(a)]^2 + [2b\sigma(b)]^2 + [2k\sigma(k)]^2 \\ &= (4 \times 6,431 \times 0,003)^2 + (2 \times 9,801 \times 0,005)^2 \\ &\quad + (2 \times 12,036 \times 0,005)^2 \\ &= (0,0772)^2 + (0,0980)^2 + (0,120)^2 \end{aligned}$$

$$\sigma(T) = (0,02996)^{\frac{1}{2}} = 0,173$$

$$\text{Now } h = \left(\frac{1}{2} T\right)^{\frac{1}{2}}, \text{ so that}$$

$$\begin{aligned} \sigma(h) &= \frac{1}{2} \left(\frac{1}{2} T\right)^{-\frac{1}{2}} \cdot \frac{1}{2} \sigma(T) \\ &= \frac{1}{4} \cdot \frac{1}{h} \cdot \sigma(T) \\ &= \frac{1}{4} \cdot \frac{1}{8,894} \cdot 0,173 \\ &= 0,00487 \end{aligned}$$

$$\text{Hence } h = 8,894 \pm 0,005 \text{ mm}$$

Error in \hat{f}_h

$$\text{Let } Z = 2(6)^{\frac{1}{2}} \cos \hat{f}_h = \frac{(18a^2 - 3b^2 - 2c^2 - 4g^2 + 6i^2 - 3k^2)}{(-6a^2 + c^2 + 2g^2)^{\frac{1}{2}} (-2a^2 + b^2 + k^2)^{\frac{1}{2}}} = p \ q \ r$$

where

$$p = 18a^2 - 2b^2 - 2c^2 - 4g^2 + 6i^2 - 3k^2 = -226,541$$

$$q = (-6a^2 + c^2 + 2g^2)^{-\frac{1}{2}} = 0,074041$$

$$r = (-2a^2 + b^2 + k^2)^{-\frac{1}{2}} = 0,079503$$

$$\therefore Z = -1,33354$$

We have

$$\begin{aligned} \frac{1}{Z} \frac{\partial Z}{\partial a} &= \frac{1}{p} \frac{\partial p}{\partial a} + \frac{1}{q} \frac{\partial q}{\partial a} + \frac{1}{r} \frac{\partial r}{\partial a} \\ &= 36a/p + \left(-\frac{1}{2}q^3\right) (-12a)/q + \left(-\frac{1}{2}r^3\right) (-4a)/r \\ &= 36a/p + 6q^2 a + 2r^2 a \end{aligned}$$

$$\begin{aligned}
&= 36(6,431)/(-226,541) + 6(0,074041)^2 (6,431) + 2(0,079503)^2 (6,431) \\
&= -1,02196 + 0,21153 + 0,08130 \\
&= -0,72913
\end{aligned}$$

$$\begin{aligned}
\frac{1}{Z} \frac{\partial Z}{\partial b} &= \frac{1}{p} \frac{\partial p}{\partial b} + \frac{1}{q} \frac{\partial q}{\partial b} + \frac{1}{r} \frac{\partial r}{\partial b} \\
&= -6b/p + 0 + \left(-\frac{1}{2}r^3\right) (2b)/r \\
&= -6b/p + 0 - r^2 b \\
&= -6(9,801)/(-226,541) + 0 - (0,079503)^2 (9,801) \\
&= -0,25958 + 0 - 0,06195 \\
&= -0,32153
\end{aligned}$$

$$\begin{aligned}
\frac{1}{Z} \frac{\partial Z}{\partial c} &= \frac{1}{p} \frac{\partial p}{\partial c} + \frac{1}{q} \frac{\partial q}{\partial c} + \frac{1}{r} \frac{\partial r}{\partial c} \\
&= -4c/p + \left(-\frac{1}{2}q^3\right) (2c)/q + 0 \\
&= -4c/p - q^2 c + 0 \\
&= -4(15,957)/(-226,541) - (0,074041)^2 (15,957) \\
&= +0,28175 - 0,08748 + 0 \\
&= +0,19427
\end{aligned}$$

$$\begin{aligned}
\frac{1}{Z} \frac{\partial Z}{\partial g} &= \frac{1}{p} \frac{\partial p}{\partial g} + \frac{1}{q} \frac{\partial q}{\partial g} + \frac{1}{r} \frac{\partial r}{\partial g} \\
&= -8g/p + \left(-\frac{1}{2}q^3\right) (4g)/q + 0 \\
&= -8g/p - 2q^2 g + 0 \\
&= -8(9,379)/(-226,541) - 2(0,074041)^2 \cdot (9,379) + 0 \\
&= 0,33121 - 0,10283 + 0 \\
&= +0,22838
\end{aligned}$$

$$\begin{aligned}
\frac{1}{Z} \frac{\partial Z}{\partial i} &= \frac{1}{p} \frac{\partial p}{\partial i} + \frac{1}{q} \frac{\partial q}{\partial i} + \frac{1}{r} \frac{\partial r}{\partial i} \\
&= 12i/p + 0 + 0 \\
&= 12(10,107)/(-226,541) \\
&= -0,53537
\end{aligned}$$

$$\begin{aligned}
\frac{1}{Z} \frac{\partial Z}{\partial k} &= \frac{1}{p} \frac{\partial p}{\partial k} + \frac{1}{q} \frac{\partial q}{\partial k} + \frac{1}{r} \frac{\partial r}{\partial k} \\
&= -6k/p + 0 + \left(-\frac{1}{2}r^3\right) (2k)/r \\
&= -6k/p + 0 - r^2 k \\
&= -6(12,036)/(-226,541) + 0 - (0,079503)^2 (12,036) \\
&= +0,31878 + 0 - 0,07608 \\
&= +0,24270
\end{aligned}$$

Hence

$$\begin{aligned}
\left[\frac{1}{Z} \sigma(Z)\right]^2 &= \left[\frac{1}{Z} \frac{\partial Z}{\partial a} \sigma(a)\right]^2 + \left[\frac{1}{Z} \frac{\partial Z}{\partial b} \sigma(b)\right]^2 + \left[\frac{1}{Z} \frac{\partial Z}{\partial c} \sigma(c)\right]^2 \\
&\quad + \left[\frac{1}{Z} \frac{\partial Z}{\partial g} \sigma(g)\right]^2 + \left[\frac{1}{Z} \frac{\partial Z}{\partial i} \sigma(i)\right]^2 + \left[\frac{1}{Z} \frac{\partial Z}{\partial k} \sigma(k)\right]^2 \\
&= [(-0,729 \sigma(a))]^2 + [(-0,322 \sigma(b))]^2 + [0,194 \sigma(c)]^2 \\
&\quad + [0,228 \sigma(g)]^2 + [-0,535 \sigma(i)]^2 + [0,243 \sigma(k)]^2 \\
&= (0,729 \times 0,003)^2 + (0,322 \times 0,005)^2 + (0,194 \times 0,007)^2 \\
&\quad + (0,228 \times 0,009)^2 + (0,535 \times 0,006)^2 + (0,243 \times 0,005)^2 \\
&= (0,00219)^2 + (0,00161)^2 + (0,00136)^2 + (0,00205)^2 \\
&\quad \quad \quad + (0,00321)^2 + (0,00122)^2
\end{aligned}$$

and

$$\frac{1}{Z} \sigma(Z) = 0,00502$$

Therefore

$$\sigma(Z) = 1,33354 \times 0,00502 = 0,0067$$

$$Z = -1,3335 \pm 0,0067$$

Now

$$\cos \underline{\hat{f}}_h = Z/2(6)^{\frac{1}{2}} = -0,2722 \pm 0,0014$$

$$\text{and } \sigma(\underline{\hat{f}}_h) = \sigma(\cos \underline{\hat{f}}_h) / |\sin \underline{\hat{f}}_h|$$

$$= 0,0014 / |\sin 105,80|$$

$$= 0,0015 \text{ rad} = 0,08^\circ$$

Therefore

$$\underline{\hat{f}}_h = 105,80 \pm 0,08^\circ$$

Error in \hat{a}_h

$$\text{Let } U = 2(2)^{\frac{1}{2}} \cos \hat{a}_h = \frac{(k^2 - b^2)}{a(k^2 - 2a^2 + b^2)^{\frac{1}{2}}} = v t w$$

where

$$v = k^2 - b^2 = 48,8057$$

$$t = a^{-1} = 0,155497$$

$$w = (k^2 - 2a^2 + b^2)^{-\frac{1}{2}} = 0,079503$$

$$U = 0,603359$$

We have

$$\begin{aligned} \frac{1}{U} \frac{\partial U}{\partial a} &= \frac{1}{v} \frac{\partial v}{\partial a} + \frac{1}{t} \frac{\partial t}{\partial a} + \frac{1}{w} \frac{\partial w}{\partial a} \\ &= 0 + (-1a^{-2})/a^{-1} + 2aw^3/w \\ &= 0 - a^{-1} + 2aw^2 \\ &= 0 - (6,431)^{-1} + 2(6,431) (0,079503)^2 \\ &= 0 - 0,155497 + 0,08130 \\ &= - 0,07420 \end{aligned}$$

$$\begin{aligned} \frac{1}{U} \frac{\partial U}{\partial b} &= \frac{1}{v} \frac{\partial v}{\partial b} + \frac{1}{t} \frac{\partial t}{\partial b} + \frac{1}{w} \frac{\partial w}{\partial b} \\ &= - 2b/v + 0 + (-bw^3)/w \\ &= - 2b/v + 0 - bw^2 \\ &= - 2(9,801)/48,8057 + 0 - (9,801) (0,079503)^2 \\ &= - 0,40163 + 0 - 0,061949 \\ &= - 0,46358 \end{aligned}$$

$$\begin{aligned} \frac{1}{U} \frac{\partial U}{\partial k} &= \frac{1}{v} \frac{\partial v}{\partial k} + \frac{1}{t} \frac{\partial t}{\partial k} + \frac{1}{w} \frac{\partial w}{\partial k} \\ &= 2k/v + 0 + (-kw^3)/w \\ &= 2k/v + 0 - kw^2 \\ &= 2(12,036)/(48,8057) + 0 - (12,036) (0,079503)^2 \\ &= 0,49322 + 0 - 0,076076 \\ &= 0,41714 \end{aligned}$$

Therefore

$$\begin{aligned}
 \left[\frac{1}{U} \sigma(U) \right]^2 &= \left[\frac{1}{U} \frac{\partial U}{\partial a} \sigma(a) \right]^2 + \left[\frac{1}{U} \frac{\partial U}{\partial b} \sigma(b) \right]^2 + \left[\frac{1}{U} \frac{\partial U}{\partial k} \sigma(k) \right]^2 \\
 &= [(-0,0742) \sigma(a)]^2 + [(-0,464) \sigma(b)]^2 + [0,417 \sigma(k)]^2 \\
 &= (0,0742 \times 0,003)^2 + (0,464 \times 0,003)^2 + (0,417 \times 0,005)^2 \\
 &= (0,0002226)^2 + (0,00139)^2 + (0,002085)^2
 \end{aligned}$$

so that

$$\frac{1}{U} \sigma(U) = 0,00252$$

and $\sigma(U) = 0,6034 \times 0,00252 = 0,0015$

i.e. $U = 0,6034 \pm 0,0015$

$$\cos \underline{\hat{a}}_h = U/2(2)^{\frac{1}{2}} = 0,21333 \pm 0,00053$$

Now $\sigma(\underline{\hat{a}}_h) = \sigma(\cos \underline{\hat{a}}_h) / |\sin \underline{\hat{a}}_h|$

$$\begin{aligned}
 &= 0,00053 / |\sin 77,68| \\
 &= 0,000542 \text{ rad} = 0,03^\circ
 \end{aligned}$$

Therefore

$$\underline{\hat{a}}_h = 77,68 \pm 0,03^\circ.$$

APPENDIX 2

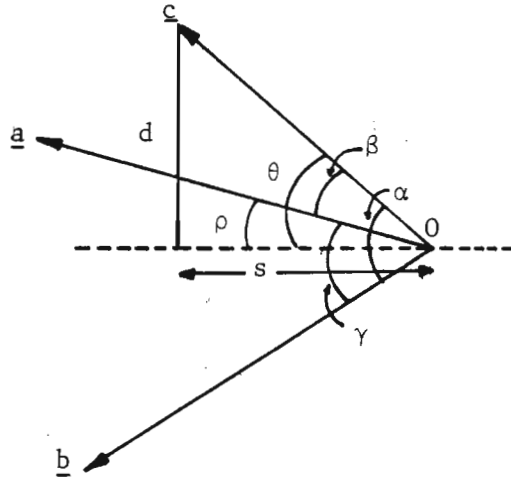
TRANSFORMATION MATRIX FROM SKEW TO ORTHOGONAL COORDINATES

Fig. A2.1 Vectors a, b and c and related angles.

Fig. A2.1 shows vectors a, b and c from the origin 0. The vector c is out of the plane formed by a and b. s is the (perpendicular) projection of c onto the a - b plane.

The following relations hold:

$$c^2 = d^2 + s^2$$

$$\tan \theta = d/s$$

$$\cos \beta = \cos \theta \cos \rho$$

$$\cos \alpha = \cos \theta \cos(\gamma - \rho).$$

(A2.1)

From these equations the following are derived:

$$\cos \theta = \cos \beta / \cos \rho$$

$$d = c \sin \theta$$

$$s = c \cos \theta$$

$$\tan \rho = \left[\frac{\cos \alpha}{\cos \beta} - \cos \gamma \right] \sin \gamma$$

(A2.2)

The lattice constants for RUCOPNP are:

$$a = 14,732\text{\AA}; \quad b = 12,386\text{\AA}; \quad c = 10,982\text{\AA}$$

$$\alpha = 104,525^\circ; \quad \beta = 100,644^\circ; \quad \gamma = 94,893^\circ$$

$$\begin{aligned} \text{Then } \tan \rho &= \left[\frac{\cos 104,525}{\cos 100,644} - \cos 94,893 \right] \sin 94,893^\circ \\ &= 1,448419 \end{aligned}$$

so that $\rho = 55,378^\circ$.

Also:

$$\cos \theta = \cos \beta / \cos \rho = \cos 100,644 / \cos 55,778^\circ = -0,325099 \rightarrow \theta = 108,972^\circ$$

$$s = c \cos \theta = 10,982 \cdot \cos 108,972 = -3,570$$

$$d = c \sin \theta = 10,982 \cdot \sin 108,972 = 10,385.$$

Fig. A2.2 shows the relationships when $\alpha, \beta, \gamma \geq 90$ as is the convention for the direct unit cell. Note that $\theta > 90$ and s is negative.

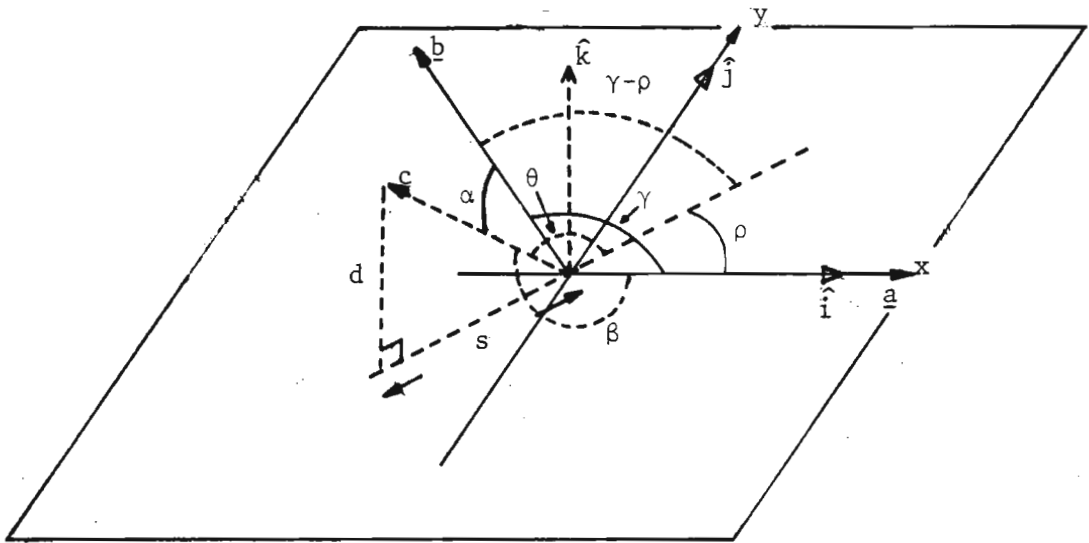


Fig. A2.2 Geometry of the x, y, z and $\hat{i}, \hat{j}, \hat{k}$ coordinate systems, common origin O .

A vector $\underline{r} = x\underline{a} + y\underline{b} + z\underline{c}$ in skew co-ordinates is transformed into the vector $\underline{r} = u\underline{\hat{i}} + v\underline{\hat{j}} + w\underline{\hat{k}}$ in right-handed rectangular co-ordinates (x, y, z are fractional co-ordinates and u, v, w are in \AA).

$$\text{Now } \underline{a} = a\underline{\hat{i}}$$

$$\underline{b} = b \cos \gamma \underline{\hat{i}} + b \sin \gamma \underline{\hat{j}}$$

$$\underline{c} = s \cos \rho \underline{\hat{i}} + s \sin \rho \underline{\hat{j}} + c \sin \theta \underline{\hat{k}} \quad (\underline{c} = \underline{s} + \underline{d})$$

Hence

$$\underline{a} = 14,732 \underline{\hat{i}} + 0,0 \underline{\hat{j}} + 0,0 \underline{\hat{k}}$$

$$\begin{aligned}\underline{b} &= (12,386 \cos 94,893) \hat{i} + (12,386 \sin 94,893) \hat{j} \\ &= -1,056 \hat{i} + 12,341 \hat{j} + 0,0 \hat{k}\end{aligned}$$

$$\begin{aligned}\underline{c} &= (-3,570 \cos 55,378) \hat{i} + (-3,570 \sin 55,378) \hat{j} + 10,385 \hat{k} \\ &= -2,028 \hat{i} - 2,938 \hat{j} + 10,385 \hat{k}\end{aligned}$$

Therefore in matrix notation,

$$\begin{bmatrix} \underline{a} \\ \underline{b} \\ \underline{c} \end{bmatrix} = \begin{bmatrix} 14,732 & 0 & 0 \\ -1,056 & 12,341 & 0 \\ -2,028 & -2,938 & 10,385 \end{bmatrix} \begin{bmatrix} \hat{i} \\ \hat{j} \\ \hat{k} \end{bmatrix} \quad (\text{A2.3})$$

Hence

$$\begin{aligned}\underline{r} &= x\underline{a} + y\underline{b} + z\underline{c} \\ &= x(14,732 \hat{i} + 0 \hat{j} + 0 \hat{k}) \\ &\quad + y(-1,056 \hat{i} + 12,341 \hat{j} + 0 \hat{k}) \\ &\quad + z(-2,028 \hat{i} - 2,938 \hat{j} + 10,385 \hat{k}) \\ &= (14,732 x - 1,056 y - 2,028 z) \hat{i} \\ &\quad + (0,0 x + 12,341 y - 2,938 z) \hat{j} \\ &\quad + (0,0 x + 0,0 y + 10,385 z) \hat{k} \\ &= u\hat{i} + v\hat{j} + w\hat{k}\end{aligned}$$

Hence finally

$$\begin{bmatrix} u \\ v \\ w \end{bmatrix} = \begin{bmatrix} 14,732 & -1,056 & -2,028 \\ 0 & 12,341 & -2,938 \\ 0 & 0 & 10,385 \end{bmatrix} \begin{bmatrix} x \\ y \\ z \end{bmatrix} = A \begin{bmatrix} x \\ y \\ z \end{bmatrix} \quad (\text{A2.4})$$

APPENDIX 3THE SHELX PROGRAM (13)

The integrated program performs crystallographic calculations simply and efficiently. It is written in a simple subset of ASA Fortran and is therefore ideal for use on any computer. The calculations are valid for all space groups, and there is no limit on the number of reflections used. In implementing the program on the ICL 2946 several dimension statements had to be changed.

The instruction cards supply the programs with various information pertinent to the crystal under study and define which calculations are to be carried out. The first four characters on a card define the type of instruction. The next 76 columns convey numerical information. The instruction cards used in this analysis are now explained.

- * TITL - any convenient title
- * CELL - specifies radiation used and the cell parameters
- * LATT n - specifies lattice type
- * SYMM - specifies the symmetry information by giving the co-ordinates of the general position
- * SFAC - sets up complex neutral atom scattering factors for common elements. The data is contained in the program. Other scattering factors may be set up as follows:
- *SFAC a1, b1, a2, b2, a3, b3, a4, b4, c, df', df'', μ , r.

The real part of the scattering factor is given by
 $a_1 \exp(-b_1 s^2) + \dots + a_4 \exp(-b_4 s^2) + c + df'$
 where $s = \sin \theta / \lambda$. df'' is the imaginary part, μ the absorption coefficient in cm^{-1} , and r the covalent radius.

*UNIT n1, n2, n3, n4 - specifies the number of atoms of each type in the unit cell in the same order as the SFAC cards.

*HKLF n,s - specifies the type of input data; s is a multiplicative scale factor.

MERG n - puts data on an approximately absolute scale and calculates an overall temperature factor. This program has options to perform other calculations related to data reduction.

OMIT s - reflections for which $s\sigma(F) > F$ are suppressed.

OMIT h, k, l - suppresses reflections hkl before doing least-squares refinement, etc.

*L.S. nls - does full matrix (or blocked full-matrix) least-squares refinement. nls = number of cycles

BOND - calculates bond lengths and angles of input atoms

LIST n, m - produces m copies of F_o/F_c tables in publication format

FMAP n, na, nl, np, s. Fourier synthesis. n specifies the type of map to be calculated (e.g. Patterson, Fourier, difference Fourier). na specifies which layers of the map are to be calculated e.g. na = 1 calculates layers of constant x, with y across the page and z down the page. Negative na is similar but has the 'across' and 'down' axes interchanged. nl = number of layers. np = number of strongest peaks to be found in the peak search. s is a weighting factor.

GRID 10, a0, d0, dl, da, dd - specifies the grid of the Fourier map. 10, a0, d0 are the starting values and dl, da, dd the increments for layers, across and down respectively, multiplied by 100 and given as integers.

PLAN n, ax - assembles and plots (on the line printer) the 'molecules' derived from the atoms plus the highest n unique Fourier peaks (if any). The 'elevation' (the height in inches above the paper) is printed to aid model building.

ax sets an axis for a projection of the asymmetric unit and the cell edges to be plotted. In this plot atoms are identified by the molecule number.

*FVAR osf, fv(2), fv(3) specifies the overall scale factor; fv(2) etc. are free variables and parameters on "atom cards" can be related to these free variables. This is useful if several parameters are to have the same value (or related values) i.e. for applying constraints to parameters.

*'ATOM CARDS' - these cards start with any four characters which do not form another instruction. They are used as the names of the atom. Isotropic and anisotropic atoms are distinguished by the number of temperature factor components, and may be given in any order: isotropic - name (4 characters), type, x/a, y/b, z/c, s.o.f., U. Type refers to the atom which has the n^{th} scattering factor on the SFAC card, (x/a, y/b, z/c) are the fractional co-ordinates of the atom, s.o.f. the site occupation factor and U the isotropic temperature factor. Anisotropic - as above but in place of U use U11, U22, U33, U23, U13, U12 (the U's are the anisotropic temperature factors). (A parameter on an 'atom card' may be fixed by adding 10). To set a parameter to be a free variable, it is given as 10^*m+p and interpreted as $p*fv(m)$; m = free variable number on FVAR card, p = integer.

ANIS n - makes the next n isotropic atoms anisotropic.

AFIX m - The card is used to generate a regular pentagon or hexagon, to add H-atoms to them or to generate the H-atoms of CH, CH₂ and CH₃ groups. The card applies constraints to all atoms until the next 'AFIX' card is read. m refers to geometrical operations before the first refinement cycle, and n to constraints during least-squares refinement.

BLOC n1, n2 - This card divides the refinement into blocks. n1, n2 refer to least squares refinement cycle numbers in which the following atoms (until the next BLOC card) are to be refined (subject to AFIX and any other constraints). Before the first BLOC card, parameters may refine in any cycle.

END n - transfer control from the present instruction stream to unit n e.g. another input file

*END - must be last instruction card.

In the above instruction cards, those marked with an * must, if used, appear in the order given. All other cards may be given in any order. The first card however, must be TITL and the last END. The CELL, SFAC and UNIT cards are also obligatory.

In order to save memory space by creating fewer long files on the computer, two files were created, the REFLDATA and ATOMDATA files. The REFLDATA file consisted of the cards TITL, CELL, SYMM, SFAC, UNIT, HKLF and the 5295 observed structure factors (terminated by a blank card) and then the END 4 card. This file remained unchanged except for the HKLF card. The END 4 card transferred control from the REFLDATA file to the ATOMDATA file. The ATOMDATA file consisted of those cards which were involved in the execution of the various crystallographic calculations. This file was continually edited to accommodate the different calculations to be carried out. These files were short and thus conveniently saved after editing (for reference) without taking up much user memory.

OBSERVED AND CALCULATED STRUCTURE FACTORS FOR RUCOPNP

PAGE 1

H	K	L	FO	FC	H	K	L	FO	FC	H	K	L	FO	FC	H	K	L	FO	FC	H	K	L	FO	FC
3	0	0	103	-111	8	2	0	55	-48	6	4	0	53	53	11	6	0	33	-41	-1	9	0	189	-197
4	0	0	143	135	9	2	0	28	-33	9	4	0	159	-165	12	6	0	72	-71	-2	9	0	128	-128
5	0	0	331	328	11	2	0	49	54	10	4	0	32	-25	13	6	0	35	30	-3	9	0	89	93
6	0	0	31	46	13	2	0	74	-80	11	4	0	58	52	11	7	0	38	47	-4	9	0	108	115
7	0	0	133	-137	14	2	0	72	-79	12	4	0	58	59	10	7	0	42	32	-9	9	0	30	20
8	0	0	91	-94	14	3	0	51	-50	13	5	0	59	62	7	7	0	54	-63	-10	9	0	41	-40
9	0	0	99	101	10	3	0	33	33	12	5	0	53	49	5	7	0	104	110	-12	9	0	60	58
10	0	0	58	63	9	3	0	32	-39	11	5	0	57	-61	4	7	0	71	72	-13	9	0	48	40
11	0	0	110	-108	8	3	0	37	-95	10	5	0	137	-143	2	7	0	52	-55	-11	10	0	31	31
12	0	0	48	-57	6	3	0	98	98	9	5	0	52	72	1	7	0	52	-49	-8	10	0	32	35
14	0	0	51	53	5	3	0	133	133	8	5	0	213	219	0	7	0	24	-32	-6	10	0	51	-48
14	1	0	47	46	4	3	0	51	51	7	5	0	59	76	-1	7	0	138	143	-3	10	0	100	103
13	1	0	70	-77	2	3	0	100	-97	6	5	0	165	-177	-2	7	0	115	111	-2	10	0	76	77
12	1	0	78	-87	1	3	0	21	-20	5	5	0	178	-184	-3	7	0	62	-66	-1	10	0	45	-56
11	1	0	47	54	-1	3	0	61	-62	4	5	0	93	100	-4	7	0	43	-49	0	10	0	122	-127
10	1	0	118	120	-2	3	0	25	-20	3	5	0	128	137	-5	7	0	37	-36	2	10	0	114	116
9	1	0	82	-87	-3	3	0	156	148	1	5	0	131	-132	-6	7	0	38	35	3	10	0	46	47
8	1	0	114	-115	-5	3	0	286	-269	-1	5	0	187	190	-10	7	0	28	29	4	10	0	65	-71
7	1	0	56	60	-6	3	0	217	-200	-2	5	0	57	59	-11	7	0	76	72	5	10	0	52	-48
6	1	0	31	45	-7	3	0	66	60	-3	5	0	218	-221	-12	7	0	37	-38	7	10	0	49	57
4	1	0	189	-189	-8	3	0	178	169	-4	5	0	43	-36	-13	7	0	51	-56	4	11	0	42	40
3	1	0	95	-89	-9	3	0	90	89	-5	5	0	162	161	-13	8	0	34	36	3	11	0	42	40
2	1	0	251	242	-10	3	0	118	-116	-6	5	0	191	181	-12	8	0	61	-74	2	11	0	35	-32
-2	1	0	298	-270	-11	3	0	126	-118	-8	5	0	193	-187	-11	8	0	66	-63	1	11	0	66	-73
-3	1	0	137	122	-12	3	0	49	51	-9	5	0	87	-83	-10	8	0	72	73	-1	11	0	60	62
-4	1	0	113	101	-13	3	0	85	74	-10	5	0	96	93	-9	8	0	43	38	-4	11	0	29	-20
-7	1	0	86	-80	-15	3	0	43	-43	-11	5	0	62	58	-3	8	0	44	-47	-5	11	0	59	-55
-8	1	0	51	43	-14	4	0	34	-40	-13	5	0	57	-50	-7	8	0	38	-32	-6	11	0	34	-25
-10	1	0	85	-79	-12	4	0	105	100	-14	6	0	45	-44	-6	8	0	31	39	-7	11	0	33	35
-12	1	0	111	105	-11	4	0	77	69	-10	6	0	37	32	-5	8	0	64	63	-8	11	0	33	24
-14	1	0	32	-24	-10	4	0	174	-164	-9	6	0	60	62	-4	8	0	70	68	-9	11	0	37	34
-14	2	0	66	68	-9	4	0	183	-174	-7	6	0	63	-63	-3	8	0	151	-158	-8	12	0	37	40
-12	2	0	90	-86	-8	4	0	76	68	-6	6	0	39	-44	-2	8	0	236	-243	-7	12	0	73	67
-11	2	0	47	37	-7	4	0	249	240	-5	6	0	64	61	-1	8	0	131	142	-5	12	0	66	-61
-10	2	0	63	62	-6	4	0	39	44	-4	6	0	92	92	0	8	0	219	226	-4	12	0	63	-47
-9	2	0	88	83	-5	4	0	251	-240	-3	6	0	74	68	2	8	0	131	-140	-2	12	0	51	55
-8	2	0	24	15	-4	4	0	275	-266	-2	6	0	91	-88	3	8	0	112	-115	0	12	0	29	3
-7	2	0	98	-94	-3	4	0	66	-63	0	6	0	38	34	4	8	0	47	51	-1	13	0	51	52
-6	2	0	154	-138	-2	4	0	280	275	1	6	0	32	-36	5	8	0	92	89	-2	13	0	43	33
-4	2	0	203	178	-1	4	0	144	-140	2	6	0	104	-110	7	8	0	67	-83	-3	13	0	56	-54
-3	2	0	107	105	0	4	0	317	-314	3	6	0	45	53	10	9	0	47	41	-4	13	0	57	-57
-2	2	0	105	-94	1	4	0	36	-34	4	6	0	132	138	8	9	0	69	-75	-2	13	1	56	58
-1	2	0	140	-134	2	4	0	68	72	5	6	0	50	55	6	9	0	58	58	0	13	1	58	-63
0	2	0	262	-255	3	4	0	37	31	6	6	0	150	-164	4	9	0	60	-60	2	13	1	88	92
1	2	0	53	-46	4	4	0	185	-192	7	6	0	113	-114	3	9	0	143	-151	4	13	1	82	-82
2	2	0	47	47	5	4	0	152	-161	8	6	0	52	53	2	9	0	29	31	8	12	1	40	37
3	2	0	78	87	6	4	0	132	133	9	6	0	105	109	1	9	0	162	167	7	12	1	65	62
7	2	0	68	-61	7	4	0	204	211	10	6	0	57	64	0	9	0	51	58	5	12	1	61	-54

LIST OF OBSERVED AND CALCULATED STRUCTURE FACTORS
AFTER JOB 43 (R = 0,0537)

OBSERVED AND CALCULATED STRUCTURE FACTORS FOR PUCOPNP

PAGE 2

H	K	L	FO	FC	H	K	L	FO	FC	H	K	L	FO	FC	H	K	L	FO	FC	H	K	L	FO	FC
3-12	1	60	62	11	-8	1	47	55	-6	-6	1	140	-133	-4	-4	1	333	-313	-5	-2	1	112	109	
1-12	1	45	-38	10	-8	1	78	80	-7	-6	1	112	-106	-6	-4	1	149	145	-8	-2	1	85	-82	
-1-12	1	50	49	8	-8	1	86	-89	-8	-6	1	49	42	-7	-4	1	116	112	-9	-2	1	44	-42	
-2-12	1	34	30	7	-8	1	66	-60	-9	-6	1	114	117	-8	-4	1	40	-38	-10	-2	1	102	102	
-3-12	1	46	-43	6	-8	1	157	156	-11	-6	1	62	-60	-9	-4	1	142	-134	-11	-2	1	120	111	
-4-12	1	48	-49	5	-8	1	208	208	-13	-6	1	50	49	-10	-4	1	55	50	-13	-2	1	89	-90	
-1-11	1	30	-27	4	-8	1	48	-42	-12	-5	1	37	26	-11	-4	1	29	16	-14	-2	1	39	-34	
0-11	1	40	-44	3	-8	1	296	-286	-10	-5	1	72	-74	-12	-4	1	32	-28	-15	-2	1	37	36	
1-11	1	66	71	2	-8	1	32	-30	-9	-5	1	68	-61	-15	-3	1	43	-37	-15	-1	1	56	55	
2-11	1	61	62	1	-8	1	288	282	-8	-5	1	168	163	-14	-3	1	46	-51	-14	-1	1	65	61	
6-11	1	42	-35	0	-8	1	95	93	-7	-5	1	164	153	-10	-3	1	50	-46	-13	-1	1	38	-36	
8-11	1	56	58	-1	-8	1	28	-24	-6	-5	1	98	-93	-9	-3	1	50	-46	-12	-1	1	147	-140	
10-11	1	36	-33	-2	-8	1	97	-91	-5	-5	1	306	-300	-8	-3	1	99	-91	-11	-1	1	33	-36	
11-10	1	30	-31	-3	-8	1	50	-48	-4	-5	1	83	-81	-7	-3	1	79	-71	-10	-1	1	195	184	
10-10	1	30	-29	-4	-8	1	48	49	-3	-5	1	216	205	-6	-3	1	89	81	-9	-1	1	143	133	
9-10	1	32	27	-6	-8	1	44	-40	-2	-5	1	307	285	-5	-3	1	150	140	-8	-1	1	127	-118	
8-10	1	39	38	-8	-8	1	56	60	-1	-5	1	189	-171	-4	-3	1	76	-61	-7	-1	1	84	-83	
6-10	1	43	-44	-10	-8	1	65	-61	0	-5	1	336	-323	-3	-3	1	70	-65	-6	-1	1	88	78	
5-10	1	47	-46	-11	-8	1	36	-31	1	-5	1	74	67	-2	-3	1	135	-125	-5	-1	1	113	102	
4-10	1	33	29	-10	-7	1	45	51	2	-5	1	199	191	-1	-3	1	110	90	-4	-1	1	41	34	
3-10	1	119	121	-9	-7	1	38	-31	4	-5	1	57	47	0	-3	1	229	211	-3	-1	1	168	-141	
2-10	1	37	38	-8	-7	1	78	-76	5	-5	1	24	-20	1	-3	1	52	-44	-2	-1	1	32	32	
1-10	1	148	-142	-6	-7	1	42	37	6	-5	1	94	97	2	-3	1	94	85	2	-1	1	323	-316	
0-10	1	72	-68	-5	-7	1	47	53	7	-5	1	75	76	4	-3	1	57	60	3	-1	1	46	45	
-6-10	1	46	40	-4	-7	1	64	59	8	-5	1	71	-67	5	-3	1	31	24	4	-1	1	198	203	
-8-10	1	74	-79	-3	-7	1	33	-31	9	-5	1	142	-142	6	-3	1	186	-188	5	-1	1	67	73	
-10-9	1	62	65	-2	-7	1	140	-127	11	-5	1	138	142	8	-3	1	150	160	6	-1	1	53	-50	
-9-9	1	90	87	-1	-7	1	52	-51	12	-5	1	36	31	9	-3	1	120	127	7	-1	1	155	-151	
-8-9	1	42	-40	1	-7	1	79	76	13	-5	1	44	-45	10	-3	1	60	-66	8	-1	1	54	-56	
-7-9	1	92	-96	2	-7	1	108	100	14	-5	1	33	-30	11	-3	1	167	-173	9	-1	1	76	76	
-6-9	1	50	54	3	-7	1	31	-29	15	-4	1	57	-52	12	-3	1	72	-70	10	-1	1	70	77	
-5-9	1	55	62	4	-7	1	162	-156	14	-4	1	63	-63	13	-3	1	77	90	14	0	1	50	58	
-4-9	1	33	-35	5	-7	1	85	-85	13	-4	1	44	52	14	-3	1	67	71	12	0	1	56	-65	
-3-9	1	65	-67	6	-7	1	90	89	12	-4	1	134	140	15	-3	1	61	-61	10	0	1	123	123	
-1-9	1	103	100	7	-7	1	89	92	10	-4	1	224	-233	15	-2	1	55	56	8	0	1	211	-220	
0-9	1	151	153	9	-7	1	36	-34	9	-4	1	86	-90	14	-2	1	34	37	7	0	1	89	-97	
1-9	1	125	-124	11	-7	1	65	61	8	-4	1	92	94	12	-2	1	42	-46	6	0	1	159	165	
2-9	1	274	-267	12	-6	1	27	-30	7	-4	1	184	193	10	-2	1	58	66	5	0	1	460	457	
4-9	1	178	177	10	-6	1	92	93	6	-4	1	31	-37	9	-2	1	132	139	4	0	1	30	-31	
5-9	1	74	79	8	-6	1	37	-34	5	-4	1	204	-202	7	-2	1	115	-117	3	0	1	538	-526	
6-9	1	74	-80	6	-6	1	35	-30	4	-4	1	30	34	6	-2	1	62	-62	2	0	1	175	-176	
7-9	1	88	-90	5	-6	1	49	-51	3	-4	1	29	24	5	-2	1	21	19	-2	0	1	139	-135	
9-9	1	57	59	3	-6	1	79	76	2	-4	1	35	-36	3	-2	1	79	-72	-3	0	1	166	-142	
10-9	1	41	39	2	-6	1	24	27	1	-4	1	286	-271	2	-2	1	141	134	-4	0	1	39	39	
11-9	1	40	-51	1	-6	1	180	173	0	-4	1	218	-200	1	-2	1	119	109	-5	0	1	140	129	
13-9	1	46	42	-1	-6	1	197	-187	-1	-4	1	242	221	0	-2	1	311	-291	-6	0	1	63	-58	
13-8	1	42	-37	-3	-6	1	184	174	-2	-4	1	69	67	-2	-2	1	39	32	-7	0	1	68	-62	
12-8	1	60	-58	-4	-6	1	182	172	-3	-4	1	141	-135	-4	-2	1	196	172	-8	0	1	166	155	

OBSERVED AND CALCULATED STRUCTURE FACTORS FOR PUCOPNP

PAGE 3

H	K	L	FO	FC	H	K	L	FO	FC	H	K	L	FO	FC	H	K	L	FO	FC	H	K	L	FO	FC
-9	0	1	99	95	-8	2	1	134	-118	-10	4	1	53	-62	-10	7	1	120	125	7	10	1	40	33
-10	0	1	88	-82	-9	2	1	110	97	-11	4	1	53	54	-8	7	1	76	-73	6	10	1	36	-28
-11	0	1	144	-138	-10	2	1	60	54	-13	4	1	35	-35	-7	7	1	58	-55	5	10	1	70	-72
-12	0	1	71	74	-11	2	1	63	-61	-13	5	1	39	29	-5	7	1	38	-35	3	10	1	82	87
-13	0	1	102	93	-12	2	1	67	-64	-10	5	1	33	28	-4	7	1	42	-46	2	10	1	79	83
-14	0	1	34	26	-15	2	1	40	-48	-9	5	1	32	-19	-2	7	1	42	44	1	10	1	47	-39
-12	1	1	32	33	-16	2	1	35	-38	-8	5	1	139	-139	-1	7	1	56	58	0	10	1	79	-78
-11	1	1	129	121	-15	3	1	49	-47	-7	5	1	42	-41	0	7	1	24	-25	-2	10	1	34	-32
-10	1	1	38	39	-11	3	1	90	-82	-6	5	1	122	126	1	7	1	123	-127	-6	10	1	34	34
-9	1	1	152	-138	-10	3	1	133	-131	-5	5	1	180	174	2	7	1	34	-30	-8	10	1	52	-46
-8	1	1	40	-39	-9	3	1	67	62	-3	5	1	241	-246	3	7	1	43	43	-10	10	1	57	57
-7	1	1	45	47	-8	3	1	202	195	-2	5	1	148	-143	5	7	1	50	48	-10	11	1	50	-45
-5	1	1	127	121	-7	3	1	60	50	-1	5	1	222	223	6	7	1	59	56	-9	11	1	58	54
-4	1	1	65	-49	-6	3	1	67	-67	0	5	1	211	209	7	7	1	49	-45	-8	11	1	65	62
-3	1	1	87	72	-5	3	1	164	-168	1	5	1	55	59	8	7	1	40	-47	-4	11	1	31	29
-2	1	1	142	-137	-4	3	1	123	-117	2	5	1	107	-110	10	8	1	36	38	-3	11	1	67	71
1	1	1	329	317	-3	3	1	310	307	3	5	1	62	62	8	8	1	40	-43	-2	11	1	59	57
2	1	1	212	209	-2	3	1	223	221	4	5	1	156	157	7	8	1	29	-31	1	11	1	40	-37
3	1	1	139	-136	-1	3	1	227	-218	6	5	1	112	-111	6	8	1	43	50	2	11	1	36	-38
4	1	1	514	-510	0	3	1	64	-75	7	5	1	43	-47	5	8	1	102	100	3	11	1	34	26
5	1	1	76	-81	1	3	1	83	-77	8	5	1	93	94	4	8	1	35	28	4	11	1	72	70
6	1	1	309	301	2	3	1	88	-86	9	5	1	139	138	3	8	1	163	-171	0	12	1	41	-39
7	1	1	103	107	3	3	1	34	38	10	5	1	48	-44	2	8	1	145	-151	-1	12	1	40	37
8	1	1	59	-57	5	3	1	57	56	11	5	1	96	-103	1	8	1	63	70	-2	12	1	94	90
9	1	1	125	-136	6	3	1	49	-47	13	5	1	92	95	0	8	1	130	131	-4	12	1	73	-75
10	1	1	36	-42	7	3	1	46	-50	12	6	1	97	-91	-2	8	1	109	-115	-5	12	1	67	-62
11	1	1	90	93	8	3	1	58	-55	10	6	1	62	67	-3	8	1	86	-95	-7	12	1	61	68
13	1	1	90	-97	9	3	1	57	-58	9	6	1	53	52	-4	8	1	30	20	5	-13	2	57	-57
14	1	1	48	-50	10	3	1	49	55	8	6	1	56	-59	-6	8	1	27	-27	3	-13	2	98	100
15	1	1	75	78	12	4	1	93	93	7	6	1	130	-129	-7	8	1	44	-47	2	-13	2	49	49
14	2	1	62	-65	10	4	1	93	-89	5	6	1	48	49	-9	8	1	111	119	1	-13	2	93	-87
12	2	1	48	51	9	4	1	61	-70	2	6	1	25	27	-11	8	1	107	-97	0	-13	2	80	-80
10	2	1	45	-50	8	4	1	104	106	1	6	1	123	120	-13	8	1	42	50	-2	-13	2	85	81
9	2	1	41	42	7	4	1	103	107	0	6	1	73	-75	-11	9	1	32	26	-1	-12	2	50	48
8	2	1	76	68	5	4	1	57	-58	-1	6	1	114	-114	-10	9	1	75	-71	1	-12	2	46	-51
7	2	1	66	59	3	4	1	103	112	-2	6	1	57	-58	-9	9	1	47	-44	2	-12	2	96	-96
6	2	1	85	-89	2	4	1	72	65	-3	6	1	60	62	-8	9	1	49	48	4	-12	2	50	49
5	2	1	192	-197	1	4	1	111	-113	-4	6	1	116	118	-5	9	1	27	-30	6	-12	2	69	-66
3	2	1	278	262	0	4	1	115	-118	-5	6	1	56	54	-2	9	1	31	-32	8	-12	2	56	63
2	2	1	142	141	-1	4	1	175	177	-6	6	1	40	-41	-1	9	1	95	-93	4	-11	2	31	-31
1	2	1	80	-78	-2	4	1	436	434	-7	6	1	97	-97	0	9	1	42	-42	-3	-11	2	50	-49
0	2	1	27	20	-3	4	1	61	-64	-11	6	1	97	92	1	9	1	109	109	-7	-11	2	46	46
-1	2	1	178	-182	-4	4	1	280	-283	-12	6	1	32	36	2	9	1	148	153	-8	-10	2	82	-86
-2	2	1	48	45	-5	4	1	135	-142	-14	6	1	69	-66	3	9	1	79	-75	-7	-10	2	42	-45
-3	2	1	197	195	-6	4	1	232	226	-14	7	1	39	45	4	9	1	166	-172	-6	-10	2	62	58
-5	2	1	96	-86	-7	4	1	221	214	-13	7	1	82	-72	6	9	1	96	93	-5	-10	2	59	62
-6	2	1	81	-81	-8	4	1	46	-44	-12	7	1	83	-90	7	9	1	56	58	-3	-10	2	45	-34
-7	2	1	77	-83	-9	4	1	146	-142	-11	7	1	48	52	9	9	1	35	-44	0	-10	2	51	50

OBSERVED AND CALCULATED STRUCTURE FACTORS FOR PUCOPNP

PAGE 4

H	K	L	FO	FC	H	K	L	FO	FC	H	K	L	FO	FC	H	K	L	FO	FC	H	K	L	FO	FC
1-10	2	73	-77	6	-7	2	66	65	-2	-5	2	281	275	-8	-3	2	56	46	-9	-1	2	243	238	
2-10	2	39	-28	5	-7	2	137	-141	-3	-5	2	120	126	-9	-3	2	87	-79	-10	-1	2	149	142	
3-10	2	52	53	4	-7	2	101	-99	-4	-5	2	46	-56	-10	-3	2	91	-89	-11	-1	2	106	-95	
4-10	2	42	40	3	-7	2	40	35	-5	-5	2	204	-201	-12	-3	2	59	55	-12	-1	2	101	-96	
5-10	2	48	-46	2	-7	2	51	50	-6	-5	2	96	-92	-13	-3	2	38	28	-14	-1	2	35	43	
6-10	2	83	-85	1	-7	2	68	65	-7	-5	2	129	126	-14	-3	2	59	-56	-15	-1	2	64	60	
9-10	2	42	47	0	-7	2	67	61	-8	-5	2	59	61	-15	-2	2	56	48	-16	0	2	38	-37	
12-9	2	41	-46	-1	-7	2	61	61	-9	-5	2	49	-48	-13	-2	2	92	-90	-14	0	2	46	42	
10-9	2	78	76	-2	-7	2	52	-51	-12	-5	2	58	47	-11	-2	2	148	143	-11	0	2	74	-66	
9-9	2	62	64	-3	-7	2	34	-35	-13	-4	2	33	24	-10	-2	2	178	168	-10	0	2	86	-83	
8-9	2	45	-48	-5	-7	2	81	87	-11	-4	2	36	-41	-9	-2	2	103	-100	-8	0	2	285	269	
7-9	2	166	-167	-6	-7	2	107	108	-9	-4	2	42	37	-8	-2	2	190	-176	-7	0	2	76	80	
6-9	2	36	-47	-7	-7	2	47	-48	-8	-4	2	35	-32	-7	-2	2	57	-49	-6	0	2	190	-175	
5-9	2	175	173	-8	-7	2	53	-52	-6	-4	2	135	125	-6	-2	2	136	124	-5	0	2	43	-43	
4-9	2	92	91	-9	-7	2	37	43	-4	-4	2	254	-248	-5	-2	2	195	182	-4	0	2	79	76	
3-9	2	88	-87	-13	-6	2	37	34	-3	-4	2	201	-192	-2	-2	2	202	-184	-3	0	2	251	232	
2-9	2	121	-115	-12	-6	2	45	32	-1	-4	2	441	421	-1	-2	2	116	-121	-2	0	2	131	-131	
1-9	2	59	58	-11	-6	2	44	-35	0	-4	2	151	149	0	-2	2	69	-61	-1	0	2	47	30	
0-9	2	83	80	-10	-6	2	76	-71	1	-4	2	289	-289	1	-2	2	36	-35	0	0	2	140	141	
-2-9	2	53	-48	-9	-6	2	60	46	2	-4	2	298	-296	3	-2	2	66	67	1	0	2	90	85	
-4-9	2	79	81	-8	-6	2	60	66	3	-4	2	100	98	4	-2	2	41	32	2	0	2	52	40	
-5-9	2	58	59	-7	-6	2	109	-108	4	-4	2	193	204	5	-2	2	52	-52	3	0	2	365	-367	
-6-9	2	77	-75	-6	-6	2	135	-130	5	-4	2	27	-25	6	-2	2	29	21	4	0	2	289	-287	
-7-9	2	105	-109	-5	-6	2	46	-38	6	-4	2	163	-170	7	-2	2	39	-36	5	0	2	221	231	
-8-9	2	42	36	-4	-6	2	138	132	8	-4	2	130	129	9	-2	2	34	28	6	0	2	234	244	
-9-9	2	80	81	-3	-6	2	91	97	9	-4	2	61	68	10	-2	2	65	65	8	0	2	271	-273	
-10-8	2	56	-51	-2	-6	2	68	-66	10	-4	2	78	-81	12	-2	2	55	-61	9	0	2	87	-94	
-8-8	2	56	49	-1	-6	2	166	-163	11	-4	2	71	-76	13	-2	2	33	-42	10	0	2	57	59	
-7-8	2	77	82	0	-6	2	102	-91	12	-4	2	35	40	15	-2	2	55	59	11	0	2	83	86	
-5-8	2	76	-76	1	-6	2	129	126	13	-4	2	113	112	12	-1	2	27	-24	13	0	2	78	-79	
-4-8	2	40	44	2	-6	2	219	215	15	-4	2	102	-105	10	-1	2	64	68	14	0	2	30	-19	
-3-8	2	62	54	3	-6	2	54	52	14	-3	2	89	95	9	-1	2	43	46	14	1	2	90	-91	
1-8	2	115	120	6	-6	2	60	-58	13	-3	2	49	56	8	-1	2	36	-41	12	1	2	84	86	
2-8	2	46	40	8	-6	2	86	89	12	-3	2	36	-30	7	-1	2	43	-54	10	1	2	74	-73	
3-8	2	121	-117	9	-6	2	36	-29	11	-3	2	54	-54	6	-1	2	65	-66	9	1	2	153	-154	
4-8	2	155	-157	14	-5	2	75	-76	10	-3	2	45	45	5	-1	2	170	175	7	1	2	242	245	
5-8	2	84	85	13	-5	2	32	-36	9	-3	2	107	112	4	-1	2	258	264	6	1	2	70	76	
6-8	2	254	256	12	-5	2	47	53	8	-3	2	34	38	3	-1	2	86	-87	5	1	2	272	-268	
8-8	2	162	-165	11	-5	2	40	46	5	-3	2	129	133	1	-1	2	89	-85	4	1	2	204	-215	
9-8	2	79	-83	10	-5	2	98	-97	3	-3	2	198	-195	0	-1	2	90	89	2	1	2	51	-49	
10-8	2	51	50	9	-5	2	27	-42	2	-3	2	40	41	-1	-1	2	76	69	1	1	2	28	-26	
11-8	2	99	103	7	-5	2	32	35	1	-3	2	319	323	-2	-1	2	20	14	-1	1	2	108	98	
13-8	2	47	-54	5	-5	2	130	-136	0	-3	2	92	97	-3	-1	2	85	-84	-2	1	2	114	-112	
14-7	2	54	-51	3	-5	2	123	132	-1	-3	2	218	-205	-4	-1	2	192	174	-3	1	2	318	-309	
12-7	2	40	39	2	-5	2	146	137	-2	-3	2	249	-238	-5	-1	2	197	183	-4	1	2	81	-75	
10-7	2	79	-77	1	-5	2	246	-235	-3	-3	2	160	-142	-6	-1	2	131	-121	-5	1	2	72	71	
9-7	2	80	-85	0	-5	2	370	-365	-5	-3	2	65	60	-7	-1	2	317	-296	-6	1	2	106	103	
7-7	2	134	134	-1	-5	2	28	13	-6	-3	2	47	47	-8	-1	2	62	-56	-7	1	2	137	135	

OBSERVED AND CALCULATED STRUCTURE FACTORS FOR PUCOPNP

PAGE 5

H	K	L	FO	FC	H	K	L	FO	FC	H	K	L	FO	FC	H	K	L	FO	FC	H	K	L	FO	FC
-8	1	2	147	-140	-12	3	2	92	80	-13	6	2	48	49	7	8	2	50	-54	3-12	3	34	-37	
-9	1	2	62	-65	-14	3	2	77	-74	-9	6	2	79	-76	8	8	2	68	-68	2-12	3	59	-54	
-10	1	2	40	-43	-16	3	2	54	51	-3	6	2	105	-112	9	8	2	42	-34	0-12	3	42	43	
-15	2	2	75	-69	-15	4	2	36	34	-7	6	2	60	-69	7	9	2	73	76	-1-12	3	47	45	
-13	2	2	76	71	-13	4	2	41	-38	-6	6	2	53	47	6	9	2	68	69	-3-12	3	32	-26	
-12	2	2	43	42	-9	4	2	87	-86	-4	6	2	79	78	5	9	2	45	-51	-6-12	3	34	-41	
-11	2	2	69	-70	-8	4	2	38	-38	-2	6	2	87	-92	4	9	2	90	-89	-7-11	3	56	61	
-10	2	2	59	-52	-7	4	2	115	114	-1	6	2	55	-61	3	9	2	29	3	-6-11	3	67	72	
-9	2	2	106	99	-6	4	2	74	81	1	6	2	84	84	2	9	2	48	51	-4-11	3	56	-57	
-8	2	2	64	57	-5	4	2	80	-76	2	6	2	106	104	1	9	2	29	24	-3-11	3	48	-42	
-7	2	2	108	-98	-4	4	2	276	-282	3	6	2	29	-24	-3	9	2	36	39	4-11	3	47	-49	
-6	2	2	173	-163	-3	4	2	143	-141	4	6	2	102	-100	-5	9	2	55	-57	6-11	3	45	51	
-5	2	2	187	180	-2	4	2	161	173	6	6	2	81	82	-6	9	2	30	30	9-10	3	35	33	
-4	2	2	332	319	-1	4	2	259	262	8	6	2	27	-14	-7	9	2	82	78	7-10	3	32	-24	
-3	2	2	109	-96	0	4	2	105	103	10	6	2	61	57	-9	9	2	83	-86	6-10	3	59	-54	
-1	2	2	241	-240	1	4	2	310	-308	6	7	2	46	-43	-10	9	2	45	-42	5-10	3	31	-7	
0	2	2	76	-77	2	4	2	101	-101	5	7	2	56	-49	-12	9	2	33	28	1-10	3	30	34	
1	2	2	118	115	3	4	2	174	171	4	7	2	91	93	-7	10	2	39	-40	0-10	3	51	49	
2	2	2	35	43	4	4	2	102	104	3	7	2	76	80	-5	10	2	43	32	-2-10	3	35	-38	
3	2	2	121	115	6	4	2	43	-37	2	7	2	59	-58	-3	10	2	37	34	-3-10	3	64	-60	
5	2	2	151	-152	9	4	2	34	19	1	7	2	78	-78	-2	10	2	33	-34	-4-10	3	42	45	
6	2	2	132	-138	10	4	2	29	-30	-3	7	2	64	-68	-1	10	2	31	-26	-5-10	3	134	128	
7	2	2	51	51	12	4	2	45	48	-5	7	2	60	52	3	10	2	58	57	-6-10	3	56	50	
8	2	2	118	120	13	4	2	60	61	-7	7	2	142	-147	5	10	2	37	-85	-7-10	3	99	-99	
10	2	2	36	-30	12	5	2	54	-61	-8	7	2	96	-102	6	10	2	42	-45	-8-10	3	66	-67	
11	2	2	41	-44	11	5	2	54	-64	-9	7	2	116	121	0	11	2	35	-38	-10-9	3	34	19	
13	2	2	56	53	9	5	2	42	50	-10	7	2	147	133	-2	11	2	45	47	-9-9	3	53	49	
13	3	2	32	-27	7	5	2	57	-55	-11	7	2	52	-59	-5	11	2	70	-69	-8-9	3	45	48	
10	3	2	30	22	6	5	2	32	-32	-12	7	2	106	-110	-6	11	2	61	-63	-7-9	3	66	-70	
9	3	2	25	11	5	5	2	77	77	-13	7	2	58	-54	-8	11	2	49	55	-6-9	3	128	-132	
7	3	2	111	-111	4	5	2	56	60	-14	7	2	55	48	-6	12	2	43	53	-4-9	3	118	116	
6	3	2	38	-42	3	5	2	103	-107	-13	8	2	55	50	-5	12	2	63	-64	-3-9	3	77	78	
5	3	2	38	33	2	5	2	173	-172	-11	8	2	104	-107	-4	12	2	100	-102	-2-9	3	87	-93	
3	3	2	114	116	1	5	2	122	120	-10	8	2	79	-89	-2	12	2	65	65	-1-9	3	73	-68	
2	3	2	112	108	0	5	2	118	130	-9	8	2	100	97	-1	12	2	75	74	1-9	3	85	83	
1	3	2	92	-94	-1	5	2	48	52	-8	8	2	136	135	0	12	2	39	-38	3-9	3	36	-21	
0	3	2	173	-183	-2	5	2	94	-95	-7	8	2	44	-48	1	12	2	75	-79	5-9	3	92	95	
-1	3	2	43	44	-3	5	2	141	-143	-6	8	2	118	-119	-2	-13	3	68	69	6-9	3	63	61	
-2	3	2	299	299	-5	5	2	169	175	-4	8	2	125	128	-1	-13	3	39	39	7-9	3	83	-83	
-3	3	2	264	267	-6	5	2	93	102	-2	8	2	40	-41	0	-13	3	53	-50	8-9	3	87	-85	
-4	3	2	37	39	-8	5	2	26	-16	-1	8	2	29	-28	1	-13	3	92	-99	10-9	3	84	90	
-5	3	2	159	-155	-10	5	2	40	-41	0	8	2	67	70	3	-13	3	80	85	11-9	3	36	29	
-6	3	2	127	-133	-12	5	2	55	51	1	8	2	80	85	4	-13	3	55	51	12-9	3	33	-27	
-7	3	2	99	104	-13	5	2	29	20	2	8	2	69	-73	5	-13	3	47	-51	12-8	3	34	26	
-8	3	2	152	155	-14	6	2	40	-39	3	8	2	111	-109	6	-13	3	76	-77	11-8	3	94	91	
-9	3	2	96	-93	-13	6	2	74	-75	4	8	2	35	-27	7	-12	3	66	-69	9-8	3	125	-130	
-10	3	2	93	-90	-12	6	2	31	-27	5	8	2	75	24	5	-12	3	75	77	8-8	3	111	-108	
-11	3	2	47	50	-11	6	2	133	132	6	8	2	70	71	4	-12	3	32	40	7-8	3	96	92	

OBSERVED AND CALCULATED STRUCTURE FACTORS FOR RUCOPNP

PAGE 6

H	K	L	FO	FC	H	K	L	FO	FC	H	K	L	FO	FC	H	K	L	FO	FC	H	K	L	FO	FC
6	-8	3	125	125	-12	-6	3	79	72	-7	-3	3	138	130	-6	-1	3	222	-213	-7	1	3	25	-20
4	-8	3	50	-50	-13	-6	3	39	34	-6	-3	3	168	158	-5	-1	3	184	180	-6	1	3	78	83
0	-8	3	59	-57	-14	-5	3	43	-47	-4	-3	3	71	62	-4	-1	3	233	226	-5	1	3	27	17
-2	-8	3	135	138	-13	-5	3	74	-71	-3	-3	3	144	136	-3	-1	3	139	-135	-4	1	3	256	-257
-3	-8	3	33	36	-11	-5	3	61	55	-2	-3	3	45	-46	-2	-1	3	336	-343	-3	1	3	274	-278
-4	-8	3	85	-81	-9	-5	3	58	-57	-1	-3	3	273	269	-1	-1	3	301	-304	-1	1	3	33	-28
-5	-8	3	87	-85	-8	-5	3	53	-49	0	-3	3	378	388	0	-1	3	148	150	0	1	3	53	51
-7	-8	3	62	66	-7	-5	3	76	76	2	-3	3	100	94	1	-1	3	48	54	1	1	3	47	-44
-13	-7	3	58	60	-6	-5	3	50	48	3	-3	3	114	-117	2	-1	3	108	-108	2	1	3	102	-103
-11	-7	3	42	-48	-5	-5	3	146	-136	4	-3	3	126	-131	3	-1	3	64	-68	3	1	3	60	-61
-10	-7	3	33	-31	-4	-5	3	106	-106	5	-3	3	99	106	4	-1	3	49	61	5	1	3	39	-41
-9	-7	3	44	44	-3	-5	3	178	174	6	-3	3	149	151	5	-1	3	187	189	7	1	3	168	174
-8	-7	3	31	40	-2	-5	3	189	198	7	-3	3	34	-36	6	-1	3	80	-75	8	1	3	86	92
-7	-7	3	31	-30	-1	-5	3	69	72	8	-3	3	100	-99	7	-1	3	169	-176	9	1	3	62	-65
-5	-7	3	54	48	0	-5	3	248	-255	12	-3	3	54	-56	8	-1	3	63	-69	10	1	3	52	-51
-3	-7	3	113	-115	1	-5	3	257	-265	13	-3	3	29	-25	9	-1	3	68	76	12	1	3	72	77
-2	-7	3	82	-87	2	-5	3	64	71	14	-3	3	59	56	10	-1	3	41	34	13	1	3	52	56
0	-7	3	44	45	3	-5	3	315	314	9	-2	3	31	-27	13	-1	3	33	-30	11	2	3	49	-37
1	-7	3	82	76	4	-5	3	51	51	8	-2	3	33	35	14	0	3	62	-62	10	2	3	28	-22
2	-7	3	55	-48	5	-5	3	207	-213	7	-2	3	88	94	13	0	3	68	-70	9	2	3	30	38
3	-7	3	100	-100	6	-5	3	88	-89	6	-2	3	26	-27	11	0	3	76	75	8	2	3	87	85
4	-7	3	48	-45	7	-5	3	55	49	5	-2	3	156	-161	9	0	3	120	-122	6	2	3	34	-38
5	-7	3	29	-25	8	-5	3	42	36	4	-2	3	73	-71	8	0	3	172	-178	4	2	3	83	-86
7	-7	3	71	73	13	-5	3	46	45	3	-2	3	68	70	7	0	3	90	86	3	2	3	98	-93
8	-7	3	109	106	14	-4	3	62	67	2	-2	3	168	169	6	0	3	209	215	2	2	3	100	108
9	-7	3	71	-77	13	-4	3	50	49	1	-2	3	119	121	5	0	3	52	57	1	2	3	198	201
10	-7	3	92	-97	9	-4	3	54	60	0	-2	3	114	115	4	0	3	101	-109	0	2	3	76	-74
12	-7	3	53	47	8	-4	3	37	35	-1	-2	3	66	-69	3	0	3	85	-87	-1	2	3	220	-218
13	-7	3	37	37	7	-4	3	142	-147	-2	-2	3	27	-35	2	0	3	138	133	-2	2	3	47	-46
11	-6	3	38	-42	6	-4	3	78	-83	-3	-2	3	123	-117	1	0	3	72	76	-3	2	3	47	46
9	-6	3	66	69	5	-4	3	130	132	-4	-2	3	47	-43	0	0	3	187	-190	-4	2	3	226	227
8	-6	3	32	33	4	-4	3	237	243	-5	-2	3	173	167	-1	0	3	115	-120	-5	2	3	43	52
6	-6	3	40	39	3	-4	3	57	-58	-6	-2	3	97	96	-2	0	3	62	-59	-6	2	3	46	-51
5	-6	3	77	-76	2	-4	3	226	-234	-7	-2	3	129	-126	-3	0	3	450	447	-7	2	3	75	79
4	-6	3	139	-135	1	-4	3	51	-52	-8	-2	3	259	-247	-4	0	3	96	-93	-8	2	3	56	55
2	-6	3	158	160	0	-4	3	32	34	-9	-2	3	35	36	-5	0	3	302	-297	-9	2	3	82	-79
1	-6	3	56	57	-1	-4	3	264	266	-10	-2	3	194	187	-6	0	3	133	-134	-10	2	3	103	-104
0	-6	3	91	-99	-3	-4	3	78	-76	-11	-2	3	49	45	-7	0	3	99	95	-12	2	3	150	145
-1	-6	3	193	-189	-5	-4	3	55	-53	-13	-2	3	86	-80	-8	0	3	175	175	-14	2	3	62	-62
-2	-6	3	94	-90	-8	-4	3	35	24	-15	-2	3	76	79	-10	0	3	76	-77	-15	2	3	99	-100
-3	-6	3	108	99	-10	-4	3	46	-45	-16	-1	3	51	-50	-11	0	3	108	-98	-14	3	3	87	-84
-4	-6	3	141	143	-12	-4	3	51	-51	-14	-1	3	91	90	-13	0	3	64	63	-13	3	3	98	-91
-5	-6	3	57	-56	-15	-4	3	41	32	-12	-1	3	134	-125	-16	1	3	56	-57	-12	3	3	54	56
-6	-6	3	64	-68	-13	-3	3	50	-37	-11	-1	3	59	-55	-14	1	3	34	31	-11	3	3	152	153
-7	-6	3	47	45	-12	-3	3	44	49	-10	-1	3	109	108	-13	1	3	79	70	-10	3	3	46	51
-8	-6	3	90	81	-11	-3	3	90	82	-9	-1	3	216	210	-11	1	3	65	-69	-9	3	3	140	-136
-9	-6	3	63	-66	-9	-3	3	158	-153	-8	-1	3	66	56	-10	1	3	76	-94	-8	3	3	25	-32
-10	-6	3	87	-83	-8	-3	3	46	-43	-7	-1	3	309	-301	-8	1	3	30	-35	-7	3	3	188	197

1

OBSERVED AND CALCULATED STRUCTURE FACTORS FOR RUCCPNP

PAGE 7

H	K	L	FO	FC	H	K	L	FO	FC	H	K	L	FO	FC	H	K	L	FO	FC	H	K	L	FO	FC
-5	3	3	224	-229	7	5	3	125	-128	-7	6	3	54	53	-4-11	4	72	-72	6	-7	4	50	52	
-4	3	3	46	-43	9	6	3	35	-21	-8	8	3	113	114	-6-11	4	71	77	5	-7	4	57	58	
-3	3	3	223	226	5	6	3	81	-80	-10	8	3	71	-78	-8-11	4	64	-62	3	-7	4	110	-111	
-2	3	3	218	225	4	6	3	60	-60	-11	8	3	62	-62	-8-10	4	36	-32	2	-7	4	71	-74	
0	3	3	211	-217	2	6	3	52	52	-13	8	3	57	57	-7-10	4	82	-85	1	-7	4	79	83	
1	3	3	194	-190	1	6	3	31	25	-12	9	3	41	37	-5-10	4	110	114	0	-7	4	36	41	
2	3	3	141	140	-1	6	3	54	-55	-10	9	3	63	-59	-4-10	4	75	79	-2	-7	4	101	-104	
3	3	3	192	199	-2	6	3	124	-129	-9	9	3	47	-53	-3-10	4	99	-93	-3	-7	4	96	-98	
5	3	3	100	-110	-3	6	3	80	-72	-7	9	3	88	83	-2-10	4	147	-151	-5	-7	4	38	-38	
6	3	3	42	-41	-4	6	3	37	45	-6	9	3	56	60	-1-10	4	37	35	-6	-7	4	72	-66	
7	3	3	30	38	-5	6	3	44	54	-5	9	3	35	-87	0-10	4	100	103	-7	-7	4	45	44	
10	3	3	46	54	-6	6	3	131	137	-4	9	3	116	-114	1-10	4	51	51	-8	-7	4	130	132	
6	4	3	158	-161	-7	6	3	34	-27	-2	9	3	45	47	2-10	4	37	-33	-10	-7	4	105	-103	
5	4	3	37	38	-8	6	3	144	-135	4	9	3	42	-46	9-10	4	40	35	-11	-7	4	63	-62	
4	4	3	235	235	-9	6	3	29	-29	5	9	3	76	-65	10-9	4	61	59	-13	-7	4	73	76	
3	4	3	69	66	-10	6	3	106	104	6	9	3	41	40	8-9	4	76	-80	-12	-6	4	92	96	
2	4	3	242	-245	-11	6	3	39	41	7	9	3	67	61	7-9	4	28	-20	-11	-6	4	61	61	
1	4	3	157	-162	-12	6	3	53	-53	4	10	3	33	28	6-9	4	58	64	-10	-6	4	81	-86	
0	4	3	51	56	-13	6	3	39	-42	1	10	3	31	30	4-9	4	59	-50	-9	-6	4	173	-168	
-1	4	3	209	212	-14	7	3	72	70	-3	10	3	30	-24	3-9	4	26	-22	-7	-6	4	142	143	
-2	4	3	210	208	-12	7	3	70	-79	-6	10	3	49	49	1-9	4	97	105	-6	-6	4	91	95	
-3	4	3	176	-184	-11	7	3	81	-77	-9	10	3	35	-41	-1-9	4	165	-169	-5	-6	4	79	-84	
-4	4	3	205	-209	-10	7	3	57	50	-10	10	3	44	-50	-2-9	4	70	-77	-4	-6	4	45	-43	
-5	4	3	49	51	-9	7	3	164	167	-7	11	3	43	40	-3-9	4	131	132	-3	-6	4	150	154	
-6	4	3	99	92	-7	7	3	202	-203	-5	11	3	55	-53	-4-9	4	122	130	-2	-6	4	69	66	
-7	4	3	57	57	-6	7	3	86	-85	-2	11	3	45	46	-5-9	4	100	-104	-1	-6	4	108	-108	
-8	4	3	83	-81	-5	7	3	172	173	0	11	3	61	-56	-7-9	4	48	-49	0	-6	4	124	-125	
-9	4	3	41	39	-4	7	3	166	179	3	11	3	44	37	-9-9	4	65	70	1	-6	4	25	16	
-10	4	3	110	120	-3	7	3	37	35	4	-13	4	66	65	-10-8	4	33	-12	2	-6	4	203	207	
-12	4	3	63	-65	-2	7	3	105	-108	3	-13	4	56	53	-9-8	4	60	61	3	-6	4	40	37	
-13	4	3	69	-58	-1	7	3	80	-76	1	-13	4	71	-65	-8-8	4	65	59	4	-6	4	105	-108	
-14	4	3	39	44	0	7	3	30	35	-1	-13	4	36	41	-6-8	4	43	-36	5	-6	4	146	-140	
-15	4	3	75	76	4	7	3	49	49	-5	-12	4	48	-55	-5-8	4	60	-65	7	-6	4	126	124	
-12	5	3	44	-43	5	7	3	63	51	-3	-12	4	46	44	-4-8	4	52	-49	8	-6	4	40	-33	
-9	5	3	36	-45	7	7	3	34	-35	1	-12	4	39	-43	-2-8	4	161	171	9	-6	4	29	-33	
-7	5	3	64	68	8	8	3	55	-51	2	-12	4	37	-38	0-8	4	73	-76	10	-6	4	36	-27	
-5	5	3	56	66	6	8	3	80	80	4	-12	4	31	16	3-8	4	81	77	11	-6	4	30	-36	
-4	5	3	65	66	5	8	3	72	75	5	-12	4	55	51	5-8	4	35	-39	12	-6	4	33	-33	
-3	5	3	131	-137	4	8	3	53	-58	6	-12	4	44	41	6-8	4	31	-16	10	-5	4	57	-52	
-2	5	3	101	-97	3	8	3	81	-79	7	-12	4	55	-45	7-8	4	65	66	9	-5	4	27	28	
-1	5	3	92	94	1	8	3	74	70	8	-12	4	49	-51	9-8	4	57	-91	8	-5	4	141	142	
0	5	3	151	149	0	8	3	38	-39	9	-11	4	37	-37	11-8	4	67	59	7	-5	4	35	38	
1	5	3	156	157	-1	8	3	57	-62	7	-11	4	63	62	12-8	4	51	46	6	-5	4	201	-206	
2	5	3	95	-98	-2	8	3	27	27	2	-11	4	38	-43	13-7	4	37	38	5	-5	4	110	-113	
3	5	3	167	-168	-3	8	3	135	135	0	-11	4	42	44	12-7	4	43	43	4	-5	4	163	166	
4	5	3	50	-54	-4	8	3	96	97	-1	-11	4	49	50	11-7	4	31	-26	3	-5	4	141	147	
5	5	3	141	138	-5	8	3	158	-160	-2	-11	4	60	65	10-7	4	40	-36	2	-5	4	24	-21	
6	5	3	34	41	-6	8	3	163	-166	-3	-11	4	73	-78	7-7	4	56	-54	1	-5	4	94	-96	

OBSERVED AND CALCULATED STRUCTURE FACTORS FOR RUCOPNP

PAGE 8

H	K	L	FO	FC	H	K	L	FO	FC	H	K	L	FO	FC	H	K	L	FO	FC	H	K	L	FO	FC
0	-5	4	226	-237	-7	-3	4	24	20	-11	-1	4	130	-128	-16	1	4	47	-43	-7	4	4	162	-164
-1	-5	4	97	94	-8	-3	4	75	-75	-13	-1	4	88	79	-15	2	4	62	-64	-6	4	4	50	-52
-2	-5	4	221	225	-10	-3	4	41	34	-14	-1	4	31	-29	-14	2	4	77	-77	-5	4	4	157	156
-3	-5	4	25	-27	-11	-3	4	27	-21	-15	-1	4	93	-91	-12	2	4	125	132	-3	4	4	183	-192
-4	-5	4	98	-99	-14	-3	4	36	30	-14	0	4	54	-53	-11	2	4	86	86	-2	4	4	32	-31
-5	-5	4	145	138	-15	-3	4	49	51	-11	0	4	55	-52	-10	2	4	83	-84	-1	4	4	194	198
-6	-5	4	80	79	-14	-2	4	102	105	-10	0	4	49	-51	-9	2	4	206	-212	0	4	4	53	51
-7	-5	4	46	-47	-12	-2	4	84	-79	-9	0	4	65	64	-7	2	4	155	153	1	4	4	153	-160
-8	-5	4	125	-128	-10	-2	4	96	102	-8	0	4	92	89	-6	2	4	82	89	2	4	4	199	-196
-9	-5	4	29	-23	-9	-2	4	68	67	-7	0	4	43	42	-5	2	4	35	32	4	4	4	210	212
-10	-5	4	119	117	-8	-2	4	104	-104	-6	0	4	73	-69	-2	2	4	55	58	5	4	4	158	162
-11	-5	4	88	88	-7	-2	4	237	-226	-5	0	4	244	-252	-1	2	4	66	65	6	4	4	136	-142
-12	-5	4	42	-42	-6	-2	4	27	24	-4	0	4	196	-189	0	2	4	87	83	7	4	4	152	-155
-13	-5	4	66	-67	-5	-2	4	282	282	-3	0	4	366	374	1	2	4	64	72	9	4	4	68	68
-12	-4	4	68	-65	-4	-2	4	90	88	-2	0	4	135	129	2	2	4	107	107	10	5	4	57	57
-10	-4	4	33	30	-3	-2	4	271	-274	-1	0	4	123	-121	3	2	4	57	57	8	5	4	62	-60
-9	-4	4	65	62	-2	-2	4	343	-347	0	0	4	192	-200	4	2	4	118	-125	7	5	4	36	-33
-8	-4	4	55	61	-1	-2	4	121	-118	1	0	4	78	-76	5	2	4	29	-39	6	5	4	121	124
-7	-4	4	37	-35	0	-2	4	196	207	2	0	4	171	179	6	2	4	53	60	5	5	4	104	99
-5	-4	4	49	-48	1	-2	4	103	106	3	0	4	34	36	7	2	4	28	29	3	5	4	138	-138
-4	-4	4	63	69	2	-2	4	36	-34	4	0	4	81	-79	8	2	4	29	31	2	5	4	97	-95
-3	-4	4	42	-38	3	-2	4	33	-37	5	0	4	112	-108	11	2	4	55	-53	1	5	4	80	80
-2	-4	4	22	16	4	-2	4	27	-35	6	0	4	121	123	8	3	4	39	41	0	5	4	86	86
-1	-4	4	212	219	6	-2	4	35	-48	7	0	4	98	105	7	3	4	62	60	-2	5	4	76	-79
0	-4	4	64	67	8	-2	4	72	78	8	0	4	86	-85	6	3	4	143	-149	-3	5	4	92	-89
1	-4	4	168	-177	9	-2	4	26	-16	9	0	4	85	-92	5	3	4	173	-186	-4	5	4	51	45
2	-4	4	184	-189	10	-2	4	49	-50	11	0	4	36	84	4	3	4	53	48	-5	5	4	61	-63
3	-4	4	39	-40	13	-1	4	38	-35	12	0	4	59	60	3	3	4	177	186	-6	5	4	68	-66
4	-4	4	121	124	12	-1	4	49	-48	13	0	4	35	-34	2	3	4	80	76	-7	5	4	43	44
5	-4	4	139	147	10	-1	4	35	34	12	1	4	72	80	1	3	4	122	-123	-8	5	4	47	36
7	-4	4	195	-203	9	-1	4	56	53	10	1	4	77	-74	0	3	4	167	-175	-11	5	4	57	-57
9	-4	4	100	106	8	-1	4	69	-68	9	1	4	27	-28	-2	3	4	142	144	-13	5	4	50	54
10	-4	4	29	33	7	-1	4	80	-88	8	1	4	50	49	-4	3	4	175	-175	-14	5	4	30	18
13	-3	4	42	-39	6	-1	4	42	44	7	1	4	51	53	-5	3	4	30	30	-14	6	4	47	43
11	-3	4	38	34	5	-1	4	108	108	5	1	4	34	37	-6	3	4	172	174	-10	6	4	35	37
9	-3	4	40	-48	4	-1	4	53	-60	2	1	4	75	-79	-7	3	4	79	-82	-9	6	4	54	54
8	-3	4	88	-93	3	-1	4	73	-73	1	1	4	63	-68	-8	3	4	218	-220	-8	6	4	62	-71
7	-3	4	59	60	2	-1	4	62	64	0	1	4	81	84	-10	3	4	114	113	-7	6	4	86	-85
6	-3	4	112	115	1	-1	4	174	185	-2	1	4	184	188	-11	3	4	134	130	-6	6	4	54	46
3	-3	4	72	-78	0	-1	4	88	91	-3	1	4	139	-141	-13	3	4	105	-105	-5	6	4	100	99
1	-3	4	63	69	-1	-1	4	233	-244	-4	1	4	143	-145	-14	3	4	47	-45	-4	6	4	26	26
0	-3	4	182	187	-2	-1	4	327	-338	-6	1	4	76	73	-15	3	4	77	75	-3	6	4	94	-103
-1	-3	4	153	162	-3	-1	4	356	350	-7	1	4	105	107	-15	4	4	57	54	-2	6	4	82	-83
-2	-3	4	27	-31	-4	-1	4	418	424	-8	1	4	123	124	-14	4	4	74	78	-1	6	4	59	-63
-3	-3	4	96	-97	-6	-1	4	280	-286	-10	1	4	121	-122	-12	4	4	99	-96	0	6	4	49	48
-4	-3	4	154	-152	-7	-1	4	115	-121	-11	1	4	49	-52	-10	4	4	78	81	1	6	4	93	91
-5	-3	4	38	-37	-8	-1	4	68	63	-12	1	4	37	38	-9	4	4	126	133	2	6	4	31	31
-6	-3	4	173	163	-9	-1	4	106	107	-14	1	4	45	37	-8	4	4	30	-25	3	6	4	61	-58

OBSERVED AND CALCULATED STRUCTURE FACTORS FOR FUCOPNP

PAGE 9

H	K	L	FO	FC	H	K	L	FO	FC	H	K	L	FO	FC	H	K	L	FO	FC	H	K	L	FO	FC
4	6	4	63	-58	-6	11	4	51	48	8	-8	5	41	72	-12	-5	5	64	-71	-9	-3	5	34	32
6	6	4	33	27	1	-13	5	50	-54	6	-8	5	42	-39	-11	-5	5	91	88	-8	-3	5	34	36
7	6	4	56	63	3	-13	5	45	39	5	-8	5	36	-37	-10	-5	5	118	116	-6	-3	5	37	40
9	6	4	36	-35	4	-13	5	39	39	4	-8	5	30	33	-8	-5	5	106	-95	-5	-3	5	58	56
7	7	4	35	-26	5	-12	5	30	26	3	-8	5	95	93	-7	-5	5	124	-127	-4	-3	5	74	-79
5	7	4	46	45	-1	-12	5	29	-10	1	-8	5	72	-77	-6	-5	5	68	73	-3	-3	5	48	-46
3	7	4	59	-53	-2	-12	5	57	63	0	-8	5	126	-130	-5	-5	5	203	209	-2	-3	5	25	26
2	7	4	54	49	-3	-12	5	39	36	-2	-8	5	101	108	-3	-5	5	228	-233	-1	-3	5	148	153
1	7	4	110	113	-5	-11	5	66	68	-5	-8	5	55	-54	-2	-5	5	89	-94	0	-3	5	30	31
-1	7	4	100	-98	-3	-11	5	98	-99	-6	-8	5	80	-85	-1	-5	5	121	125	2	-3	5	67	-68
-2	7	4	108	-108	-1	-11	5	92	89	-8	-8	5	47	53	0	-5	5	40	-37	3	-3	5	164	-171
-3	7	4	62	63	0	-11	5	83	84	-13	-7	5	58	56	1	-5	5	141	-154	5	-3	5	74	73
-4	7	4	189	197	2	-11	5	51	-58	-12	-7	5	52	57	-2	-5	5	55	-60	6	-3	5	59	67
-5	7	4	29	33	3	-11	5	32	-29	-10	-7	5	85	-91	3	-5	5	152	159	8	-3	5	71	-78
-6	7	4	142	-143	5	-11	5	61	63	-9	-7	5	39	-37	4	-5	5	131	140	9	-3	5	38	-38
-7	7	4	54	-59	9	-10	5	36	40	-8	-7	5	79	80	5	-5	5	30	-32	11	-3	5	43	48
-8	7	4	49	53	7	-10	5	51	-46	-7	-7	5	150	148	6	-5	5	168	-178	8	-2	5	28	-29
-9	7	4	79	82	6	-10	5	49	41	-5	-7	5	174	-178	7	-5	5	111	-113	6	-2	5	33	40
-11	7	4	47	-50	5	-10	5	53	49	-4	-7	5	41	-49	8	-5	5	159	159	5	-2	5	37	32
-13	7	4	58	55	4	-10	5	37	-40	-3	-7	5	67	74	9	-5	5	106	107	4	-2	5	149	-150
-12	8	4	33	30	3	-10	5	91	-89	-2	-7	5	43	46	10	-5	5	31	-26	3	-2	5	208	-211
-10	8	4	47	-38	2	-10	5	28	-15	1	-7	5	42	-42	11	-5	5	74	-78	2	-2	5	54	-53
-8	8	4	107	107	1	-10	5	115	116	2	-7	5	47	-43	13	-5	5	49	53	1	-2	5	123	129
-7	8	4	94	108	0	-10	5	94	95	3	-7	5	32	-34	12	-4	5	85	-79	0	-2	5	123	132
-6	8	4	38	-31	-1	-10	5	39	-35	4	-7	5	33	-38	11	-4	5	58	-26	-1	-2	5	104	-106
-5	8	4	143	-140	-2	-10	5	154	-158	6	-7	5	65	72	10	-4	5	96	101	-2	-2	5	275	-286
-3	8	4	178	180	-4	-10	5	99	97	9	-7	5	29	-17	9	-4	5	61	60	-3	-2	5	105	-113
-2	8	4	91	95	-5	-10	5	62	60	10	-6	5	45	-43	8	-4	5	109	-113	-4	-2	5	169	175
-1	8	4	84	-85	-7	-10	5	45	-41	8	-6	5	72	71	7	-4	5	135	-139	-5	-2	5	143	148
0	8	4	128	-126	-9	-10	5	52	58	7	-6	5	161	166	6	-4	5	38	40	-6	-2	5	95	-101
2	8	4	107	97	-10	-9	5	34	-45	5	-6	5	92	-95	5	-4	5	130	133	-7	-2	5	83	-85
3	8	4	33	38	-7	-9	5	32	-29	4	-6	5	31	-28	4	-4	5	110	117	-8	-2	5	60	61
4	8	4	96	-95	-6	-9	5	65	-63	3	-6	5	39	42	3	-4	5	71	-80	-9	-2	5	59	60
5	8	4	40	-35	-5	-9	5	56	-63	2	-6	5	80	78	2	-4	5	54	-57	-11	-2	5	96	-96
6	8	4	61	59	-4	-9	5	77	78	1	-6	5	65	77	1	-4	5	42	38	-13	-2	5	105	107
5	9	4	38	-43	-3	-9	5	140	141	0	-6	5	53	-56	-3	-4	5	95	99	-14	-2	5	35	34
1	9	4	85	-82	-1	-9	5	177	-181	-2	-6	5	124	126	-4	-4	5	207	215	-15	-2	5	55	-51
0	9	4	32	-35	0	-9	5	77	-74	-3	-6	5	66	-70	-5	-4	5	94	-98	-15	-1	5	40	-51
-1	9	4	96	107	1	-9	5	148	153	-4	-6	5	223	-229	-7	-4	5	73	-70	-14	-1	5	92	-92
-2	9	4	86	85	2	-9	5	154	159	-5	-6	5	28	-26	-8	-4	5	55	50	-12	-1	5	98	97
-3	9	4	37	-34	4	-9	5	91	-90	-6	-6	5	176	182	-9	-4	5	36	87	-10	-1	5	96	-92
-4	9	4	115	-112	5	-9	5	39	-34	-7	-6	5	103	99	-10	-4	5	51	50	-8	-1	5	101	99
-6	9	4	107	110	6	-9	5	60	56	-8	-6	5	114	-116	-11	-4	5	73	-67	-6	-1	5	176	-181
-7	9	4	43	47	7	-9	5	47	47	-9	-6	5	131	-131	-12	-4	5	50	-49	-5	-1	5	56	-57
-9	10	4	63	-61	8	-9	5	59	-58	-11	-6	5	103	103	-15	-3	5	51	52	-4	-1	5	143	158
-3	10	4	69	-70	9	-9	5	56	-50	-12	-6	5	52	56	-14	-3	5	50	60	-3	-1	5	329	342
-1	10	4	38	40	10	-8	5	46	-40	-13	-6	5	65	-59	-13	-3	5	35	-28	-2	-1	5	49	-57
-4	11	4	31	-22	9	-8	5	38	-38	-13	-5	5	43	-42	-12	-3	5	58	-51	-1	-1	5	312	-332

OBSERVED AND CALCULATED STRUCTURE FACTORS FOR PUCOPNP

PAGE 10

H	K	L	FO	FC	H	K	L	FO	FC	H	K	L	FO	FC	H	K	L	FO	FC	H	K	L	FO	FC
0	-1	5	125	-126	2	1	5	70	-78	7	4	5	97	-103	-4	7	5	100	107	-2	-12	6	37	39
1	-1	5	242	253	3	1	5	52	51	5	4	5	101	100	-3	7	5	112	106	8	-11	6	44	-37
2	-1	5	263	274	4	1	5	50	50	4	4	5	91	97	-2	7	5	79	-81	7	-11	6	43	-43
3	-1	5	55	-52	5	1	5	63	66	3	4	5	36	-39	-1	7	5	126	-128	6	-11	6	34	22
4	-1	5	208	-219	6	1	5	32	-29	2	4	5	128	-125	0	7	5	36	-37	5	-11	6	69	66
5	-1	5	59	-61	9	1	5	41	34	0	4	5	91	92	1	7	5	92	86	2	-11	6	76	-71
6	-1	5	126	132	10	1	5	35	-32	-2	4	5	113	-119	2	7	5	80	75	0	-11	6	84	80
7	-1	5	49	44	11	1	5	45	-47	-3	4	5	29	36	4	7	5	81	-73	-1	-11	6	38	27
8	-1	5	69	-75	12	1	5	36	41	-4	4	5	169	171	6	7	5	47	40	-2	-11	6	49	-55
10	-1	5	48	43	7	2	5	45	44	-6	4	5	223	-231	5	8	5	73	-67	-3	-11	6	41	-34
12	-1	5	35	-35	5	2	5	52	-50	-7	4	5	137	-147	3	8	5	82	76	-5	-11	6	33	35
12	0	5	72	75	1	2	5	29	26	-8	4	5	37	45	2	8	5	71	72	-6	-11	6	46	-43
11	0	5	52	56	0	2	5	75	70	-9	4	5	98	98	1	8	5	64	-58	-7	-11	6	41	-39
10	0	5	54	-59	-2	2	5	33	32	-10	4	5	48	41	0	8	5	133	-126	-8	-10	6	68	61
9	0	5	68	-68	-3	2	5	41	-47	-11	4	5	63	-63	-2	8	5	133	129	-6	-10	6	46	-50
8	0	5	51	52	-4	2	5	245	-254	-12	4	5	79	-79	-3	8	5	61	67	-5	-10	6	32	-26
7	0	5	66	69	-6	2	5	191	200	-11	5	5	34	-34	-4	8	5	71	-72	-4	-10	6	50	51
6	0	5	40	-47	-7	2	5	156	161	-10	5	5	41	-36	-5	8	5	69	-71	-3	-10	6	54	56
5	0	5	149	-150	-8	2	5	108	-108	-9	5	5	45	42	-7	8	5	40	41	-2	-10	6	75	-76
3	0	5	165	174	-9	2	5	146	-148	-8	5	5	94	93	-9	8	5	33	-34	-1	-10	6	110	-103
2	0	5	139	146	-11	2	5	-68	66	-7	5	5	41	45	-11	8	5	55	54	1	-10	6	112	105
1	0	5	144	-151	-12	2	5	119	116	-5	5	5	84	-85	-4	9	5	55	-47	3	-10	6	99	-100
0	0	5	228	-235	-14	2	5	77	-77	-3	5	5	38	35	-3	9	5	78	-72	4	-10	6	94	-95
-1	0	5	43	38	-15	3	5	57	58	-2	5	5	28	35	-2	9	5	33	38	6	-10	6	95	95
-2	0	5	293	302	-14	3	5	34	19	-1	5	5	59	-59	-1	9	5	105	104	8	-10	6	54	-59
-3	0	5	111	118	-13	3	5	104	-104	0	5	5	54	46	1	9	5	74	-77	9	-10	6	47	-48
-4	0	5	81	-76	-12	3	5	40	-49	1	5	5	52	53	2	9	5	51	-44	9	-9	6	42	-52
-5	0	5	134	-137	-11	3	5	110	112	3	5	5	109	-105	4	9	5	62	60	8	-9	6	31	31
-6	0	5	63	67	-10	3	5	97	100	4	5	5	93	-98	0	10	5	57	58	7	-9	6	106	104
-7	0	5	54	51	-8	3	5	187	-192	5	5	5	47	46	-2	10	5	57	-49	5	-9	6	92	-92
-11	0	5	71	70	-7	3	5	170	-178	6	5	5	94	92	-3	10	5	40	-35	4	-9	6	106	-111
-13	0	5	81	-87	-6	3	5	116	117	8	5	5	89	-87	-6	10	5	57	59	3	-9	6	72	73
-15	0	5	54	58	-5	3	5	241	242	9	5	5	70	-66	-7	10	5	37	40	2	-9	6	147	145
-14	1	5	38	31	-3	3	5	175	-182	7	6	5	47	46	2	-13	6	41	-41	0	-9	6	119	-118
-13	1	5	57	51	-2	3	5	58	-63	4	6	5	57	-59	0	-13	6	56	54	-1	-9	6	68	-78
-11	1	5	78	-78	-1	3	5	60	64	2	6	5	39	32	-2	-12	6	45	39	-2	-9	6	62	65
-10	1	5	56	-54	0	3	5	27	34	1	6	5	68	66	4	-12	6	31	15	-3	-9	6	28	20
-9	1	5	56	-54	1	3	5	81	-82	0	6	5	33	29	3	-11	6	45	-37	-5	-9	6	36	-35
-8	1	5	81	78	3	3	5	78	79	-2	6	5	62	-66	7	-11	6	42	-43	-9	-9	6	62	-54
-7	1	5	81	87	4	3	5	93	95	-3	6	5	62	-61	4	9	5	60	60	-9	-8	6	43	44
-6	1	5	27	-31	6	3	5	111	-114	-4	6	5	61	58	0	10	5	61	58	-6	-8	6	43	-41
-5	1	5	100	-101	8	3	5	70	63	-5	6	5	42	46	-2	10	5	47	-49	-3	-8	6	34	37
-4	1	5	58	-62	9	3	5	60	61	-10	6	5	33	-31	-3	10	5	36	-35	-1	-8	6	37	37
-3	1	5	28	-19	10	3	5	44	-43	-12	7	5	53	65	-6	10	5	54	50	0	-8	6	65	-66
-2	1	5	71	73	11	3	5	43	-46	-10	7	5	56	-43	-7	10	5	45	40	1	-8	6	130	-141
-1	1	5	150	153	10	4	5	69	78	-8	7	5	53	48	2	-13	6	41	-41	3	-8	6	131	131
0	1	5	104	107	9	4	5	87	88	-6	7	5	79	-36	1	-13	6	37	14	5	-8	6	67	-63
1	1	5	119	-122	8	4	5	50	-48	-5	7	5	37	-35	0	-13	6	54	54	6	-8	6	56	-60

OBSERVED AND CALCULATED STRUCTURE FACTORS FOR RUCOPNP

PAGE 11

H	K	L	FO	FC	H	K	L	FO	FC	H	K	L	FO	FC	H	K	L	FO	FC	H	K	L	FO	FC
8	-8	6	72	70	-7	-5	6	130	-137	-5	-2	6	24	14	10	0	6	74	-77	-4	3	6	118	121
4	-7	6	52	49	-8	-5	6	92	-89	-2	-2	6	150	-154	11	0	6	37	-31	-5	3	6	150	156
2	-7	6	38	-43	-9	-5	6	40	42	-1	-2	6	56	-60	11	1	6	43	-38	-7	3	6	82	-82
0	-7	6	34	-34	-10	-5	6	103	106	0	-2	6	71	73	9	1	6	38	43	-8	3	6	138	-139
-1	-7	6	58	67	-13	-5	6	57	49	1	-2	6	106	112	8	1	6	43	-41	-10	3	6	101	108
-2	-7	6	151	154	-13	-4	6	60	-60	3	-2	6	97	-104	5	1	6	62	59	-11	3	6	34	22
-3	-7	6	31	33	-10	-4	6	35	29	4	-2	6	85	-84	4	1	6	111	116	-12	3	6	71	-74
-4	-7	6	85	-94	-9	-4	6	75	76	5	-2	6	32	25	2	1	6	133	-142	-14	4	6	31	-25
-5	-7	6	119	-119	-7	-4	6	80	-84	6	-2	6	115	111	1	1	6	25	-26	-11	4	6	52	-54
-7	-7	6	80	91	-6	-4	6	126	-125	7	-2	6	89	96	0	1	6	81	84	-10	4	6	39	40
-8	-7	6	38	43	-5	-4	6	102	-105	8	-2	6	43	-39	-1	1	6	24	27	-9	4	6	104	104
-10	-7	6	79	-83	-4	-4	6	32	39	11	-1	6	64	67	-2	1	6	58	59	-8	4	6	37	40
-12	-7	6	38	36	-3	-4	6	116	121	9	-1	6	80	-76	-3	1	6	63	65	-7	4	6	97	-98
-13	-6	6	38	-41	-1	-4	6	177	-187	7	-1	6	147	148	-4	1	6	82	-81	-6	4	6	82	-83
-11	-6	6	84	85	1	-4	6	63	65	6	-1	6	52	47	-5	1	6	49	-42	-4	4	6	123	126
-9	-6	6	94	-95	3	-4	6	54	-55	5	-1	6	171	-179	-6	1	6	85	-90	-3	4	6	143	142
-8	-6	6	78	-73	5	-4	6	86	90	4	-1	6	142	-143	-7	1	6	41	44	-2	4	6	87	-91
-7	-6	6	65	67	6	-4	6	29	25	2	-1	6	239	245	-8	1	6	89	91	-1	4	6	186	-185
-6	-6	6	183	189	7	-4	6	54	-58	1	-1	6	89	97	-9	1	6	51	43	1	4	6	106	106
-5	-6	6	104	111	8	-4	6	71	-75	0	-1	6	182	-184	-11	1	6	49	-57	3	4	6	71	-74
-4	-6	6	100	-105	10	-4	6	92	89	-1	-1	6	161	-171	-12	1	6	43	40	5	4	6	50	46
-3	-6	6	182	-190	11	-4	6	47	55	-3	-1	6	144	151	-15	1	6	34	-14	6	4	6	56	56
-2	-6	6	37	30	12	-4	6	82	-80	-4	-1	6	31	21	-15	2	6	38	41	7	4	6	62	-57
-1	-6	6	261	268	11	-3	6	54	55	-5	-1	6	44	-44	-13	2	6	62	-66	8	4	6	67	-67
0	-6	6	38	39	9	-3	6	68	-72	-7	-1	6	101	101	-12	2	6	33	31	7	5	6	54	53
1	-6	6	79	-83	8	-3	6	63	-60	-9	-1	6	117	-119	-11	2	6	100	99	6	5	6	31	28
2	-6	6	24	-26	6	-3	6	61	57	-10	-1	6	36	-46	-9	2	6	111	-114	4	5	6	36	-27
3	-6	6	59	62	5	-3	6	28	30	-11	-1	6	83	85	-7	2	6	132	132	3	5	6	28	22
4	-6	6	33	39	3	-3	6	24	-24	-12	-1	6	85	86	-6	2	6	139	145	2	5	6	50	45
5	-6	6	40	-43	1	-3	6	36	-40	-14	-1	6	57	-58	-5	2	6	78	84	1	5	6	39	-35
6	-6	6	53	-57	0	-3	6	24	-37	-13	0	6	43	-29	-4	2	6	166	-170	0	5	6	80	-81
8	-6	6	59	63	-1	-3	6	57	58	-12	0	6	42	-47	-3	2	6	135	-138	-2	5	6	152	152
10	-6	6	79	-77	-3	-3	6	28	-17	-11	0	6	52	52	-2	2	6	88	94	-3	5	6	48	52
12	-5	6	58	-59	-4	-3	6	40	-38	-10	0	6	100	105	-1	2	6	121	125	-5	5	6	51	-52
11	-5	6	82	-84	-5	-3	6	73	-68	8	0	6	40	-45	0	2	6	61	56	-6	5	6	27	-24
9	-5	6	75	81	-6	-3	6	29	-40	-7	0	6	51	-50	1	2	6	36	-35	-7	5	6	48	37
7	-5	6	100	-103	-8	-3	6	55	55	-6	0	6	37	41	2	2	6	42	-36	-11	5	6	34	-40
6	-5	6	47	-43	-9	-3	6	93	98	-4	0	6	51	53	3	2	6	74	-74	-12	5	6	50	-60
5	-5	6	30	22	-11	-3	6	75	-72	-3	0	6	32	-45	5	2	6	41	44	-11	6	6	73	-77
4	-5	6	89	92	-12	-3	6	96	-96	-2	0	6	113	116	6	2	6	43	-46	-10	6	6	46	-46
3	-5	6	28	-31	-14	-3	6	72	75	-1	0	6	145	151	9	3	6	59	53	-9	6	6	39	29
2	-5	6	110	-113	-15	-2	6	46	-47	0	0	6	112	-115	7	3	6	38	-39	-6	6	6	45	-49
1	-5	6	43	49	-13	-2	6	115	111	1	0	6	225	-230	6	3	6	30	-33	-3	6	6	36	-27
0	-5	6	167	173	-11	-2	6	106	-110	3	0	6	222	236	2	3	6	59	-62	-2	6	6	53	-50
-2	-5	6	211	-215	-10	-2	6	102	-100	4	0	6	122	126	0	3	6	106	107	-1	6	6	50	44
-3	-5	6	70	-78	-8	-2	6	94	93	5	0	6	125	-132	-1	3	6	49	50	0	6	6	78	78
-4	-5	6	191	196	-7	-2	6	33	-30	6	0	6	129	-132	-2	3	6	183	-186	2	6	6	31	-25
-5	-5	6	166	168	-6	-2	6	56	-58	8	0	6	92	96	-3	3	6	184	-186	3	6	6	28	-6

H	K	L	FO	FC	H	K	L	FO	FC	H	K	L	FO	FC	H	K	L	FO	FC	H	K	L	FO	FC
4	6	6	54	-38	3	-9	7	111	111	-5	-5	7	44	42	6	-2	7	54	53	-5	0	7	26	29
7	6	6	34	30	4	-9	7	48	-49	-4	-5	7	79	76	4	-2	7	43	-43	-7	0	7	122	-127
5	7	6	62	-65	5	-9	7	132	-127	-3	-5	7	59	-53	3	-2	7	105	-108	-8	0	7	75	-81
4	7	6	49	-45	6	-9	7	39	-39	-2	-5	7	174	-178	1	-2	7	63	67	-9	0	7	44	39
2	7	6	70	66	7	-9	7	68	61	-1	-5	7	121	-125	0	-2	7	53	53	-10	0	7	39	49
1	7	6	73	71	8	-9	7	60	63	0	-5	7	146	153	-1	-2	7	93	-99	-14	0	7	40	-31
0	7	6	32	-22	9	-8	7	46	43	1	-5	7	193	196	-2	-2	7	35	-34	-14	1	7	52	-49
-1	7	6	75	-76	8	-8	7	52	39	3	-5	7	135	-139	-3	-2	7	107	108	-13	1	7	61	-58
-3	7	6	72	72	7	-8	7	42	-39	5	-5	7	74	76	-4	-2	7	74	-78	-12	1	7	41	41
-5	7	6	61	-58	6	-8	7	99	-97	7	-5	7	46	-43	-5	-2	7	110	-108	-11	1	7	50	54
-7	7	6	37	36	4	-8	7	109	108	10	-5	7	56	55	-6	-2	7	38	-34	-10	1	7	38	-35
-10	7	6	48	-52	2	-8	7	67	-73	11	-4	7	69	69	-7	-2	7	72	73	-8	1	7	79	78
-10	8	6	41	36	-1	-8	7	52	-57	9	-4	7	35	-38	-8	-2	7	138	138	-7	1	7	50	51
-8	8	6	38	-43	-3	-8	7	62	57	6	-4	7	28	21	-10	-2	7	118	-123	-6	1	7	73	-76
-4	8	6	39	-42	-4	-8	7	45	44	4	-4	7	83	-85	-11	-2	7	87	-91	-5	1	7	80	-76
-2	8	6	67	57	-5	-8	7	67	74	3	-4	7	39	44	-12	-2	7	76	75	-4	1	7	112	-117
0	8	6	65	-60	-7	-8	7	51	-46	2	-4	7	150	153	-13	-2	7	81	94	-3	1	7	62	58
1	8	6	78	-70	-9	-8	7	31	24	1	-4	7	45	48	-14	-1	7	35	-41	-2	1	7	71	62
3	8	6	85	79	-11	-7	7	59	58	0	-4	7	150	-156	-12	-1	7	66	70	0	1	7	42	-46
1	9	6	40	-39	-10	-7	7	35	-40	-1	-4	7	100	-104	-11	-1	7	69	72	3	1	7	74	-78
0	9	6	38	38	-9	-7	7	49	-49	-3	-4	7	74	78	-10	-1	7	42	-41	4	1	7	59	61
-1	9	6	41	35	-8	-7	7	39	39	-4	-4	7	99	99	-9	-1	7	104	-105	5	1	7	64	62
2	-12	7	35	31	-7	-7	7	77	79	-6	-4	7	56	-62	-8	-1	7	43	-36	6	1	7	43	-47
-6	-11	7	67	-60	-5	-7	7	93	-103	-10	-4	7	54	53	-7	-1	7	86	85	7	1	7	59	-58
-3	-11	7	43	50	-4	-7	7	49	-49	-11	-4	7	44	47	-6	-1	7	147	151	8	1	7	38	-40
-2	-11	7	31	-25	-3	-7	7	36	40	-12	-4	7	40	-42	-5	-1	7	30	30	9	1	7	37	27
2	-11	7	39	-33	-2	-7	7	130	132	-13	-4	7	62	-72	-4	-1	7	40	-39	10	1	7	49	44
3	-11	7	39	-39	-1	-7	7	71	75	-14	-3	7	62	63	-3	-1	7	39	42	9	2	7	33	-21
5	-11	7	52	40	0	-7	7	74	-76	-13	-3	7	38	38	-2	-1	7	90	94	5	2	7	29	26
7	-10	7	44	47	1	-7	7	89	-96	-12	-3	7	101	-106	0	-1	7	72	-76	4	2	7	28	19
6	-10	7	64	64	5	-7	7	62	61	-11	-3	7	108	-109	2	-1	7	169	173	2	2	7	31	-32
4	-10	7	80	-69	6	-7	7	29	-27	-10	-3	7	46	50	3	-1	7	66	62	1	2	7	52	-44
3	-10	7	45	-43	10	-7	7	30	8	-9	-3	7	113	118	4	-1	7	86	-86	0	2	7	51	51
1	-10	7	78	75	7	-6	7	40	-39	-7	-3	7	68	-64	5	-1	7	94	-99	-1	2	7	115	112
-1	-10	7	54	-58	4	-6	7	76	73	-6	-3	7	61	-60	7	-1	7	77	70	-3	2	7	138	-139
-2	-10	7	44	43	2	-6	7	133	-132	-5	-3	7	40	-53	8	-1	7	75	81	-4	2	7	88	-91
-3	-10	7	29	18	1	-6	7	46	-40	-4	-3	7	41	40	9	-1	7	54	-50	-6	2	7	84	83
-5	-10	7	74	-73	0	-6	7	144	145	-3	-3	7	64	71	10	-1	7	83	-74	-7	2	7	84	87
-7	-10	7	65	65	-1	-6	7	197	200	-1	-3	7	42	43	9	0	7	87	83	-8	2	7	43	-44
-8	-10	7	41	49	-2	-6	7	50	-51	0	-3	7	26	-37	8	0	7	53	52	-9	2	7	91	-88
-9	-9	7	55	-47	-3	-6	7	128	-137	1	-3	7	76	-80	7	0	7	43	-32	-10	2	7	58	61
-7	-9	7	36	30	-4	-6	7	56	-55	2	-3	7	40	-38	6	0	7	103	-100	-11	2	7	41	40
-6	-9	7	78	81	-6	-6	7	101	100	3	-3	7	42	44	5	0	7	43	-41	-12	2	7	73	-73
-4	-9	7	41	-41	-8	-6	7	90	-95	4	-3	7	27	29	4	0	7	94	94	-13	2	7	31	-27
-2	-9	7	38	33	-10	-6	7	48	57	6	-3	7	32	44	3	0	7	63	79	-14	2	7	46	43
0	-9	7	63	-62	-12	-6	7	47	-47	10	-3	7	37	-34	2	0	7	61	-89	-11	3	7	40	-40
1	-9	7	32	-37	-12	-5	7	40	41	11	-2	7	32	25	1	0	7	40	-38	-10	3	7	43	47
2	-9	7	62	67	-7	-5	7	91	-97	7	-2	7	47	43	-4	0	7	56	64	-9	3	7	45	38

OBSERVED AND CALCULATED STRUCTURE FACTORS FOR RUCOPNP

PAGE 13

H	K	L	FO	FC	H	K	L	FO	FC	H	K	L	FO	FC	H	K	L	FO	FC	H	K	L	FO	FC
-8	3	7	97	-99	-9	6	7	39	44	6	-8	8	41	-35	-7	-4	8	39	-46	-3	-1	8	71	-79
-7	3	7	104	-99	-10	6	7	76	-77	7	-8	8	36	-29	-5	-4	8	45	49	-4	-1	8	103	-104
-6	3	7	50	55	-11	6	7	104	-106	2	-7	8	39	-32	-4	-4	8	34	85	-6	-1	8	156	158
-5	3	7	123	125	-10	7	7	80	-81	3	-7	8	75	67	-3	-4	8	47	50	-7	-1	8	67	70
-4	3	7	41	41	-9	7	7	96	-98	1	-7	8	62	-60	-2	-4	8	45	-43	-8	-1	8	83	-87
-3	3	7	93	-95	-7	7	7	57	54	0	-7	8	70	-68	0	-4	8	59	-65	-9	-1	8	129	-134
-2	3	7	162	-159	-6	7	7	34	37	-1	-7	8	54	49	2	-4	8	107	112	-11	-1	8	48	55
-1	3	7	34	-38	-5	7	7	33	-33	-2	-7	8	113	108	3	-4	8	78	78	-12	-1	8	32	35
0	3	7	138	140	-4	7	7	37	-38	-4	-7	8	48	-47	4	-4	8	80	-76	-13	0	8	34	-32
1	3	7	95	92	-2	7	7	33	34	-6	-7	8	44	50	5	-4	8	83	-76	-12	0	8	56	61
2	3	7	77	-74	-1	7	7	52	-50	-7	-7	8	45	46	7	-4	8	41	38	-11	0	8	39	40
3	3	7	68	-68	0	7	7	53	-57	-8	-7	8	38	-39	4	-3	8	75	75	-8	0	8	73	-70
4	3	7	37	39	1	7	7	34	36	-10	-7	8	64	72	2	-3	8	52	-53	-7	0	8	84	-79
5	3	7	50	47	2	7	7	67	63	-11	-7	8	46	44	-1	-3	8	40	-40	-5	0	8	73	72
4	4	7	51	-48	1	8	7	69	-61	-12	-6	8	45	-41	-3	-3	8	116	114	-2	0	8	82	-81
3	4	7	50	-53	-1	8	7	40	36	-11	-6	8	46	-48	-4	-3	8	87	94	-1	0	8	42	-36
2	4	7	90	94	-6	8	7	43	29	-9	-6	8	43	54	-5	-3	8	62	-67	0	0	8	28	27
1	4	7	107	104	-7	8	7	33	-25	-7	-6	8	57	-57	-6	-3	8	118	-118	4	0	8	42	40
0	4	7	81	-78	-8	8	7	72	-67	-6	-6	8	77	79	-7	-3	8	81	-82	6	0	8	55	-57
-1	4	7	142	-139	-1	-11	8	50	-45	-5	-6	8	83	82	-8	-3	8	77	80	7	0	8	49	-49
-3	4	7	82	84	-2	-11	8	31	12	-4	-6	8	64	-62	-9	-3	8	144	147	9	0	8	66	59
-4	4	7	120	123	-3	-11	8	55	53	-3	-6	8	96	-95	-11	-3	8	110	-122	8	1	8	53	-51
-6	4	7	86	-86	-6	-11	8	75	-77	-1	-6	8	103	97	-13	-3	8	48	51	3	1	8	42	44
-7	4	7	44	-36	-8	-10	8	38	43	0	-6	8	83	82	-13	-2	8	34	35	2	1	8	46	47
-8	4	7	39	38	-7	-10	8	72	69	2	-6	8	129	-128	-12	-2	8	63	62	1	1	8	84	-87
-13	4	7	46	-40	-5	-10	8	75	-79	3	-6	8	52	-48	-10	-2	8	154	-158	0	1	8	74	-71
-12	5	7	89	-90	-4	-10	8	32	-37	4	-6	8	95	92	-9	-2	8	46	-46	-2	1	8	76	73
-11	5	7	35	-41	-3	-10	8	31	-8	5	-6	8	38	38	-8	-2	8	158	160	-3	1	8	46	46
-10	5	7	40	49	-2	-10	8	53	48	7	-6	8	45	-46	-7	-2	8	131	131	-4	1	8	44	-45
-9	5	7	77	79	0	-10	8	65	-53	8	-5	8	42	-40	-6	-2	8	49	-46	-8	1	8	28	-27
-8	5	7	44	44	2	-10	8	50	45	6	-5	8	50	48	-5	-2	8	148	-150	-9	1	8	33	-36
-6	5	7	72	-71	4	-10	8	47	-54	5	-5	8	58	58	-4	-2	8	57	-60	-10	1	8	36	43
-4	5	7	29	35	6	-10	8	36	34	4	-5	8	106	-109	-3	-2	8	81	82	-11	1	8	69	71
-3	5	7	35	28	7	-9	8	44	43	3	-5	8	140	-136	-2	-2	8	100	101	-12	1	8	40	-40
-2	5	7	58	64	5	-9	8	44	-43	2	-5	8	29	28	0	-2	8	65	-67	-13	1	8	87	-91
-1	5	7	42	41	4	-9	8	42	41	1	-5	8	101	97	2	-2	8	71	73	-12	2	8	95	-88
0	5	7	56	-54	3	-9	8	40	51	-1	-5	8	58	-65	3	-2	8	49	-52	-11	2	8	44	-41
1	5	7	82	-77	-3	-9	8	42	-45	-2	-5	8	110	-108	4	-2	8	49	-51	-10	2	8	84	88
3	5	7	52	51	-5	-9	8	51	55	-3	-5	8	73	-75	6	-2	8	50	52	-9	2	8	76	77
4	5	7	30	-34	-6	-9	8	49	51	-4	-5	8	51	56	8	-1	8	45	40	-8	2	8	42	-49
3	6	7	33	-32	-8	-9	8	52	-50	-5	-5	8	55	55	7	-1	8	47	44	-7	2	8	88	-90
2	6	7	48	-32	-9	-9	8	37	-26	-6	-5	8	30	-29	5	-1	8	84	-86	-6	2	8	77	83
1	6	7	35	23	-9	-8	8	30	-19	-8	-5	8	36	28	4	-1	8	43	-51	-5	2	8	54	59
0	6	7	45	42	-6	-8	8	51	-54	-10	-5	8	35	-37	3	-1	8	92	96	-4	2	8	70	-67
-5	6	7	59	-55	-4	-8	8	32	18	-12	-4	8	50	-55	2	-1	8	32	43	-3	2	8	100	-103
-6	6	7	30	-32	-1	-8	8	57	-51	-10	-4	8	78	84	1	-1	8	52	-53	-1	2	8	115	114
-7	6	7	54	56	0	-8	8	34	-31	-9	-4	8	30	28	-1	-1	8	36	85	0	2	8	87	80
-8	6	7	74	79	2	-8	8	29	29	-8	-4	8	26	-90	-2	-1	8	40	36	1	2	8	94	-91

OBSERVED AND CALCULATED STRUCTURE FACTORS FOR RUCOPNP

PAGE 14

H	K	L	FO	FC	H	K	L	FO	FC	H	K	L	FO	FC	H	K	L	FO	FC	H	K	L	FO	FC
2	2	8	116	-116	-6	7	8	80	81	-3	-6	9	78	-75	2	-2	9	54	51	4	2	9	57	54
4	2	8	32	32	-7	7	8	89	87	-4	-6	9	51	60	1	-2	9	67	-64	3	2	9	37	-41
5	2	8	33	31	-3	-11	9	74	69	-5	-6	9	38	20	0	-2	9	79	-77	2	2	9	79	-71
3	3	8	115	-114	-2	-11	9	33	15	-6	-6	9	102	-103	-1	-2	9	45	43	0	2	9	89	85
2	3	8	32	-25	-1	-11	9	66	-53	-7	-6	9	60	-67	-2	-2	9	122	119	-1	2	9	46	41
1	3	8	128	117	0	-11	9	50	-54	-8	-6	9	54	54	-3	-2	9	81	82	-2	2	9	53	-52
0	3	8	90	82	2	-11	9	55	57	-9	-6	9	85	91	-4	-2	9	93	-88	-4	2	9	52	52
-1	3	8	35	-32	3	-10	9	54	46	-11	-6	9	70	-74	-5	-2	9	163	-163	-5	2	9	44	44
-2	3	8	96	-96	1	-10	9	51	-47	-10	-5	9	63	-63	-7	-2	9	154	153	-6	2	9	64	-61
-3	3	8	62	-66	-1	-10	9	43	35	-8	-5	9	45	43	-8	-2	9	57	58	-7	2	9	74	-80
-4	3	8	89	75	-2	-10	9	79	76	-7	-5	9	62	61	-9	-2	9	81	-86	-8	2	9	58	62
-5	3	8	73	72	-3	-10	9	41	26	-2	-5	9	50	-50	-10	-2	9	40	-46	-9	2	9	107	102
-6	3	8	64	-54	-4	-10	9	64	-58	-1	-5	9	39	-35	-9	-1	9	48	-50	-11	2	9	101	-106
-8	3	8	58	66	-5	-10	9	78	-74	0	-5	9	38	33	-8	-1	9	76	-78	-12	2	9	78	-80
-9	3	8	51	63	-6	-9	9	42	40	1	-5	9	76	81	-7	-1	9	46	41	-11	3	9	59	-62
-10	3	8	41	-42	-4	-9	9	46	-44	3	-5	9	55	-46	-6	-1	9	159	163	-10	3	9	105	-110
-11	3	8	64	-60	-3	-9	9	34	-40	4	-5	9	91	-91	-5	-1	9	43	39	-8	3	9	77	70
-11	4	8	34	33	-1	-9	9	45	45	5	-5	9	35	28	-4	-1	9	124	-124	-7	3	9	33	36
-6	4	8	44	-39	0	-9	9	57	51	6	-5	9	73	74	-3	-1	9	104	-98	-6	3	9	70	-76
-4	4	8	79	80	2	-9	9	36	-30	7	-5	9	32	32	-1	-1	9	112	113	-4	3	9	59	61
-3	4	8	41	35	6	-9	9	33	-39	8	-5	9	58	-49	0	-1	9	46	39	-3	3	9	45	46
-1	4	8	86	-86	4	-8	9	31	-19	8	-4	9	37	40	1	-1	9	66	-69	-2	3	9	67	-63
0	4	8	51	-51	2	-8	9	39	41	7	-4	9	63	52	2	-1	9	82	-82	-1	3	9	63	-59
1	4	8	65	60	-1	-8	9	35	-39	5	-4	9	57	-60	4	-1	9	56	58	0	3	9	65	63
2	4	8	97	90	-6	-8	9	42	36	2	-4	9	35	25	5	-1	9	36	-37	1	3	9	80	79
4	4	8	78	-78	-7	-8	9	44	37	1	-4	9	43	45	6	-1	9	73	-72	3	3	9	73	-64
6	4	8	33	32	-8	-8	9	41	-28	-1	-4	9	55	-54	3	0	9	41	-35	4	3	9	62	-58
3	5	8	38	42	-9	-8	9	61	-65	-2	-4	9	53	-54	2	0	9	27	-26	5	3	9	46	44
1	5	8	40	-32	-10	-7	9	90	89	-3	-4	9	29	28	1	0	9	47	42	3	4	9	42	38
0	5	8	36	-40	-8	-7	9	93	-98	-4	-4	9	62	60	0	0	9	39	37	2	4	9	46	49
-3	5	8	76	74	-7	-7	9	54	-61	-5	-4	9	64	65	-1	0	9	42	-48	0	4	9	37	-37
-4	5	8	33	27	-6	-7	9	32	38	-7	-4	9	62	-57	-2	0	9	77	-78	-1	4	9	53	-46
-5	5	8	36	-34	-5	-7	9	52	41	-12	-3	9	44	47	-3	0	9	59	-55	-3	4	9	59	49
-6	5	8	62	-67	-3	-7	9	30	-34	-10	-3	9	54	-57	-4	0	9	47	50	-8	4	9	43	-38
-9	5	8	73	70	-1	-7	9	51	53	-9	-3	9	49	43	-5	0	9	97	101	-9	4	9	48	-46
-11	5	8	64	-58	0	-7	9	33	-24	-8	-3	9	126	131	-6	0	9	30	-25	-7	5	9	36	-33
-8	6	8	98	98	1	-7	9	86	-81	-6	-3	9	141	-141	-8	0	9	56	-57	-6	5	9	59	-57
-7	6	8	67	69	3	-7	9	62	57	-5	-3	9	72	-72	-11	0	9	45	48	-3	5	9	37	43
-6	6	8	46	-42	4	-7	9	78	79	-4	-3	9	91	93	-12	1	9	64	-73	-1	5	9	34	-30
-5	6	8	93	-84	6	-7	9	35	-40	-3	-3	9	103	107	-11	1	9	39	41	-2	6	9	65	60
-3	6	8	56	56	7	-6	9	67	-55	-2	-3	9	32	27	-10	1	9	101	107	-4	6	9	47	-40
-2	6	8	57	66	5	-6	9	80	72	-1	-3	9	71	-75	-8	1	9	70	-66	-5	6	9	101	-99
0	6	8	36	-26	4	-6	9	45	44	0	-3	9	95	-89	-7	1	9	73	-76	-2	-10	10	90	87
0	7	8	37	-35	3	-6	9	69	-62	2	-3	9	59	67	-6	1	9	32	39	-1	-10	10	53	50
-1	7	8	53	49	2	-6	9	106	-103	8	-2	9	39	-33	1	1	9	54	-53	0	-10	10	53	-43
-2	7	8	46	47	0	-6	9	87	84	6	-2	9	49	45	3	1	9	47	37	1	-10	10	72	-64
-3	7	8	53	-52	-1	-6	9	31	36	5	-2	9	31	-36	4	1	9	37	29	2	-9	10	49	-41
-4	7	8	69	-63	-2	-6	9	44	-44	3	-2	9	62	57	5	2	9	43	45	0	-9	10	61	61

1

OBSERVED AND CALCULATED STRUCTURE FACTORS FOR RUCOPNP

PAGE 15

H	K	L	FO	FC	H	K	L	FO	FC	H	K	L	FO	FC	H	K	L	FO	FC	H	K	L	FO	FC
-1	-9	10	66	61	-5	-5	10	75	-74	4	-1	10	60	60	-2	3	10	42	48	-8	-3	11	57	-55
-3	-9	10	68	-67	-6	-5	10	36	26	3	-1	10	35	-33	-3	3	10	52	51	-6	-3	11	39	30
-4	-9	10	34	-28	-7	-5	10	80	83	2	-1	10	95	-81	-5	3	10	94	-91	-5	-3	11	35	-37
-5	-9	10	33	26	-8	-5	10	30	19	0	-1	10	88	86	-7	3	10	93	87	-3	-3	11	41	41
-8	-8	10	68	-62	-10	-5	10	50	-52	-1	-1	10	126	123	-2	3	10	48	45	0	-3	11	36	-33
-6	-8	10	60	61	-5	-4	10	45	49	-3	-1	10	135	-134	-6	4	10	60	55	2	-3	11	34	32
4	-7	10	65	61	1	-4	10	30	24	-4	-1	10	55	-51	-4	4	10	60	-61	3	-3	11	56	50
0	-7	10	34	32	2	-4	10	53	58	-5	-1	10	80	78	1	-8	11	33	26	3	-2	11	49	43
-2	-7	10	31	-42	5	-4	10	36	-37	-6	-1	10	33	27	-1	-8	11	30	-2	2	-2	11	32	-26
-3	-7	10	47	-50	5	-3	10	44	-34	-9	0	10	43	-43	-3	-8	11	55	-55	1	-2	11	71	-59
-4	-7	10	41	47	4	-3	10	41	-40	-5	0	10	52	-50	-6	-7	11	55	-55	0	-2	11	31	-29
-5	-7	10	78	78	3	-3	10	69	65	-6	0	10	37	34	-5	-7	11	69	59	-1	-2	11	69	69
-7	-7	10	98	-93	2	-3	10	70	56	-3	0	10	38	-28	-4	-7	11	88	87	-2	-2	11	48	43
-8	-7	10	52	-47	0	-3	10	74	-68	-2	0	10	84	-80	-2	-7	11	72	-64	-3	-2	11	41	-42
-9	-7	10	79	71	-1	-3	10	71	-71	-1	0	10	37	-37	-1	-7	11	37	-31	-4	-2	11	41	-37
-9	-6	10	76	82	-2	-3	10	43	37	0	0	10	64	63	2	-6	11	33	24	-5	-2	11	37	39
-8	-6	10	75	77	-3	-3	10	88	88	1	0	10	65	59	1	-6	11	34	30	-7	-2	11	41	-48
-6	-6	10	82	-89	-4	-3	10	45	46	3	0	10	40	-34	0	-6	11	34	-28	-3	-1	11	43	-35
-5	-6	10	59	-53	-5	-3	10	63	-61	4	1	10	31	21	-1	-6	11	77	-64	-2	-1	11	56	-54
-4	-6	10	88	80	-6	-3	10	42	-40	-1	1	10	43	-37	-3	-6	11	101	98	-1	-1	11	37	32
-3	-6	10	49	43	-7	-3	10	31	31	-2	1	10	29	-17	-4	-6	11	53	45	0	-1	11	75	72
-2	-6	10	60	-49	-9	-3	10	42	-41	-4	1	10	53	55	-5	-6	11	78	-71	2	-1	11	73	-68
-1	-6	10	69	-61	-8	-2	10	41	-36	-5	1	10	68	65	-6	-6	11	73	-69	1	0	11	54	41
0	-6	10	28	18	-6	-2	10	63	67	-7	1	10	90	-88	-7	-6	11	32	20	0	0	11	35	27
1	-6	10	61	60	-5	-2	10	89	-87	-8	1	10	41	-32	-8	-5	11	34	26	-1	0	11	48	-46
2	-6	10	38	-28	-4	-2	10	139	-139	-9	1	10	40	37	-7	-5	11	36	38	-6	0	11	43	33
3	-6	10	65	-61	-2	-2	10	130	127	-10	1	10	85	80	-5	-5	11	46	-40	-7	1	11	74	-79
5	-6	10	89	88	-1	-2	10	66	64	-9	2	10	86	84	-4	-5	11	76	-66	-5	1	11	76	67
6	-6	10	49	37	0	-2	10	84	-75	-2	2	10	82	74	-2	-5	11	83	71	-4	1	11	47	43
6	-5	10	56	54	1	-2	10	107	-105	-7	2	10	38	-35	-1	-5	11	45	36	-3	2	11	65	60
4	-5	10	59	-51	2	-2	10	38	-36	-6	2	10	104	-99	0	-5	11	55	-52	-4	2	11	62	58
2	-5	10	36	25	3	-2	10	78	73	-4	2	10	73	67	2	-5	11	33	37	-5	2	11	45	-44
0	-5	10	38	-39	4	-2	10	62	53	-3	2	10	36	45	-1	-4	11	39	36	-6	2	11	98	-90
-1	-5	10	38	-33	5	-2	10	63	-56	3	2	10	56	-59	-3	-4	11	35	-44	-3	-5	12	31	-23
-3	-5	10	57	51	6	-2	10	35	-38	2	3	10	46	42	-9	-3	11	33	-32	-2	-4	12	33	-26
-4	-5	10	59	-56	5	-1	10	37	39	-1	3	10	38	-37										